Modeling and simulation of photovoltaic systems under partial shading conditions

Bonie Johana Restrepo Cuestas

Universidad Nacional de Colombia
Facultad de Ingeniería y Arquitectura, Departamento de Eléctrica, Electrónica y Computación
Manizales, Colombia
2023

Modeling and simulation of photovoltaic systems under partial shading conditions

Bonie Johana Restrepo Cuestas

Doctoral Thesis

Supervised by:
Carlos Andrés Ramos Paja, Ph.D.
Luz Adriana Trejos Grisales, Ph.D.

Línea de Investigación:
Energías Renovables
Grupo de Investigación:
GAUNAL

Universidad Nacional de Colombia
Facultad de Ingeniería y Arquitectura, Departamento de Eléctrica, Electrónica y Computación
Manizales, Colombia
2023

Acknowledgments

I want to express my most sincere gratitude to my advisors, professors Carlos Andrés Ramos Paja and Luz Adriana Trejos Grisales, for allowing me to experience this doctoral process with them. Thanks to their patience and dedication, I learned that, despite the fact that we all have different learning processes and times, with perseverance and step-by-step progress, we can achieve the goals we long for. They are excellent professionals and advisors, but the most important thing is that they are wonderful people who have given me the best example to continue developing my teaching and research activities.

I also want to thank my family, especially my mother, María Consuelo (Chelito), who is the proudest of my achievement. She is the one who has given everything for her family and who has supported me in every possible way to complete my process. To my husband, Mauricio, and my son, Matías, I thank you for your patience, understanding, love, and unconditional support. To my brothers, Lean and Nena, and my nephew Samu, thank you for always being there for my family and me. I love you infinitely.

Looking back on my process, I understand it would not have been possible without a support group. For this reason, I want to thank Professor Luis Fernando Grisales, who encouraged and motivated me to start my doctoral studies and gave me advice and help at each stage that allowed everything to flow better. To professors Mariana Durango, Jhon Jairo Rojas, and Jhony Guzmán who gave a vote of confidence to my work, I hope that life allows us to continue working together for a long time. To the students David Restrepo, Alejandra Ortiz, and Juan Manuel Arango, I thank you for your invaluable support during these years. You can't imagine how much your support meant to me. I know that amazing things await you in your lives. I also want to thank people like Sebastián, Robison, María Elena, Bernardo, and Cristian, who always had a moment to listen to me, encourage me, and make me laugh at my sorrows and theirs. I carry them in my heart.

Finally, I would like to thank the members of the Electric Energy and Power, Electronics, and Renewable Energy laboratories at Instituto Tecnológico Metropolitano (ITM), especially Juan Pablo Villegas, Santiago Acevedo, Cristian Escudero, and Kevin Montes, who were always willing to help me with the equipment and spaces I needed for the experimental tests of my thesis.

Agradecimientos

Quiero expresar mi más sincero agradecimiento a mis asesores, los profesores Carlos Andrés Ramos Paja y Luz Adriana Trejos Grisales, por permitirme vivir este proceso doctoral junto a ellos. Gracias a su paciencia y dedicación, aprendí que, a pesar de que todos tenemos procesos y tiempos de aprendizaje diferentes, con perseverancia y paso a paso, podemos alcanzar los logros que anhelamos. Son excelentes profesionales y asesores, pero lo más importante es que son personas maravillosas que me han dado el mejor ejemplo para continuar desarrollando mis actividades de docencia e investigación.

También quiero agradecer a mi familia, especialmente a mi madre, María Consuelo (Chelito), quien es la persona más orgullosa de mi logro. Ella es quien lo ha dado todo por nosotros y me ha apoyado de todas las formas posibles a culminar mi proceso. A mi esposo, Mauricio, y a mi hijo, Matías, les agradezco por su paciencia, comprensión, amor y apoyo incondicional, a mis hermanos Lean y Nena, y a mi sobrino Samu, por siempre estar allí para mi y para mi familia. Los amo infinitamente.

Mirando hacia atrás en mi proceso, entiendo que no hubiera sido posible sin un grupo de apoyo. Por ello, quiero agradecer al profesor Luis Fernando Grisales, quien me impulsó y motivó a comenzar mis estudios doctorales y me brindó en cada etapa consejos y ayuda que permitieron que todo fluyera de una mejor forma. A los profesores Mariana Durango,Jhon Jairo Rojas, y Jhony Guzmán, quienes dieron un voto de confianza a mi trabajo, espero que la vida nos permita seguir trabajando juntos por mucho tiempo. A los estudiantes David Restrepo, Alejandra Ortiz y Juan Manuel Arango, les agradezco por su apoyo invaluable durante estos años. Ustedes no se imaginan cuánto significó para mi contar con su respaldo. Sé que les esperan cosas maravillosas en sus vidas. También quiero agradecer a personas como Sebastián, Robison, María Elena, Bernardo y Cristian, quienes siempre tuvieron un momento para escucharme, alentarme y hacerme reír de mis pesares y de los suyos. Los llevo en mi corazón.

Por último, quiero agradecer a los integrantes de los laboratorios de Energía Eléctrica y Potencia, y de Electrónica y Energías Renovables del Istituo Tecnológico Metropolitano (ITM), en especial a Juan Pablo Villegas, Santiago Acevedo, Cristian Escudero y Kevin Montes, quienes siempre estuvieron dispuestos a ayudarme con los equipos y espacios que necesitaba para las pruebas experimentales de mi tesis.

Abstract

Modeling and simulation of photovoltaic systems under partial shading conditions

This thesis introduces a methodology for modeling commercial photovoltaic panels at the cell level operating under partial shading conditions. In the first part, a review of the literature is presented, focusing on the proper representation of the current-voltage characteristics in both forward and reverse bias, the mathematical formulation, the circuit model, and the estimation of parameters for photovoltaic cells.
In the second part, the single diode model (SDM), the direct-reverse model (DRM), and Bishop's model are introduced, emphasizing their current-voltage relationship, mathematical formulation, circuit model, and parameter requirements.
In the third part of the thesis, a procedure to obtain I-V curves in panel terminals without the need for any physical intervention is detailed. This procedure is necessary to compare the behavior of the three models analyzed in both quadrants. The procedure requires a panel without a bypass diode and measurement equipment capable of acquiring current, voltage, temperature, and irradiation.
After considering the evaluation of some metrics such as root mean square error (RMSE) and mean absolute percentage error (MAPE), Bishop's model is selected for use in the methodology.
In the fourth part, a methodology to estimate the parameters of Bishop's model is proposed, which formulates the estimation of the parameters as an optimization problem. The methodology uses a genetic algorithm, and it is validated using information from two commercial panels. The curve reconstructions for each technology are evaluated using metrics such as RMSE and MAPE to assess the accuracy of the models.

Keywords: single diode model, Bishop's model, partial shading, photovoltaic cell, circuit modeling, direct mode, reverse mode

Resumen

Modelado y simulación de sistemas fotovoltaicos bajo condiciones de sombreado parcial

Esta tesis presenta una metodología de modelado de paneles fotovoltaicos comerciales a nivel de celda operando bajo condiciones de sombreado parcial. En la primera parte se realiza una revisión de la literatura sobre la representación de celdas fotovoltaicas, en la que se consideran características importantes como la formulación matemática, el modelo circuital, la representación apropiada del comportamiento en modo directo e inverso y la estimación de parámetros.

En la segunda parte, se exponen algunos de los modelos más utilizados en la literatura para el modelado de celdas fotovoltaicas, Modelo de un solo diodo (SDM), Modelo DRM y el modelo de Bishop, prestando especial atención a la relación corriente-voltaje, la formulación matemática, el modelo circuital y los parámetros necesarios para su evaluación. Para modelar los paneles a nivel de celda, la tercera parte se enfoca en detallar un procedimiento para obtener las curvas I-V en terminales de un panel, sin necesidad de ninguna intervención física. Para lo se requiere un panel sin diodo de bypass, información del panel obtenida al sombrear el panel y algunos equipos de medida que permitan adquirir corriente, voltaje, temperatura e irradiación.

En la tercera parte de la tesis se detalla un procedimiento para obtener curvas I-V en terminales del panel sin necesidad de intervención física alguna. Este procedimiento es necesario para comparar el comportamiento de los tres modelos analizados en ambos cuadrantes. El procedimiento requiere un panel sin diodo de derivación y un equipo de medición capaz de adquirir corriente, voltaje, temperatura e irradiación.

Después de considerar la evaluación de algunas métricas como el error cuadrático medio (RMSE) y el error porcentual absoluto medio (MAPE), se selecciona el modelo de Bishop para su uso en la metodología.

En la cuarta parte, se propone una metodología para estimar los parámetros del modelo de Bishop, formulando el problema de estimación de parámetros como un problema de optimizavión. La metodología utiliza un algoritmo genético y se valida con información de dos paneles comerciales. Las reconstrucciones de curvas para cada tecnología se evalúan utilizando métricas como RMSE y MAPE para evaluar la precisión de los modelos.

Palabras clave: modelo de un solo diodo, modelo de Bishop, sombreado parcial, celda fotovoltaica, modelado circuital, modo directo, modo inverso.

Contents

1 Introduction

The need to supply the energy demand in a sustainable way has generated the growth of renewable sources participation in the worldwide energy matrix [1]. From 2012–2021, the installed capacity of renewable energy has grown exponentially. The year 2021 was decisive for the energy transition because renewable energies contributed to 81 % of global energy additions, resulting in 257 GW of additional installed capacity. Photovoltaic systems accounted for more than half of renewable additions, with a record 133 GW by 2021, followed by 93 GW of wind power.

In Colombia, for example, photovoltaic technologies are attractive due to their energy potential [2]. According to the solar radiation atlas, Colombia has an average irradiation of 3.9 $kWh/m^2/day$, which is above the average of Germany, which is one of the countries with the largest installed photovoltaic capacity. Some Colombian regions that are above the national average are La Guajira (6 $kWh/m^2/day$), Atlantic Coast (5 $kWh/m^2/day$), and the Orinoquia and Andean Region (4.5 $kWh/m^2/day$). Also, the approval of Law 1715 [3] in Colombia promoted an increment in the number of renewable energy projects. That law establishes promotional instruments for the use of non-conventional energy sources. Some of the tax benefits included in the law are annual rent reduction; VAT exclusion; duty exemption; and accelerated depreciation of assets, among others. At the end of 2022, the Colombian mining-energy planning unit, UPME by its acronym in Spanish (Unidad de Planeación Minero Energética), had received a total of 4745 benefits applications and certificated 3262 renewable projects. 91.6 % of the approved projects correspond to photovoltaic projects. Antioquia had 456 projects with approved certifications, based on non-conventional energy source, of which 93.64 % corresponded to photovoltaic solar installations [4].

Although photovoltaic systems have advantages such as a life cycle of approximately 20 years and reduced maintenance, their energy production depends on the weather conditions of the place where the system is installed, which can change quickly [5, 6]. The behavior of the PV cell under particular environmental conditions is described by using the current-voltage (I-V) curve because it provides relevant information about the transformed energy, and can be used to calculate the maximum power that can be delivered to a load [7]. The cell behavior for different irradiance and temperature conditions can be modeled using an equivalent electrical circuit, which helps to represent the electrical phenomena associated with the energy transformation process [8, 9, 10, 11]. Therefore, it is necessary to include all the elements that intervene in its operation, and also studying the phenomena involved in its energy production to obtain more accurate predictions.

When analyzing the behavior of PV arrays, aspects such as power generation, shading impact, Maximum Power Point Tracking (MPPT) controller design [12], and degradation are examined. However, power generation is one of the most important aspects because it is associated with performance and reliability. The power output in PV systems is mainly affected by partial shading, a condition that forces the shaded cells to consume power rather than produce it [13]. This condition, known as reverse bias, imposes a negative voltage on its terminals, making the cell operate in the second quadrant Q_2 (negative cell voltage and positive cell current), thus consuming power.

The first step in performing a proper analysis of PV arrays is to represent the operation of the PV cells and modules using circuit models such as the Single Diode Model (SDM) [14, 15, 16, 17], which is widely used due to its tradeoff between complexity and accuracy [18], or the Double Diode Model (DDM), which is more accurate to represent the p–n junction at low irradiance levels [19, 20]. Both SDM and DDM have been used to model commercial PV cells, modules, and panels made of monocrystalline silicon (mc-SI) or polycrystalline silicon (pc-SI).

However, when a PV panel is under partial shading, the shaded PV cells might not generate energy; on the contrary, they might consume the energy produced by the other cells in the panel. It is worth noting that neither SDM nor DDM can accurately represent this phenomenon at the cell level. This condition can be addressed by using an avalanche mechanism to represent the reverse bias at the cell level. This is the case of the Bishop model [21, 22], which introduces a variation to the SDM that affects the shunt resistance current (R_{sh}) by means of an ohmic term and a non-linear multiplication factor. Such a model, proposed in [23], was evaluated in I-V curves of mc-SI cells, taken from a database of the ESTI laboratory (the European Solar Test Installation) [24]. In particular, the parameters proposed in [23] correspond to the average value of the parameters obtained for each cell in the database; unfortunately, that study does not include a detailed procedure to estimate the model parameters. Other authors have used the Bishop model to analyze PV systems [25, 26, 27] because it estimates the cell behavior under partial shading conditions at the cell level, but in general, the parameters suggested by Bishop are adopted when the second quadrant is analyzed [23]. Another model designed to study the behavior of PV cells under partial shading conditions is the Direct Reverse Model (DRM). This model introduces a variation to the DDM using linearized parts from the I-V curve in Q_2. The DRM can reproduce the operation of cells in either direct or reverse biasing modes to account for the influence of variations in temperature and solar irradiance [28].

Although the Bishop model is one of the most cited and adopted models to represent a PV cell operating under partial shading conditions [13, 29, 30, 31], there is not a clear procedure to estimate its parameters; instead, authors typically use parameters already reported in the literature. A similar situation occurs for the DRM [32]. Given the importance of having an accurate model for PV power generation analysis under partial shading conditions, there is a need for procedures to identify the parameters of those models. Moreover, procedures

with a good relationship between complexity and accuracy, and the ability to be applied to different PV models, are also needed.

The previous mathematical models require the accurate identification of a set of parameters to obtain a high–performance in the reproduction of the cell behavior. Several parameter estimation techniques have been reported in the literature for the different PV cell models. Those techniques can be divided into two categories: analytical and optimization techniques [33, 34, 35]. Each one of these techniques requires some initial data, which can be obtained from the manufacturer's datasheet or experimental tests.

Analytical methods use a series of mathematical equations for parameter extraction, based on equations that relate the output current and voltage of the system, and, despite those approaches determining the representative parameters of a PV model, those depend on variables under standard test conditions (STC). If those parameters are not adequately defined, analytical methods are unable to reproduce the variations in PV profiles due to changes in temperature and irradiance. Typically, these techniques depend on the technical data provided by the solar panel manufacturer. However, there are certain disadvantages when using this information, since there may be some variability between the behavior of the panels within the same manufacturing batch. Additionally, over time and use under real operating conditions, it is to be expected that the fill factor of a panel will not remain constant. In other words, the information in the data sheet may not accurately reflect the behavior of the panel as usage time increases. Furthermore, so far, only techniques based on technical data have been developed to estimate the parameters that represent the first quadrant in photovoltaic cells or panels. No study has been carried out to effectively evaluate the parameters of models that represent the behavior of photovoltaic cells in the first and second quadrants using data sheet information. Although these methods are simple but have several complex mathematical operations, which increases the computational time. Also, the resulting models have low performance in the reproduction of different real operating conditions [36, 37, 38].

The optimization techniques are classified into two groups, the deterministic and the stochastic ones. For the deterministic ones, there are solution methods such as Newton-Raphson [39], Gauss-Seidel [40] and other [41] that are related to methods that require a convex, continuous and differentiable expression, given this context, it is necessary to clarify that the convergence of an algorithm can trapped within a local minimum due to the complexity and nonlinearity of the mathematical model. On the other hand, the stochastic methodology is divided into two groups: heuristics and metaheuristics. For parametric estimation, the metaheuristics approach has been more adopted because it includes random selections of candidate solutions and setting parameters. Here, an objective function is evaluated to find the best solution, also a statistical analysis is required to validate the results [42, 33]. These alternatives do not require an accurate mathematical model; instead, they need an objective function and a parameter search range, which can be more effective and less time-consuming. Furthermore, those techniques evolve several individuals for the problem, which reduces the

procedure's sensitivity to the initial guess and provides a strong ability to jump out of a local optimum [35].

In short, optimization techniques can be applied in many PV applications as long as the equation to be optimized can be expressed in terms of an objective function, i.e. a mathematical model that can be used in an iterative process [43, 44, 33]. However, the use of optimization techniques requires trade-offs between accuracy, computation time, and computational resources, which are defined by the method programming and objective function. Optimization techniques have been widely used for estimating the parameters of cells (or modules) mostly using the SDM or the DDM, which do not represent the behavior of the cell in the second quadrant in a proper way. On the other hand, the Bishop model improves the representation of the cell behavior in the second quadrant, but eight parameters of an implicit model must be determined. However, to the best of the authors knowledge, procedures for estimating its parameters are not reported in the literature. Most of the works concerning PV cell or arrays analysis based on Bishop model, adopt the parameters from other studies previously reported.

Recent publications on the parameter estimation problem suggest that metaheuristics methods have become a relevant research area for all PV circuit models. For instance, the Slime Mold Algorithm (SMA) [45], the Grasshopper Optimization Algorithm (GOA) [33], Principal Component Analysis (PCA) [46], Particle Swarm Optimization (PSO) [47], Triple-Phase Teaching–Learning–Based Optimization (TPTLBO) [48], and Perturbed Stochastic Fractal Search (pSFS) [49] have been used to extract the parameters of the SDM. For the DDM, some of the solutions that have been adopted include the Moth Flame Optimization [50], improved Differential Evolutionary Algorithm [51], the Pattern Search (PS) algorithm [19], the Crow Search Algorithm [52], and the Wind-Driven Optimization (WDO) algorithm [53]. However, Genetic Algorithms (GA) are the most widely adopted solution for parameter estimation in PV systems.

For example, the work reported in [54] proposes a new variant of the GA, which integrates a new crossover operation to provide a good balance between the search for the best solutions and the diversification of the search space; such a solution was designed to identify the electrical parameters of different PV cell models (SDM and DDM). Similarly, in [55] the authors extract the solar cell parameters for a Kyocera panel (KC200GT) using GA. In [56], an inverse modeling method for PV panel is proposed, which is based on parameter identification through GA. Such a process generates random groups of 5 parameters which are used in the SDM; then, the parameters that generate a power output most similar to the experimental value are selected. On the other hand, [57] proposes an algorithm for datasheet parameter extraction of photovoltaic modules for the SDM, where the extracted parameters are obtained by approximation using a GA. Authors in [58] present the implementation of a continuous population genetic optimization algorithm (CGA) as a solution method for the parameter estimation of the diode model (SDM) in a PV panel from experimental data. Such a procedure was validated with four different panels: Solarex MSX60, SOLAR SJ65,

KYOCERA KC200GT, and STP245S. In [59] a GA is used to analyze the behavior of the estimated parameters as irradiation and temperature changes. Similarly, in [60] is performed a comparative analysis of the parameter estimation of the SDM, evaluating the results provided by the Newton Raphson algorithm against optimization techniques such as GA and particle swarm optimization (PSO). Besides, hybrid techniques, which use both analytical formulations and numerical algorithms, have been proposed to improve computation time or accuracy. In [61], mathematical formulations to translate I-V curves and a Moth Flame algorithm are used to take into account the PV cell parameters sensitivity to weather conditions of the SDM.

All the works reviewed in the previous paragraph use models such as the SDM and the DDM, which focus exclusively on the analysis of the first quadrant. However, it was not possible to find research works focused on the problem of parameter estimation for models representing both the first and second quadrants as an optimization problem. From the analysis of the results obtained, no analysis of the quality of the solutions was observed that goes beyond the evaluation of the objective function and the computing time. That is, there is no evidence of the repeatability of the responses when executing the technique multiple times, or the variability of the parameters obtained in each execution.

In the literature, research efforts have focused on comparing the performance of models at the cell level [62, 63] but the analysis only extends to the module level, not to arrays. On the other hand, there is the evaluation of the operation in the second quadrant of a photovoltaic cell (non-uniform radiation condition) [64, 23], but this analysis is not generalized to the configurations of known photovoltaic systems. In other cases, a comparison of the behavior of each configuration is made, but the shading study is carried out at the module level and not at the cell level, which reduces the precision of the results [64, 65, 66]. Additionally, there are studies that use the model that best fits the mode of operation in the second quadrant, but the methodology used to estimate the model parameters is not specified [67, 22, 21].

Chapter 2 focuses on the state of the art of modeling photovoltaic cells in both the first and second quadrants, considering information such as topology systems, models, parameter estimation techniques, and simulation tools. Some concepts related to the circuital model representation of solar cells, hot spot conditions, direct mode, and reverse mode operation are presented in Chapter 3. Also, Chapter 3, includes the circuital representation and the relationship of current-voltage for SDM, Bishop model, and DRM. The final section of Chapter 3 presents the parameter estimation problem as an optimization problem. Next, Chapter 4 details the non-invasive procedure for the extraction of the I-V cell curve in photovoltaic panels, including a description of the experimental platform, and showing the I-V cell curves obtained for two different photovoltaic panels. Chapter 5 presents the behavior comparison between three models (SDM, Bishop, DRM) when the estimation of the I-V curve in both Q_1 and Q_2 is needed. For this analysis, the estimation of the parameters of each model was developed using genetic algorithms and Simulink simulations. Each model was validated by comparing two error measures (RMSE and MAPE) obtained from the I-V curve reconstruc-

tion of an experimental PV cell for each model, i.e. in both the first (Q_1) and second (Q_2) quadrants.

The purpose of Chapter 6 is to propose a methodology to estimate the parameters of the Bishop mathematical model to represent a PV cell, this using a Chu-Beasley genetic algorithm. The estimation process is divided into two stages; in the first stage, the curve in the first quadrant is modeled based on the estimation of SDM parameters; then, using the first five calculated parameters, the Bishop parameters are estimated to reproduce the I-V curve in both the first and second quadrants. In the second stage, the behavior in the first and second quadrants is modeled entirely by the Bishop model. Both estimation stages are validated based on the I-V curves of two PV cells (with different technologies) using the root mean square error (RMSE).

Finally, the conclusions and future lines of research derived from this work are given in the Chapter 7.

2 State of the art about the representation of photovoltaic cells in the first and second quadrants

The modeling of photovoltaic systems is a required topic in energy estimation studies, the analysis under partial shading conditions, and the design and development of controllers, among other applications. Modeling can be done through simulation tools or using analytical formulation. Both solutions require a representation of the physical phenomena through a circuital model and a set of equations that describe their behavior; both, in general, are validated using experimental schemes. Commonly, the complexity of the system of equations requires iterative algorithms to achieve its solution. Some of the most commonly used circuit models are the SDM [68, 16, 69], the DDM [62, 63, 70], and the Bishop model [23, 21, 26, 25]. The granularity of the model can be considered at the cell, module, or array level in a generalized way, and these models are applied to evaluate the system's behavior under a given operating condition. This behavior will depend on the panels' manufacturing characteristics and the radiation and temperature conditions [71]. Ideally, those two variables are assumed to be constant for all the cells in the panel or array; however, some conditions, such as lack of maintenance, shading, or heat sources, can provide non-uniform conditions [66, 72].
The parameters of a photovoltaic cell model can be obtained through the information provided in the manufacturer datasheet, or using tests that include electrical measurements and environmental conditions [73]. Conventional procedures to estimate these parameters can be classified into analytical and numerical methods. In the case of analytical methods [74], several points of interest are taken from the Current-Voltage (I-V) curve, such as the open circuit voltage V_{oc}, the short circuit current I_{sc}, the voltage and current at the point of maximum power (V_{mpp} and I_{mpp}), and the slopes of the axial intersection of the curve. This methodology has the advantage of a simpler and faster calculation of the parameters, but the accuracy of this technique depends on the correct selection of these points in the curve. On the other hand, numerical methods are based on fitting an experimental curve using iterative algorithms [73]. These techniques have a higher computational cost since adjusting all points of the curve is necessary. Here, the accuracy will depend on selecting the initial parameters, the cost function, and the fitting algorithm. In the literature, it is possible to find the application of evolutionary algorithms in estimating parameters of electrical models for photovoltaic cells. These algorithms optimally estimate the parameters, minimizing an

objective function, where it is also required to define a search space per parameter to be estimated [18].
The objective function allows to evaluate the performance of the estimation method effectively. The most common objective functions are the root mean squared error (RMSE) [75], the mean absolute error (MAE) [76] and the relative absolute error (RAE) [73]. The objective function must be minimized during the estimation process, using the parameter values defined in the search range. Some of the most common techniques for estimating parameters of the electrical model of a photovoltaic cell are: genetic algorithms (GA) [14], differential evolution algorithm (DE) [77], pattern search (PS) [78], particle swarm optimization (PSO) [11] and Simulated Annealing (SA) [79].
The cell technologies used in most of the research works found in the state of art are monocrystalline and polycrystalline silicon, using the SDM and the DDM as representation models [18, 79, 80].
Another important aspect of the PV system is the integration of bypass diodes in the modules as a partial solution to the mismatching problem; this is because the bypass diode limits, but does not eliminates, the impact on the power production. Such diodes must also be included in the mathematical models of photovoltaic systems; and they can be represented through different voltage-current relationships such as the ideal model, the linear model, and the exponential model (higher complexity) [81, 82].
In this sense, to evaluate a photovoltaic system in a given condition, it is necessary to take into account the considerations identified in the previous paragraphs; and, in general, simulation tools are used to manage the complexity of the problem [23, 83, 28].
The following is a review of the information found in the literature on circuit representation models for photovoltaic systems, which considers the granularity of the study and the most common simulation tools.

2.1. Modeling of the first quadrant behavior

The most commonly used circuit model for solar photovoltaic representation in the literature is the SDM [66, 84, 85]. This model allows considering non-uniform operating conditions at the module, panel, or array level, but it is not possible to evaluate the condition of mismatching due to partial shading at the cell level, since it is not valid in the second quadrant.
SDM and DMM have been used to model commercial cells such as monocrystalline and polycrystalline silicon, but have also been used to represent cells with emerging technologies such as bifacial. For example, in [86, 87] bifacial cells; were modeled using the SDM to evaluate energy production, presenting as the main challenge the estimation of the irradiation received on the back side. The DDM has also been used to model the bifacial cells, in [88] each cell has been represented by two monofacial cells in parallel, which allows to evaluate the effect of the operation of one face on the other. It is also possible to find some analyses

in bifacial cells that are not based on circuit models, such as the one presented in [89], which proposes an estimation of power that depends on front and rear irradiation, on temperature, on the temperature coefficient at the cell level, and the nominal power of the module.

For example, in [90], non-uniform operating conditions in photovoltaic arrays are analyzed using the Lambert-W function, which helps to obtain an explicit relationship between the voltage and the current at the module level, assuming that the entire module has the same irradiation condition. Then, using Kirchhoff's laws, a system of equations is obtained and then described using a Jacobian matrix, which can be solved using toolboxes included in simulation tools. In [91], authors analyzed the influence of partial shading of a string (2×1), considering two modules per panel. Here, each module is protected through a bypass diode, which was simulated, assuming that would receive two different irradiance levels. Then, the authors proposed a centralized controller for the DC-DC converters stage to reduce the number of sensors needed for MPP tracking. Similarly, it is possible to find the SDM in power estimation applications extended to different array configurations proposed in the literature (Series (S), Parallel (P), Series-Parallel (SP), Total-Cross-Tied (TCT), Bridge-Linked(BL), and Honey-Comb(HC)), as in the case of [66, 84, 92], where the susceptibility of each configuration under specific shading conditions is evaluated. The SDM has also been used for the design of photovoltaic array simulators that allow the evaluation of shading conditions, such as those presented in [93, 94, 95, 96, 97]. In [94] a Matlab simulator that provides the I-V and P-V curves was developed. This, for extensive arrays, i.e. an SP photovoltaic array with 10 modules per branch, and 100 branches connected in parallel. This modeling method also considers shading conditions at the module level. On the other hand, authors in [93], developed a simulation in Simulink, using the datasheet information of MSX 60 PV. Three bypass diodes were included in the simulation, one by region (12 cell series each). Each region is exposed to a different irradiation level, and then the P-V curve is reconstructed, and the maximum power point is calculated. In [97] authors also used Simulink to analyze the behavior of different configuration when are affected by different shading patterns. In [98], using the Simulink tool, the behavior of different configurations is analyzed when are affected by typical shading patterns. The authors included a comparison through V_{oc}, I_{sc}, and P_{mpp} values, highlighting the configuration Honey-Comb because presented better performance under the proposed scenarios.

In [95] a procedure to adjust the 3 points of interest of the curve (short circuit, open circuit, and maximum power point) is proposed: the procedure considers changes in irradiation and temperature using linear equations. This procedure requires knowing at least the standard conditions (STC) and two I-V curves (at different temperatures and irradiation). Then, the five model parameters are calculated using the equation that describes the I-V relationship in the SDM, evaluated at the three points of interest described above. In [96], a simulator based on the LTspice IV software is shown, which is used to calculate the I-V curve at the module level. This work was experimentally validated using a string of six monocrystalline modules.

The authors in [99] propose extracting parameters of the STM6-40/36 modules using the tree seed algorithm. The analysis includes comparing results between different optimization techniques and the analysis of the answer quality when the number of iterations of the technique is increased.

In [100], an I-V curve is used, in addition to the information from the panel in the STC, to estimate the temperature and irradiation of the panel at the time of the test, as well as the resistance values of the SDM. The parameter estimation is performed through the Trust region algorithm, and it is necessary to adjust the parameters in relation to temperature and irradiation. Here, to solve the model, the Lambert-W function is used.

DDM is commonly found in the literature for modeling photovoltaic systems [28]. In [101] a comparative analysis is made between the models of one diode, two diodes, and the variations resulting from neglecting the series and shunt resistances. The estimation of the parameters in each model was carried out with the help of the Levenberg Marquard algorithm, using a set of equations for the problem of the initial parameters that allow a good relationship between computational cost and accuracy. Another comparative study is presented in [102], using SDM and DDM with some variations, such the inclusion of the series and shunt resistances. Here, all models were simulated and then compared with an experimental curve evaluating the RMSE metric. The DDM, like the SDM, does not allow the impact of partial shading to be evaluated at the cell level.

Table **2-1** compares the reviewed works that use the SDM (first-quadrant analysis). In all the works reviewed in the table, the modeling procedures were developed at the module level. None of the works presented analysis at the cell level. Also, Table **2-1** includes information on the analyzed reference: panel, string, or a typical configuration (Topology system), the modeling of the system: circuital model, which generally uses a circuit simulation tool (Simulation Tool); or through a set of equations that relate voltages and currents of the system (Mathematical formulation). The parameters estimation technique used can be based on the datasheet parameters at STC conditions such as (I_{sc}, V_{oc}, and P_{mpp}), using I_{sc}, V_{oc}, and P_{mpp} obtained experimentally (Experimental) or through GA. The latter requires a technique that allows the evaluation of the implicit current-voltage relationship (I-V evaluation); for references that do not include this information, it will be found (N.I. - not included) or (N.A. - not apply) in case a circuital simulation tool was used, N-R for Newton-Raphson, L-W for Lambert-W function, and L-M for Levenberg–Marquardt. Information related to the simulation tool was also sought, but if the reference does not indicate information about the tool used for the analysis, then (N.I. - not included) is reported. Finally, it is considered whether experimental validation of the results obtained was carried out. It is also analyzed at what level the voltage and current data were taken (cell, panel, or array terminals). If there are measurements at the cell level, how the data was acquired will be reviewed since, to access the terminals of each cell in a module, it is necessary to affect the rear face of the panel.

It should be noted that only in some works, such as [84, 90, 92, 95, 101], the validation of

Ref.	Topology system	Modeling	Parameter estimation	I-V evaluation	Simulation tool	Experimental validation	Acquisition terminals
[84]	SP-TCT BL-HC	Mathematical formulation	Fit using (Irr, T) Datasheet	N.I.	N.I.	Yes	String and panel
[90]	String	Math. form.	N.A.	L-W	Matlab	Yes	String
[91]	Array	Mathematical formulation	Fit using (Irr, T) Datasheet	N.I.	Matlab	No	N.A.
[92]	SP-TCT BL	Mathematical formulation	Fit using de (Irr, T) Datasheet	L-W	Matlab/ Simulink	Yes	String
[95]	Panel (4 modules)	Circuital model	Experimental Fit using (Irr, T)	N.A.	PSCAD	Yes	Panel
[101]	Panel	Mathematical formulation	Fit using (Irr, T) Datasheet, GA	N–R L–M	Matlab/ Simulink	Yes	Panel
[93]	String	Circuital model	Fit using (Irr, T) Datsheet	N.I.	Matlab	No	N.A.
[97]	S-SP-HC	Circuital model	Fit using (Irr, T) Datasheet	N.I.	Matlab/ Simulink	No	N.A.
[98]	S-SP BL-HC	Circuital model	Fit using (Irr, T) Datasheet	N.I.	Matlab/ Simulink	No	N.A.

Table 2-1: Summary of works based on the single diode model

the modeling stage was performed using experimental I-V curves. In [95, 101], the curves are taken at panel terminals, considering that each analyzed panel has more than one bypass diode to do the shading analysis per module. On the other hand, in [84, 90, 92], current and voltage measurements are taken at the terminals of the analyzed arrays to evaluate power losses due to partial shading. In none of the cases were curves analyzed at the cell level or study of power losses at the cell level due to partial shading.

2.2. Modeling of the second quadrant at cell level

Since the models analyzed in the previous section only adequately analyze the cell behavior in the first quadrant, it is necessary to consider a model that evaluates the mismatching conditions due to partial shading at the cell level. It can reproduce the inverse mode of operation, which is generally associated with avalanche mechanisms that affect the primary cell currents.

Bishop's model generally represents the behavior of PV cells in the second quadrant. The model was proposed in [23], and it analyzes the ESTI database made up of the I-V curves of monocrystalline silicon cells. The parameters proposed in the article refer to the mean value of the parameters obtained for each cell in the database. Unfortunately, there are no details on the procedure used to estimate the parameters of each curve. Many authors have also considered Bishop's model for the analysis of photovoltaic systems [26, 25, 103], since it allows to estimate the behavior under conditions of partial shading at the cell level. However, no emphasis is placed on the estimation of the model parameters. In general, for

the case of the parameters that affect the reverse characteristic, those proposed by Bishop in [23] are adopted. For example, in [25], a simulation method for diagnosing photovoltaic systems is proposed. The photovoltaic current of the shaded region is calculated as a ratio between the photovoltaic current under standard operating conditions, the irradiance value, and the transmittance of the applied shade. Although there is no details concerning the estimation of the parameters related to the first quadrant, it can be observed that those reported in [26] are assumed for the parameters associated with the second quadrant. In [103] a general method for modeling arrays and modules is proposed, seeking to generate the I-V relationship regardless of whether the arrays or modules have different electrical and geometric configurations. Through Kirchhoff's laws, the general system of equations is obtained, and the damped Newton method is used for its solution. The construction of the array is done in layers, the first from cell to module, and the second from module to array. The document does not specify how the estimation of the model parameters is carried out. On the other hand, this approach does not have a theoretical foundation based on circuit analysis, so it requires a detailed study for its validation, in which different array configurations can be evaluated, and results contrasted with experimental data.

Bishop's model has also been used to develop tools to evaluate the behavior of cells, modules, arrays, and large-scale photovoltaic systems, as is the case of PVSIM [26]. The computer program allows to consider elements such as bypass and blocking diodes. Regarding the model parameters, the tool included data for different operating points (irradiation and temperature), allowing it to interpolate based on the temperature defined by the user. In addition, the user can include the desired set of parameters in the simulation; hence, information would be required at the cell level to estimate the parameters.

The authors of [104] propose to improve the power generation, under shading conditions using the KenDoKu reconfiguration. For the simulation stage, the Bishop model is used in LTSpice software. The results are compared with TCT, BC, HC, and SP configurations using the power losses, fill factor and global maximum power.

Some works have used the Simulink tool to simulate the Bishop model [21, 105, 106]. As with [21], the authors simulate and analyze PV arrays under uniform and partial shading conditions for all different PV array configurations (S, P, TCT, BL, and HC). A PV module block diagram is created in Simulink. Then, different shading patterns are applied to estimate the power losses using the different array configurations. While the authors in [105] analyze the incidence of parameters such as the series resistance R_s, the shunt resistance R_{sh}, and the saturation current I_0 in the reproduction of the I-V curve. On the other hand, in [106], the hot spot phenomenon and the power dissipated in a shaded cell of a panel are simulated. In the case of [107], the PSpice environment is used to model solar modules working partially shaded when they work with different configuration connections of the bypass diode.

In addition, Bishop's model is used to analyze faults for the photovoltaic generator, as presented in [108], starting from a set of parameters that represent a panel under normal operating conditions. Then, each parameter is varied separately to identify how it affects

the reproduction of the I-V and P-V curves. In the case of [109], a Neuro-fuzzy classifier for fault detection in photovoltaic modules is presented. Here, the classification of faults is bypass diode fault, blocking diode fault, and increased series resistance. In [110], a fuzzy logic approach is used in the fault classification, based on the level of shading (acceptable, or serious).

Some of the studies reviewed use the Newton-Raphson algorithm to evaluate the current-voltage relationship, as is the case of [22], where a method for modeling and simulating the electrical behavior of PV installations under any shading situation is presented. The model discretizes currents and voltages in PV cells, which are connected in series and parallel associations. In the study proposed in [111], the analysis of the effect of the bypass diode in a PV panel under shading conditions is presented. While the work presented in [112], cell-by-cell models a large-scale PV system using the Jacobian matrix. In [113], the effect of the bypass diode in reducing power losses due to partial shading is also analyzed, estimating the contributions of sets of shaded and unshaded cells. On the other hand, in [114], the Lambert-W function is used to model the voltage-current relationship, to estimate the maximum power point in shading conditions.

Table **2-2** presents the consolidation of articles that use the Bishop model for modeling or PV analysis purposes. In addition to the reference, the level of granularity of the modeling is included, which can be cell or module level. Modeling can be done circuital using a simulator or mathematical formulation (Circuital or Mathematical, respectively). Parameter estimation can be developed using the parameters in the datasheet, although in some cases, the parameters presented in [23] (Bishop) are used. Implicit current and voltage (I-V) evaluation can be performed using the Newton-Raphson (N-R), Damped Newton (DN), Lambert-W (L-W) algorithm, or the Jacobian matrix (JM). Regarding the model simulation tools, the following were found: Matlab, Simulink, PVNet, and Pspice. In only a few cases is experimental validation performed through current and voltage data. However, this information is acquired at panel terminals. In some of these works, although modeling is carried out with granularity at the cell level, electrical information is not acquired at the same level. That is, no information is acquired in cell terminals. It is noted that most of the studies have granularity at the cell level in the first and second quadrants. However, those works generally use the same parameters for all cells. No studies were found in which a general modeling procedure is proposed. Many studies assess performance at the panel or array level. On the other hand, there is a need to estimate the model parameters since, in the reviewed works, data from the literature is almost always adopted. The authors present their parameters in other cases without emphasizing the model estimation process.

In the case of shading analysis in photovoltaic systems using the Bishop model, some studies present the validation of the modeling through comparison with experimental I-V curves, as is the case of the works presented in [25, 31, 111, 103, 109]. In all cases, the experimental voltages and currents data were obtained at the terminals of the panels. In these works, as in those presented in Table **2-1**, there was no analysis of the cell behavior regarding partial

Ref.	Gran.	Modeling	Parameter estimation	I-V evaluation	Simulation tool	Experimental validation	Acquisition terminals
[21]	Cell	Circuital	Bishop	N.A.	Simulink	No	N.A.
[22]	Cell	Mathematical	N.I.	N-R	N.I.	No	N.A.
[23]	Cell	Mathematical	Database mc-SI cells	Sweep on V_d	PVNet	No	N.A.
[25]	Cell	Mathematical	N.A.	N-R	N.I.	Yes	Panel
[31]	Module	Circuital	N.I.	N.I	N.I.	Yes	Panel
[107]	Cell	Circuital	Bishop	N.A.	Pspice	No	N.A.
[111]	Cell	Mathematical	N.A.	N-R	N.I.	Yes	Panel
[103]	Cell	Mathematical	N.I.	DN	Matlab	Yes	Panel
[115]	Cell	Mathematical	N.I.	N.I.	N.I.	No	N.A.
[105]	Cell	Circuital	N.I.	N.A.	Simulink	No	N.A.
[114]	Cell	Mathematical	N.I.	L-W N-R	N.I.	No	N.A.
[112]	Cell	Mathematical	N.I.	JM N-R	Matlab	No	N.A.
[109]	Module	Circuital	Fit using (Irr, T) Datasheet	N.A.	Matlab/ Simulink	Yes	Panel
[110]	Cell	Mathematical	N.I.	N.I.	Matlab	No	N.A.
[113]	Cell	Mathematical	N.I.	N-R	N.I.	No	N.A.
[106]	Module	Mathematical	N.I.	N.A.	Simulink	No	N.A.

Table 2-2: Summary of works based on the Bishop model

shading.

2.3. Reverse mode characteristic

The characterization of commercial photovoltaic cells in both direct and reverse operation modes has been the goal of different studies [116, 117, 118], since manufacturers generally do not provide information about the behavior of cells in reverse polarization. For example, in [116], the electrical characterization was carried out on a set of photovoltaic cells through dark curves (i.e., without incident irradiation). Seven groups of cells were selected, of which 4 were monocrystalline (mc-SI) and the rest polycrystalline (pc-SI). From the experiments developed, it was demonstrated that the behavior under reverse polarization conditions of cells of the same reference is subject to considerable variations. This affects both the slope of the reverse characteristics at low bias voltages and the breakdown voltage value.
The breakdown voltages (V_{br}) for pc-SI cells are within the range [12V, 20V], while for mc-SI cells, the breakdown voltages can extend up to 30V. The slope of the curves is slightly higher in the case of pc-SI cells, indicating a larger current component due to leakage currents. On the other hand, in the case of mono-Si cells, the breakdown voltage can have a wide variation range.

In [117], 10 cells from 12 different manufacturers were selected. In this case, dark curves were also used, but analysis through thermal images was included. To obtain the I-V curves, each cell was subjected to a reverse voltage sweep for approximately 1 minute. Data acquisition ends when the test current exceeds the cell short circuit current (I_{sc}). The curves obtained show a great dispersion, even when comparing cells within the same batches. The variation of avalanche rupture and thermal rupture is highlighted.

Finally, Alonso et al. [118] present the characterization of 33 cells that form a photovoltaic panel. To achieve this, the panel had to be prepared to access the terminals of all the cells. Then, each cell was characterized by obtaining the dark and illuminated I-V curves by means of a four-quadrant programmable source. In this work, it is also possible to find a high dispersion in the inverse characteristic; For example, it is highlighted how some cells have high slopes in the reverse zone that achieve high currents at small reverse voltages.

After analyzing the information presented by the authors in [116, 117, 118], an experiment was carried out to characterize 9 photovoltaic cells from the same batch. The cells were connected in series, and the voltage sweep was achieved using a programmable electronic source. Then, the cell of interest was shaded 50 % of its area. The I-V curve cells are presented in Figure **2-1**.

The behavior in the first quadrant is within the range $[0V, V_{oc}]$, while in the second quadrant, it is limited by the breakdown voltage (V_{br}). For low reverse bias voltages, near to I_{sc}, the current is approximately a linear function of the voltage (ohmic behavior - ohmic region). The slope measures the leakage currents that appear as an additional component to the saturation current. Leakage currents originate from cellular defects and impurity centers in the semiconductor (represented by a shunt resistor).

At low bias voltages, the current is distributed over the entire cell area, and heating occurs more or less uniformly. As the bias voltage increases negatively, the cell suffers high currents. Since the cells do not have a homogeneous structure, can suffer irreversible damage by thermal breakdown. Under this condition, the current is locally concentrated, heating the focal spot occurs, and damage to the cell encapsulation is expected [117].

Therefore, if a detailed analysis of a PV system is needed, it requires characterizing the operation at the cell level. This information can be obtained from the I-V curve. However, the cells are encapsulated within the modules, so it is not possible to take measurements of the voltage and current directly from the cells in a non-invasive way.

However, only one work related to obtaining I-V cell curves in panels was found [119]. The work presents the inverse characteristic of each cell in a commercial panel. Still, this procedure requires the welding of cables on the terminals of each cell for the voltage injection (see Figure **2-2**), which is necessary for the construction of the I-V curves. However, as shown in Figure **2-2**, the physical integrity of the panel was compromised, so it may not be able to be used outdoors. Therefore, a contribution to the state of the art can focus on proposing strategies that allow calculating the I-V cell curves in the first and second quadrants for commercial panels.

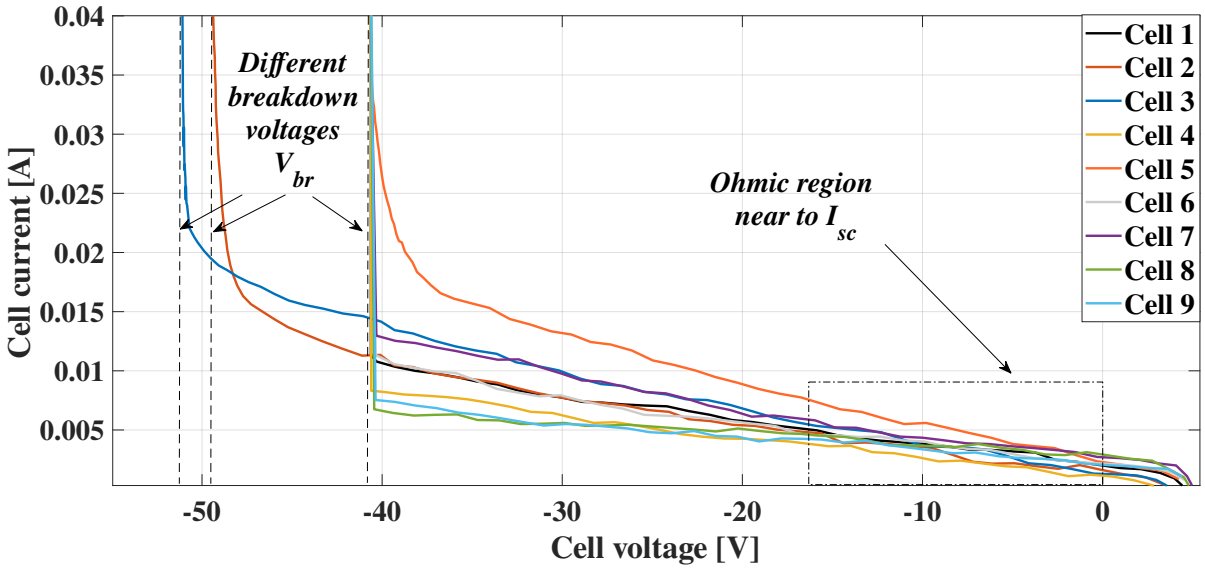

Figure 2-1: I-V curves in direct and reverse mode for cells of the same batch.

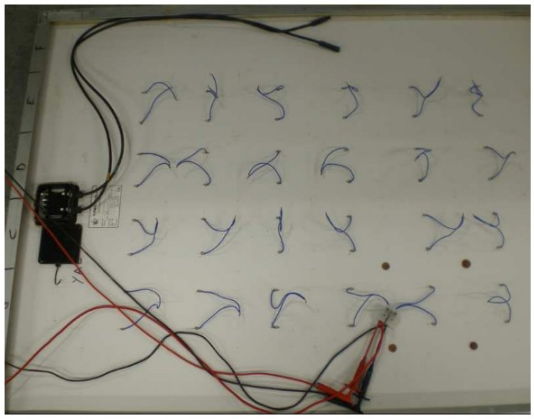

Pa

Figure 2-2: Invasive method to obtain cell-level curves in commercial panels proposed by [119].

On the other hand, in [120], modules with a standard structure (glass-EVA-cells-EVA-substrate) were created from groups of crystalline PV cells. To access the terminals of each cell, cables were soldered to the interconnections of the cells from the collector tape to allow the measurement of the reverse voltage. This connection allows to select the number of cells connected in series that form the module.

Therefore, a detailed analysis of a photovoltaic system requires characterizing the operation of each panel at the cell level. This analysis can be achieved through the I-V curves of the cells. However, as presented in the state of the art, it is not possible to directly measure

the voltage and current of a cell in commercial panels without compromising the panels' physical integrity, since accessing the terminals of each cell requires to affect the encapsulating material of the panel. This intervention on the panel would prevent it from being used outdoors. Hence, a contribution to the state of the art can focus on proposing strategies that allow calculating the I-V cell curves in the first and second quadrants for commercial panels without affecting the encapsulation.

2.4. Parameter estimation techniques

A photovoltaic cell, array, or system can be represented through I-V and P-V curves. The nonlinearities of both curves can be reproduced using mathematical models such as those described in Sections 2.1 and 2.2. Nevertheless, each model requires a set of parameters to build the curves properly. There are different methods to estimate or extract the parameters of some of the most common models. These methods can be classified as analytical, deterministic, or metaheuristic.

The analytical methods use information from some of the points of interest, such as I_{sc}, V_{oc}, and P_{mpp}. The relationship between voltage and current is evaluated at each point, obtaining a number of equations equal to the number of parameters to be extracted. Analytical methods can easily obtain the unknown parameters but rely on the values available in the manufacturer's datasheet, which may lead to a lack of accuracy [121].

Deterministic methods, such as Lambert W-function and Newton-Raphson, have a high local search capacity but are highly dependent on the initial solution conditions, so can fall into local optima [122].

Analytical and deterministic methods use forward modeling because they use manufacturer information to reproduce the I-V curves. However, these methods don't work correctly for complex situations, such as if manufacturer information is unavailable or if the original manufacturer parameters are inaccurate due to prolonged usage of the devices.

Finally, the metaheuristic method uses a fitting procedure to predict the I-V curve [121]. For this reason, some authors define these methods as inverse modeling [56]. The metaheuristic methods search for optimal solutions regardless of the initial solution and the problem's nature. Basically, they can overcome the limitations of the traditional modeling methods [122].

Metaheuristic methods turn the estimation problem into an optimization problem, where the objective is to minimize a function, generally an error between experimental I-V curve data and estimated data. These methods can be classified as bio-inspired, evolution-based, nature-based, or human-based [121].

Within the evolutionary-based are: differential evolution (DE) and genetic algorithm (GA) [59, 55]. Some of the nature-inspired based are pattern search (PS), wind-driven optimization (WDO), and flower pollination algorithm (FPA). Regard to bio-inspired based are found: particle swarm optimization (PSO) [123, 124], artificial bee colony (ABC) [125], and cuc-

koo search optimization (CSO) [122]. Finally, in the human-based are: simulated annealing (SA)[122], and Jaya [126].

Table **2-3** presents a consolidated list of publications in which parameter estimation for photovoltaic models was developed through metaheuristic optimization techniques. Some of the most relevant information has been included, such as the reference (Ref.), the optimization technique used to solve the parameter estimation problem (Optimization Technique), the panel technology used for the validation of the method (Technology), the objective function to be minimized (O.F.), the photovoltaic model (Model), and the simulation tool used to test the performance of the optimization technique (Simulation Tool). Finally, consider when a repeatability analysis of the response of the optimization technique was performed (Rep.), i.e., the algorithm was evaluated several times independently, to analyze the behavior of the objective function in terms of its mean value and standard deviation, and also consider whether the parameter values of each model were included in the repeatability analysis (Param. Analysis).

One of the most widely used optimization techniques for parameter extraction in photovoltaic models is the genetic algorithm (GA) [55, 56, 57, 58, 59]. In [55], a binary codification with 16 bits per individual, the roulette wheel parent selection, and a single parent crossover are used for the estimation of the SDM parameters. The validation was developed using a RTC France solar cell at STC (26 I-V data points) and a mc-SI Kyocera solar panel KC200GT (26 I-V data points). The estimated parameters were compared with the results of other works by means of the relative error of each parameter. Nonetheless, the information on the O.F. and search space of the parameters is not included, nor is there any metric error between the experimental and the estimated data. Otherwise, in [56], a total of 101 data (voltage, current, temperature, and irradiation) were acquired at different load conditions without needing the complete I-V curve. Two estimation schemes were carried out. First, the data set was divided into training and validation. Second, all acquired data were used for the training and validation stages. The analysis results were performed with the voltage's root mean square error (RMSE), and five hours of continuous data were used in the validation. Unfortunately, information regarding the optimization technique and panel reference is not included.

In the case of [57], GA is executed for generating I-V curves using the datasheet information (number of cells connected in series, I_{sc}, V_{oc}, and P_{mpp}). Regarding the GA parameters, selection parents using roulette, with a single point crossover, and the mutation stages, with a random replacement in the case of mutation. Here, three different O.F. were used: (1)the I-V relationship evaluated in maximum power point, (2) the I-V relationship derivated at maximum power point, and the sum of the squares of (1) and (2). For the validation stage, the information of the mc Samsung panel LPC235SM-08 at STC was used. The authors developed a Python GUI for parameter PV estimation using GA and shared it on GitHub. This document does not describe the search ranges established in the algorithm. In [58], the efficiency of the GA techniques, the continuous population genetic algorithm (CGA), and

Ref.	Optimization technique	Technology	O.F.	Model	Simulation tool	Rep.	Param. analysis
[54]	GACCC	Not indicated	1/RMSE	SDM, DDM	Not indicated	No	No
[55]	GA	KC200GT	Not indicated	SDM	Matlab	No	No
[56]	GA	Not indicated	RMSE	SDM	Not indicated	No	No
[57]	GA	LPC235SM-08	MO	SDM	Python	No	No
[58]	CGA, GA, PSO	MSX60, SOLAR SJ65, KC200GT, STP245S	RMSE	SDM	Matlab	1000	No
[59]	GA	HIT 215, KC200GT, ST 40	AE	SDM	Simulink	No	No
[60]	PSO,GA	PX-170, PT-SP250P-6-60	MASE	DDM	Matlab	No	No
[122]	AEO	PWP 201, CKC200GT	RMSE	SDM, DDM	Not indicated	50	No
[123]	FPSO	RTC, STM6-40/36	RMSE	SDM, DDM	Matlab	No	No
[124]	PSO, SA	STM6 40/36,STP6 120–36	MO	SDM	Matlab	No	No
[125]	BABCO	PWP 201, CSTM6-140/36, CLS220P	RMSE	SDM, DDM	LabVIEW	30	No
[127]	WHHO	RTC, PWP 201, SM55, KC200GT, SW255	RMSE	SDM, DDM	Matlab	Yes	No
[128]	DOA	PWP 201, CSTM6-140/36, CLS220P	RMSE	SDM	Matlab	30	No
[75]	PSO, GA	PWP 201	RMSE	SDM	Matlab/ Simulink	No	No
[129]	ECJAYA	RTC, STP6-120/36 STM6-40/36	RMSE	SDM, DDM	Matlab	Yes	No
[130]	IMFOL	PWP 201, STM6-40/36	RMSE	SDM, DDM	Not indicated	No	No
[131]	CIWPSO	RTC	RMSE	SDM, DDM	Not indicated	100	No
[132]	RSO	TDS265D60	SSE, AE, MAE, MSE, RMSE	mSDM	Not indicated	Yes	No
[133]	HS-WOA	Shell SQ85, KC200GT	MO	SDM, DDM	Matlab	Yes	No
[134]	RCGA	PWP201	MO	TDM	Matlab	Yes	No
[135]	EADE	RTC, PWP201 STM6-40/36, STP6-120/36	RMSE	SDM, DDM	Matlab	30	No
[136]	GAMNU	RTC, ESP-160 PPW, TP6-120/36, PWP201	RMSE	SDM, DDM	Matlab	No	No
[137]	AGA	Not indicated	MO	SDM	Simulink	No	No

Table 2-3: Optimization-based parameter estimation summary

particle swarm optimization (PSO) is compared when they are used to estimate the parameters of the SDM model, taking the RMSE as the objective function. CGA generates a set of offsprings of the same size from the initial population in each generation through selection, recombination, and mutation stages. Four commercial panels were selected to compare the results of the techniques (MSX60, SJ65, KC200GT, and STP245S), evaluating the objective function's minimum, maximum, average value, and standard deviation. They are achieved after repeating the estimation using each technique 1000 times (repetitions). Although the RMSE results and computation times are analyzed, the estimated parameter variation was not considered. The paper neither includes parametrization information techniques nor I-V graphical curve reproduction.

Ismail et al. [59] compare the solutions obtained with MATLAB optimization Toolbox genetic algorithm and the developed MATLAB code. The parameterization of the GA MATLAB

optimization Toolbox includes: population size = 20, selection function: stochastic uniform reproduction, reproduction, elite count: 2, crossover fraction: 0.8, and generations: 100. For the GA code, the parameters are: population size = 30, crossover and mutation rate: 0.9, and generations: 100. Then, SDM and DDM parameters were estimated using the information of Sanyo – HIT 215, Kyocera – KC200GT, and Thin-film shell solar – ST 40 panels. This validation focused on the comparison of V_{oc}, I_{sc}, and I_{mpp} datasheet and estimated values employing the absolute error (AE). There is no shared space range information or repeatability analysis in this case.

Moreover, in [60], authors compare the parameter DDM values from equations that depend on datasheet information (analytical method), GA, and PSO techniques. The selected O.F. is the minimum absolute square error (MASE), and the estimation process was applied to two modules, PX-170 and PT-SP250P-6-60. After evaluating the estimation for different irradiation values, it was possible to establish that the PSO technique presented the lowest estimation errors. A repeatability analysis was not performed in this study.

In [75], through the RMSE, the parameters of an RTE cell and a PWP-201 module were estimated. Two estimation stages were compared: (a) using a set of 26 current-voltage data, (b) using only the datasheet data (V_{oc}, I_{sc},P_{mpp}). For this purpose, a GA and a PSO were evaluated, with the former obtaining the best RMSE value in the estimation results when only three points were used. In this study, no repeatability analysis was performed.

In other studies, some modifications to traditional genetic algorithms have been proposed to be applied to the extraction of parameters in photovoltaic systems [54, 134, 136, 137]. For example, in [54], a crossover by convex combination is applied to produce individuals to diversify the search, explore non-visited areas in the search space, and find new solutions. This study proposes the inverse of the RMSE (1/RMSE) as an objective function for a cell and a panel. The proposed modification presents the best results in terms of RMSE, but the computational time and repetition analysis were not considered. In [134] uses the real coded genetic algorithm (RCGA) with a tournament selection, a suggested directional mutation, and a directional crossover based on directional probabilities. The estimated parameters of the PWP201 module using the three-diode model (TDM) were compared when the sunflower optimization (SFO) algorithm, hybrid grey wolf optimization -cuckoo search algorithm (GWCS), Artificial Ecosystem-based Optimization algorithm (AEO), and Gradient-based optimizer (GBO), and RCGA were used. Through a repeatability analysis, it was possible to observe that the proposed technique presents the best results from the average value and standard deviation of the RMSE, but the variation of model parameters or computation times was not analyzed. Another modification to GA is presented in [136], where a genetic algorithm based on non-uniform mutation (GAMNU) with a Blend crossover operator was proposed. Here, an RTC cell and the SP-160 PPW PV, STP6-120/36, and PWP 201 modules were analyzed, and the result of the proposed technique was compared with several optimization techniques using metric error such as a mean absolute error in terms of current and power. Still, in this case, computational time or repeatability analysis was not conducted.

The Adaptive Genetic Algorithm (AGA) based multiobjective (MO) optimization is proposed in [137], where least mean square error (LSE) plus Pearson residual error (PRE) are introduced as multiobjective function. The STC manufacturer data were used with predefined initial electrical parameter values (synthetic data). Then, the panel's behavior in different temperature and irradiation operation points was evaluated using Simulink. The validation consists of comparing the synthetic data with the estimated data,but the paper does not include the parameterization data of the optimization technique.

In other studies, GA, with different techniques, is used as a baseline to contrast the results of some proposed approaches in evaluating objective function and computing time [122, 127, 129]. These works have in common RMSE as O.F., parameter estimation of SDM and DDM, and repeatability analysis focused on assessing average values and standard deviation of the RMSE. They are validated using experimental data from solar cells and modules. In [122], an artificial ecosystem-based optimization technique (AEO) was compared with some techniques such as GA and PSO, among others, and also with more than ten different techniques results from the literature. The advantage here is that AEO does not need more control parameters and presents the best results in terms of RMSE value. Authors in [127] use a Whippy version of Harris Hawks Optimization Algorithm (WHHO) that allows high convergence speed, global exploration, and high robustness. The study analyzes the parameters' behavior of four solar modules for different irradiance values. Premkumar et al., in [129], proposed an Enhanced chaotic JAYA algorithm (ECJAYA) for parameter estimation of photovoltaic cell/modules. The proposed algorithm introduces a self-adaptive weight and more than twenty multimodal functions to regulate the trend to reach the optimal solution and avoid the worst solution of the search space. The results are compared with some techniques, such as time-varying PSO (TPSO), improved Teaching–Learning optimization (ITLO), and GA. From the point of RMSE view, the proposed algorithm presents the best results in maximum, minimum, and average values.

Another widely used technique in parameter estimation is PSO [123, 124, 131]. In [124], the estimation of SDM is assessed using a multiobjective function, which is a combination of a set of equations that relates the current and voltage in some point of interest (I_{sc}, V_{oc}, and P_{mpp}). The validation stage is evaluated using two solar modules and the datasheet information without performing a repeatability analysis. In [123, 131] a modified PSO is implemented. A flexible PSO (FPSO) and a Chaotic Inertia Weight Particle Swarm Optimization (CIWPSO) are proposed, respectively. Both techniques were implemented using SDM and DDM through RMSE O.F. and validated by means of experimental data. In the case of [123], a certain number of worst particles are deleted at the beginning of each phase algorithm, and some new particles are replaced in the new search space. The results are compared with PSO and Bird Mating Optimize (BMO), using some error metrics such as MAE and RMSE. On the other hand, in [131], a chaotic map through a coefficient is created.

Finally, Other techniques have also been applied to the estimation of parameters in photovoltaic models, as is the case of Dingo Optimization Algorithm (DOA) [128], in which

Table 2-4: Search space for SDM parameter estimation in a PV cell

Ref.	Boundaries	n	R_s [Ω]	R_{sh} [Ω]	I_0 [A]	I_{ph} [A]
[122],[125],[75],[126],[123],[129],[130],[131], [135],[136],[54],[138],[139],[140]	**Min**	1	0	0	0	0
	Max	2	0,5	100	1×10^{-6}	1

the calculation of the voltage-current relationship is simplified, using experimental voltage and current data, so iterative solution techniques such as Newton-Raphson are not required. The simplification reduces the algorithm execution time by 28 %. Authors in [130], proposed an improved moth flame algorithm with local escape operators (IMFOL), improving the exploitation performance and population variety of MFOs.

Also, Rat Swarm Optimizer (RSO) [132] was used to estimate the parameters of a modified SDM (mSDM), that includes a supplementary resistance n series with the diode, which reflects losses in the quasi-neutral area of the semiconductor material. The results of the technique were compared with HHO and PSO, among others, using a Friedman ranking test based on the sum of square error (SSE), absolute error (AE), mean absolute error (MAE), mean squared error (MSE) and RMSE metrics.

An enhanced adaptive differential evolution algorithm for parameter extraction of photovoltaic models was presented in [135], where an adapted crossover rate value is assigned for each individual according to their fitness values. Also, a dynamic population reduction strategy is used to improve the convergence speed and balance the exploration and exploitation. In [133], two combinatorial social group whale optimization algorithms were implemented (HS-WOA and HS-WOA+) using a MO function that includes the sum of squares of the errors in three points of interest (V_{oc}, I_{sc}, and P_{mpp}), when are evaluated in the current-voltage relationship.

Hybrid techniques have also been proposed to solve the problem of parameter estimation, as is the case of [125] where a new Bat Artificial Bee Colony optimizer (BABCO) is proposed. This study uses Lambert-W function to evaluate the current-voltage relationship for SDM and DDM.

Regarding the search ranges used for the cell-level parameter estimation stage, validated through experimental data, information associated with a silicon solar cell (RTC France) at $1000W/m^2$ and 33°C was found. Table **2-4** consolidates the search range information found for the single diode model.

After analyzing the information found in the literature, it was possible to establish the following:

- Many estimation approaches reviewed are based on the datasheet panel information. However, it is possible that such information is unavailable or needs to be adjusted to the actual behavior of the panel when it has had many years of use.
- All estimation approaches found are applied to SDM, DDM, or TDM models. However,

these models adequately represent the direct mode of operation rather than the reverse mode.

- Genetic algorithms are an optimization technique widely used to estimate photovoltaic cell and panel model parameters.
- The solution for the photovoltaic model's estimation problem based on optimization techniques, that represent both the first and second quadrant's behavior, was not found in the literature review.

Based on the issues found in the literature review, this thesis focused on developing the following contributions:

1. A Python application for analysis of photovoltaic cells operating in both the first and second quadrant.
2. A Graphical user interface (GUI) was developed in QT and Python for programming the BK 8500 electronic load.
3. Development of a non-invasive procedure to extract the experimental characteristic curves at the cell level in a photovoltaic panel with partial shading.
4. Generation of a database of experimental current-voltage (I-V) curves based on the proposed procedure for two solar panel technologies.
5. Evaluation of the performance of the most common mathematical models, reported in the literature, for the representation of photovoltaic cells in both the first and second quadrants.
6. Formulation of a methodology for estimating parameters in photovoltaic panels at the cell level.

3 Circuital model representation for photovoltaic system

Solar cells are the basic unit of a photovoltaic system. A cell transforms the energy radiated by the Sun into electrical power. In the same way, the basis for any representation model of an array is the I-V and P-V relationship at cell level [141], since they allow to obtain the points of interest necessary to analyze its behavior. Typical I-V and P-V curves for a cell under normal operating conditions are shown in Figure **3-1**.

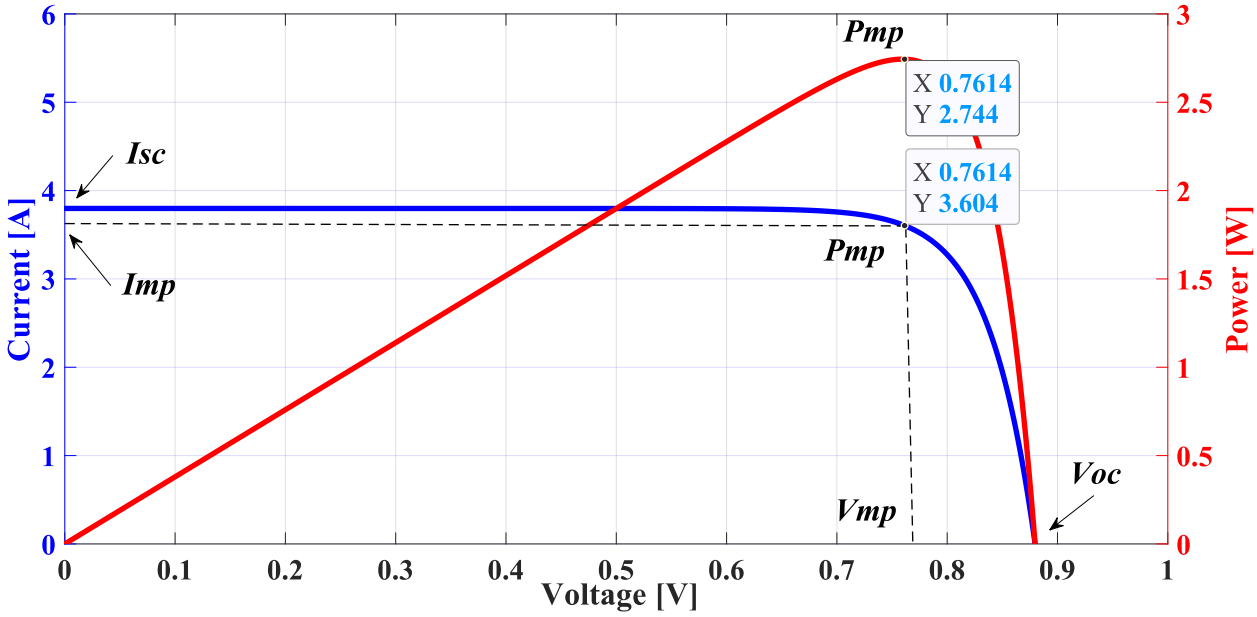

Figure 3-1: Typical curves at the cell level: Current and Power versus Voltage.

The I-V and P-V curves shown in Figure **3-1** can be obtained experimentally by performing a voltage sweep across the load terminals. In this way, it is possible to find where the maximum power is transferred to the load. The points of interest marked in the figure are: the short-circuit current (I_{sc}) obtained when the voltage at the cell terminals is 0V, the maximum power point P_{mpp} (V_{mpp}, I_{mpp}), and the open-circuit voltage (V_{oc}) that occurs when the current through the load terminals is 0 A. Each characteristic curve varies with irradiation and temperature. That is, a family of curves describes the behavior of a cell depending on

the temperature and irradiation conditions. At the level of solar panels or photovoltaic generators, it is impossible to ensure that their cells have identical electrical characteristics or are under the same lighting conditions [111]. Therefore, to model a photovoltaic system, it is convenient to use a model that includes the impact of these variations at the cell level.

3.1. Hot spot condition

Hot spots in photovoltaic systems refer to the overheating that cells experience when they consume power instead of generating it. This phenomenon occurs when the cell operates in the second quadrant and exhibits a negative voltage at the terminals, generally due to partial shading caused by nearby structural elements[142, 117, 143]. These shadows generally vary over time and have complex geometries. As a result of the nature of the electrical characteristics of solar cells, the energy losses are not proportional to the shaded areas. Evaluation of such losses is necessary to determine the power produced by the system [141]. The degree of heating of the hot spot in an affected cell depends on the number of cells that form the panel, the connection, the level of irradiation, and the overcurrent in the affected cell [144]. The type of heating can become localized and severe, especially if a single cell is shaded [117].

In the latter case, the shaded cell will be reverse-biased and dissipate a considerable part of the power generated by the other cells as heat. This operating mode can cause irreversible damage in cells where the current is concentrated at high intensity, reaching hot spots with temperatures above 150 °C. In the worst case, there may be a loss of the insulating properties of the module [116] or damage to the encapsulation materials, which permanently affects the power delivered by the array due to irreversible damage to the panels [23]. A representation of the nonuniformity condition is shown in Figure **3-2**. The figure shows the behavior of a module formed by 36 cells connected in series. The black I-V curve describes the operation of 35 cells without shading, and the blue curve describes the operating condition of only a shaded cell. The orange curve represents the module behavior. Generally, a shadow causes a reduction in the irradiation received by the affected cell, and also, a lower I_{sc}. Because of the series connection, all the cells conduct the same current.

In terms of voltage, the operating point will depend on the impedance of the load supplied by the photovoltaic (PV) system. Figure **3-2** indicates two operating points for both curves. In the first (green dotted line), it is observed that for curves with a current of 0.25A, the voltages delivered for both unshaded and shaded cells are positive, but as the charging current increases and approaches the maximum power point of the unshaded cells, the voltage of the shaded cell starts to decrease until it becomes negative; that is, the cell is reverse biased. Such a case is represented by the red dotted line, where the shaded cell consumes the energy supplied by the cells operating in forward bias. This condition causes negative voltage at its terminals, and the cell operates in the second quadrant Q_2 (reverse mode). Figure **3-3** shows the experimental I-V curve of a monocrystalline cell with short-circuit current $I_{sc} = 0.43A$

and open-circuit voltage $V_{oc} = 0.5V$. Such a figure shows the first and second quadrants Q_1 and Q_2, respectively, where Q_1 exhibits positive cell voltage and current, hence producing power (called direct mode).

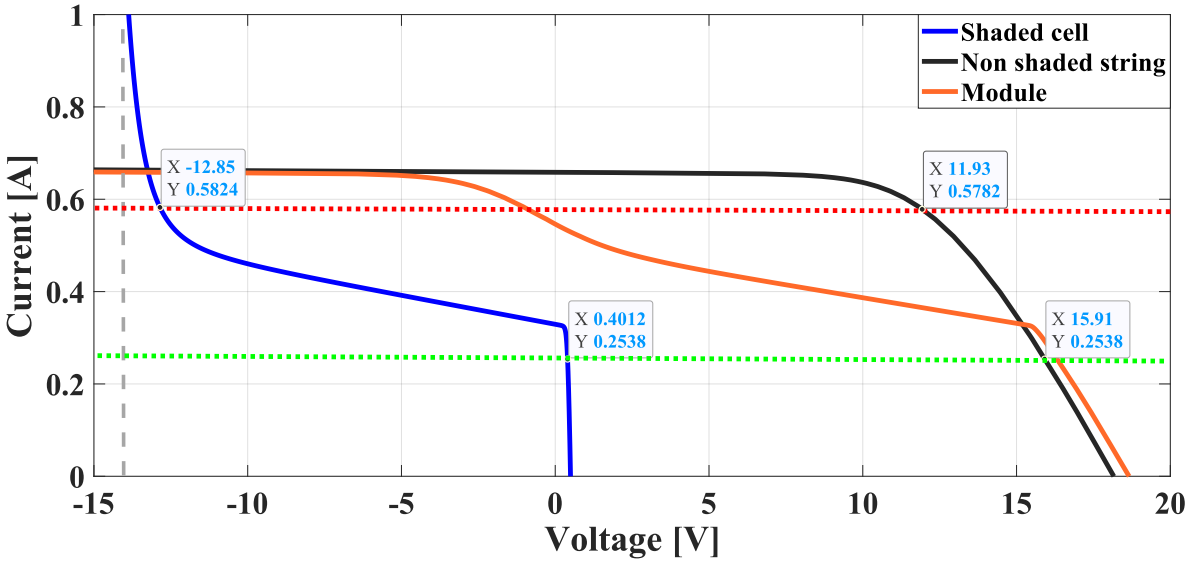

Figure 3-2: Comparison of two operating points for a string of 35 cells without shading (black) and a shaded cell (blue).

The first step in performing a proper analysis of PV arrays it is to represent the operation of the PV cells and modules using circuit models such as the SDM, which is widely used due to its tradeoff between complexity and accuracy [18], or the DDM, which is more accurate to represent the p–n junction at low irradiance levels. The Bishop model [23], instead, aims to represent the behavior of a PV cell operating under partial shading conditions, which requires considering the second quadrant (Q_2). Another model proposed to study the behavior of PV cells under partial shading conditions is the Direct Reverse Model (DRM). This model can reproduce the operation of cells in either direct or reverse biasing modes to account for the influence of variations in both temperature and solar irradiance [28].

The effect of partial shading can be partially mitigated using bypass diodes. The bypass diodes are connected in antiparallel with series-connected cell groups to limit the disparities in current [23, 141, 111]. It is important to note that the bypass diode reduces the power dissipation but not eliminated.

The bypass diode provides an additional path of current that occurs only when the voltage in the reverse mode increases [145], causing the P-V curve to develop multiple peaks [91], where the number of peaks is related to the number of active bypass diodes in the system.

Figure **3-4** shows the simulation of a panel with two modules. Each module has 18 cells connected in series and includes the antiparallel connection of a bypass diode. A single cell is partially shaded so that its PV current is reduced to half the current of the unshaded cells.

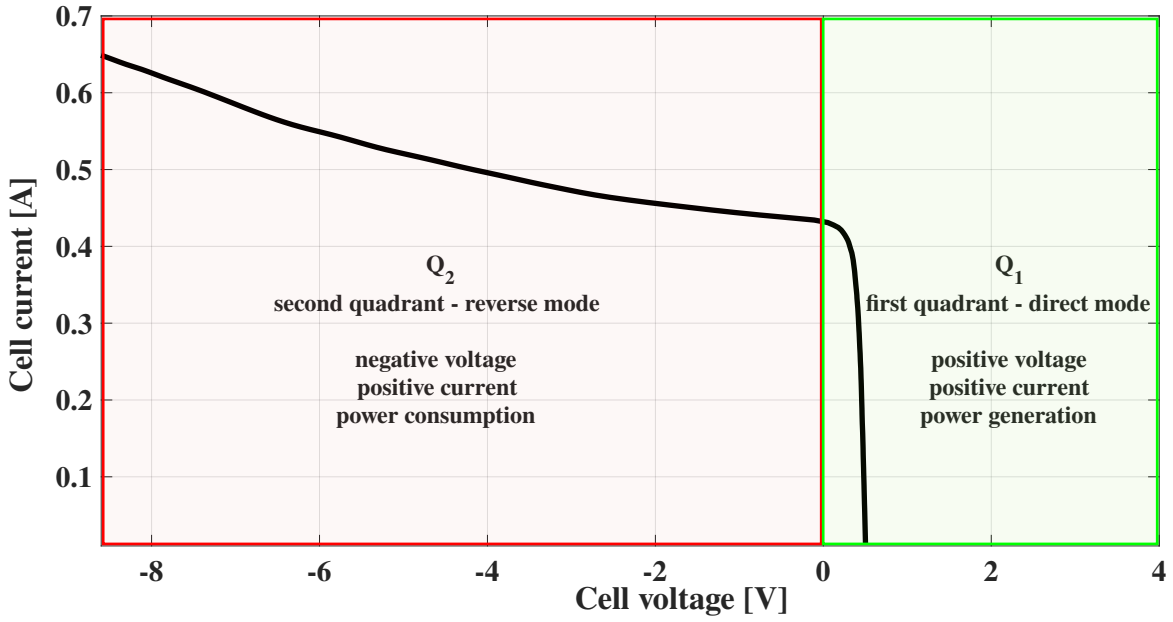

Figure 3-3: Electrical characteristic for a PV cell.

The blue I-V curve exhibits an inflection point [145], and the red I-V curve shows the local maximum and global maximum power points.

A complete description of the effects of partial shading mismatching in real arrays can be obtained by acquiring operating voltages and currents. The reverse characteristic of individual cells allows to determine the power dissipated in a single cell under reverse bias [117]. However, since cells are encapsulated within modules, it is not possible to directly measure the operating points of each cell [23]. From here arises the need to have procedures that allow estimating such behavior without physically compromising the panel.

The representation of a photovoltaic system starts by analyzing the I-V relationship at the cell level, which can be obtained through experimental tests under standard conditions. The cell can be considered a two-port element; the input port receives light energy, and the output port delivers current, voltage, and impedance [146]. The representation of cell behavior can be modeled through circuit models, where two of the best known are the SDM and the DDM. The SDM and the DDM are described below. Since those models cannot represent the behavior of cells in the second quadrant, this section also describes models that include the avalanche mechanism in solar cells.

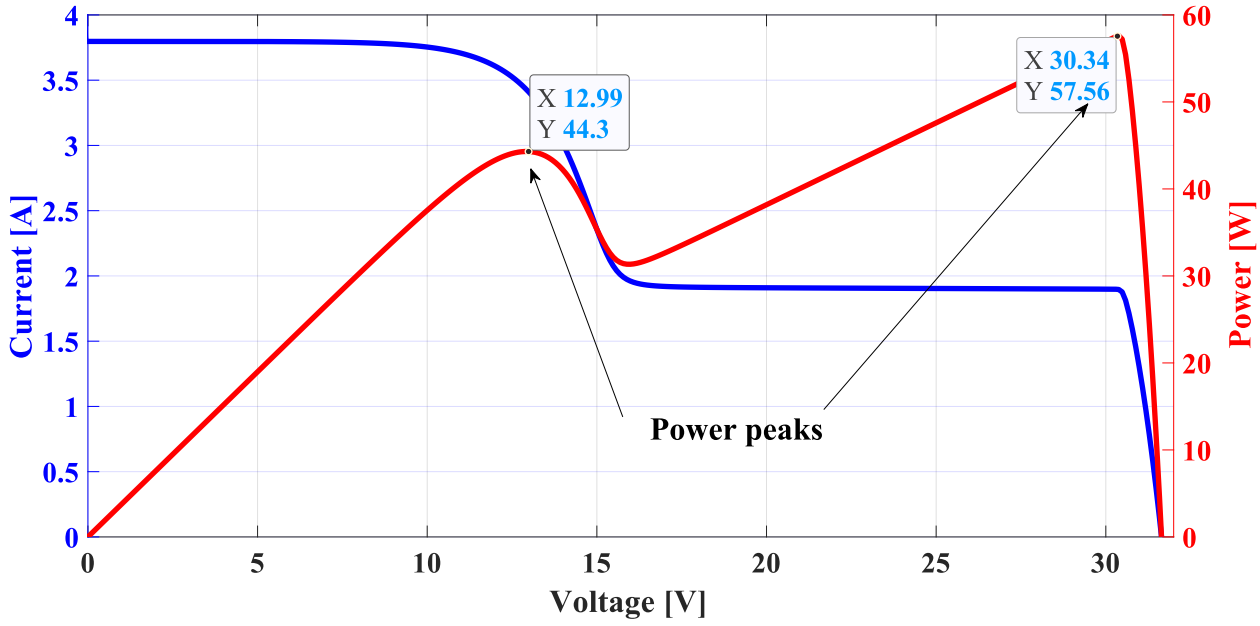

Figure 3-4: Simulation of a 36-cell module with a bypass diode: current-voltage curve and power-voltage curve (blue and red, respectively)

3.2. Single diode model

This model, also known as the five–parameter model, is represented by the equivalent circuit in Figure **3-5**. In this circuit, the current source is associated with the PV current and, the diode represents the energy level threshold for photons to trigger significant production and circulation of electron-hole pairs through the junction [147]. Losses are represented by a series resistance (R_s), which is related to the metal–semiconductor contact resistance, the contacts' ohmic resistance, and the semiconductor material's ohmic resistance. The leakage currents along the edges of the cell are represented by a shunt resistor (R_{sh}).

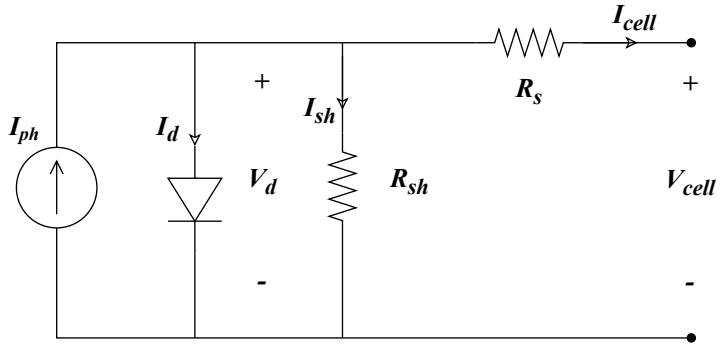

Figure 3-5: Circuit diagram of the Single Diode Model

The cell current (I_{cell}) is obtained as the algebraic sum of the currents through the diode (I_d), the current through the shunt resistor (I_{sh}) and the photocurrent (I_{ph}). Shockley's equation [148] models the current–voltage relationship in the diode ($I_d - V_d$). Thus, (3-1) represents the resulting cell current (I_{cell}).

$$I_{cell} = I_{ph} - I_0 \left[e^{(V_{cell}+I_{cell}R_s)/nV_T} - 1\right] - \frac{(V_{cell} + I_{cell} * R_s\ )}{R_{sh}} \tag{3-1}$$

In Eq. (3-1), V_{cell} is the cell voltage; and I_0 and n, are the reverse saturation current and the ideality factor of the diode, respectively. Finally, V_T represents the thermal voltage expressed in Eq. (3-2), where k is the Boltzmann constant; T, the temperature of the cell; and q, the electron charge.

$$V_T = kT/q \tag{3-2}$$

According to the previous equations, five parameters (R_s, R_{sh}, I_{ph}, I_0, and n) must be evaluated in the SDM to obtain the I–V characteristics of a PV cell. It is important to consider that, this model is only able to represent the behavior of PV cell in Q_1 when energy is delivered.

3.3. The Bishop model

The model proposed by Bishop incorporates an avalanche mechanism into the SDM. As depicted in Figure **3-6**, this mechanism represents the reverse characteristics of the PV cell, which is controlled by the current through R_{sh}. This current term consists of an ohmic term and a nonlinear multiplication factor [23] as shown in Eq. (3-3).

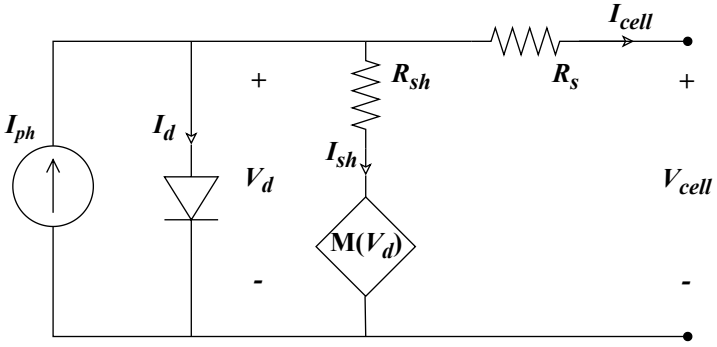

Figure 3-6: Circuit diagram of the Bishop Model

In the Bishop model, Eq.(3-3) relates the output current and the voltage of a PV cell, where a is the ohmic fraction of the current related to the avalanche breakdown; m, the avalanche breakdown exponent; and V_{br}, the junction breakdown voltage.

$$I_{cell} = I_{ph} - I_0 \left[e^{\frac{(V_{cell}+I_{cell}R_s)}{nV_T}} - 1 \right] - \frac{(V_{cell} + I_{cell} * R_s)}{R_{sh}} \left[1 + a * \left(\frac{1 - (V_{cell} + I_{cell}R_s)}{V_{br}} \right)^{-m} \right] \tag{3-3}$$

To evaluate the Bishop model, eight parameters (R_s, R_{sh}, I_{ph}, I_0, n, V_{br} ,m, a) must be estimated. This model is commonly used to represent the behavior of a PV cell in both Q_1 and Q_2, where the cell consumes power instead of producing it.
In order to analyze the effect of the curve in the second quadrant, due to each of the parameters proposed by Bishop to represent the behavior in reverse polarization, a cell was simulated with the following characteristics: $I_{ph} = 0.41$ A, $I_0 = 9 \times 10^{-8}$ A, $n = 1.1$, $R_s = 0.13\Omega$, $R_{sh} = 52.5\Omega$, $m = 4$, $a = 2 \times 10^{-2}$ and $V_{br} = -28$ V. Figure **3-7** presents how the variation of the parameters proposed by Bishop to represent the second quadrant affects the reproduction of the I-V curve. In Figure **3-7** (a), the term a is varied in the range $a = [1 \times 10^{-5}, 1 \times 10^{-1}]$. As the parameter a decreases, the ohmic region extends, and its negative slope decreases. In Figure **3-7** (b), the variation of m in the range $[2, 6]$ is analyzed. It is possible to observe how this variation affects the exponential curvature. Finally, Figure **3-7** (c), presents the variation on the breakdown voltage V_{br} in the range $[-30V, -10V]$, the value at which the current through the cell rises rapidly.

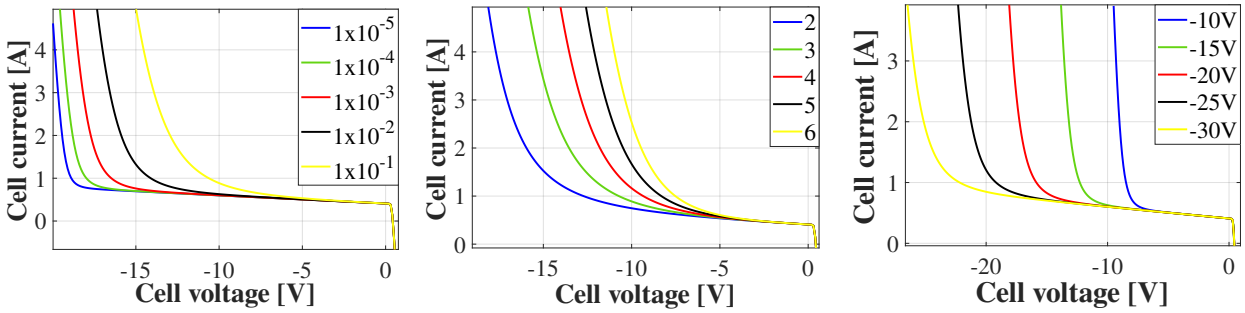

(a) (b) (c)

Figure 3-7: Variation of parameters of the second quadrant in the I-V curve:
(a) $a = [1 \times 10^{-5}, 1 \times 10^{-1}]$, (b) $m = [2, 6]$, and (c) $V_{br} = [-30V, -10V]$

A GUI, using Python, was developed to evaluate the impact that each parameter has on Bishop's model. These results were published in Narváez, Fabián, et al. Smart Technologies. SmartTech-IC 2021: Proceedings of the Second International Conference on Smart Technologies, Systems and Applications. (2022).“Python application for analysis of photovoltaics cells operating in both first and second quadrant.” Bonie J. Restrepo-Cuestas, Cristian Guarnizo-Lemus, Adriana Trejos, Carlos A. Ramos-Paja. Pages:51-67. This work can be found on the publisher's website at ¡`https://dspace.ups.edu.ec/bitstream/123456789/22473/4/SmartTechnologiesabril-2022.pdf`

3.4. Direct–Reverse model

The Direct–Reverse Model (DRM) allows to model the behavior of PV cells in both direct and reverse polarization modes. Using the I–V characteristics from the same sorted series cells, the authors of [32, 83, 149] studied the variability of the curves, not only in the value of the breakdown voltage but also in the slopes of the ohmic regions in Q_2. Based on this characterization, it is possible to observe parts of the curve in Q_2 that could be linearized. In this model, a Thevenin equivalent in series with an ideal diode in the opposite mode models each linear part; the Thevenin resistance represents the slope of the linear region. As shown in Figure **3-8**, this model evaluates the behavior of a PV cell in Q_1 using the DDM.

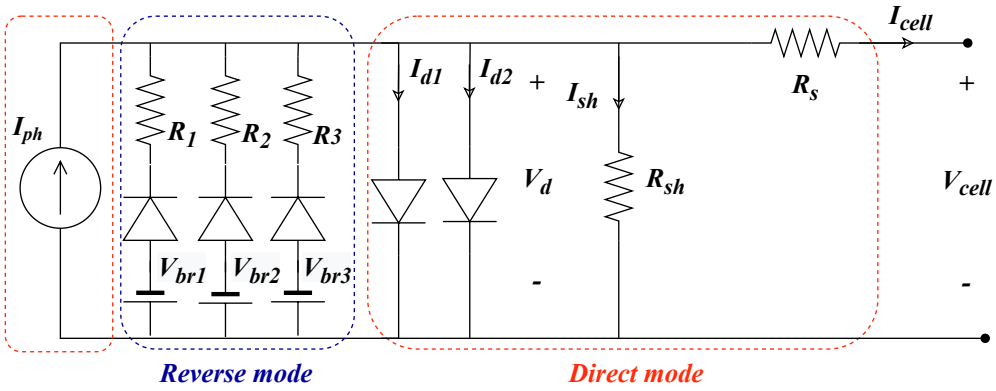

Figure 3-8: Circuit diagram of the Direct-Reverse Model

The number of PV parameters that must be estimated depends on the number of branches used to represent the linear approximation. In the example of Figure **3-8**, the circuit is represented by 13 parameters (7 for the direct mode and 6 for the reverse mode). The DRM can be used for both Q_1 and Q_2 representation.

3.5. Parameter estimation problem

In the representation models presented above, the relationship between the cell current I_{cell} and the cell voltage V_{cell} is nonlinear. Also, I_{cell} is implicit in the equation through an exponential function. Therefore, iterative algorithms are required for its evaluation. The Newton-Raphson algorithm has been widely used to find approximations to the zeros or roots of a real function. In order to apply this algorithm to the solution of a function, the function must be differentiable with respect to the variable to be found. Calculating the current I_{cell} requires the terms of Eq.(3-1) to be grouped on the same side to get an equation equal to zero. The resulting function depicted in Eq.(3-4) and called $f(I_{cell}, V_{cell}, \theta)$, will be evaluated through the algorithm Newton-Raphson to find the value of the variable I_{cell} that satisfies $f(I_{cell}, V_{cell}, \theta) \approx 0$.

$$f(I_{cell}, V_{cell}, \theta, T) = I_{ph} - I_d - I_{sh} - I_{cell} = 0 \tag{3-4}$$

In 3-4, θ is the set of parameters required for the evaluation of the function $f(I_{cell}, V_{cell}, \theta)$. Named $\theta_{BM} = \{I_{ph}, R_s, R_{sh}, I_0, n, a, V_{br}, m\}$ for representing the set parameters of Bishop's model and $\theta_{SDM} = \{I_{ph}, R_s, R_{sh}, I_0, n\}$ for SDM. The evaluation algorithm for calculating the current I_{cell} based on the Newton-Raphson method is detailed in Algorithm 1. The steps of the algorithm are listed below:

1. The first step is to choose an initial value for the I_{cell}, in this case, 0 A.
2. Then, the function $f(I_{cell}, V_{cell}, \theta, T)$ is calculated at the initial value defined for I_{cell}.
3. The function's derivative $f(I_{cell}, V_{cell}, \theta, T)$ must be calculated with respect to the variable of interest (I_cell). The derivative is presented in (3-5). This derivative represents the slope of the tangent of the function F at a given point. The derivative must also be evaluated at the starting point for I_{cell}.
4. The point of intersection of the tangent with the variable I_{cell} must be calculated, as presented in (3-6). This evaluation will return the new value for I_{cell}
5. Steps 2 to 4 are repeated until an error measure is reached (tol).

The algorithm requires as inputs the value of each parameter of the model θ, and the operating point data i (voltage $V_{cell_m}(i)$ and temperature T), at which the current $I_{cell_e}(i)$ is to be calculated. Suppose you want to reproduce an I-V curve at a given temperature and irradiation condition. In that case, the algorithm will calculate the current value in vector form for a given vector voltage. The algorithm stops when the tolerance tol has been reached. As seen in Eq.(3-4) tol is given in Amperes, and in this case, was defined $tol = 1 \times 10^{-6}$ A.

$$\begin{aligned}\frac{\partial f(I_{cell}, V_{cell}, \theta, T)}{\partial I_{cell}} = &- \frac{R_s I_0}{nV_T} e^{\frac{(V_{cell} + I_{cell} R_s)}{nV_T}} - \frac{R_s}{R_{sh}} - \frac{aR_s}{R_{sh}} \left[1 - \frac{(V_{cell} + I_{cell} R_s)}{V_{br}}\right]^{-m} \\ &- \frac{amR_s}{V_{br}} \left[\frac{V_{cell} + I_{cell} R_s}{R_{sh}}\right] \left[\frac{V_{cell} + I_{cell} R_s}{V_{br}}\right]^{(-m-1)} - 1\end{aligned} \tag{3-5}$$

$$I_{cell_e} = I_{cell_e} - \frac{f(I_{cell_e}(i), V_{cell_m}, \theta)}{\partial f(I_{cell_e}, V_{cell_m}, \theta, T)/\partial I_{cell}} \tag{3-6}$$

The parameter estimation of a model evaluates a function through the exploration of the parameter's search space. Optimization techniques allow a non-exhaustive search to find a good quality solution. In the case of circuit modeling of photovoltaic cells, it is generally based on known information, which relates the output voltage behavior and current, called the I-V

Algorithm 1: Pseudocode for the evaluation of I_{cell} using Newton-Raphson.

Load Parameters θ, T, (V_{cell_m}, I_{cell_m})
Initialize a zeros vector (I_{cell_e})
Solve Newton-Raphson
$N = length(V_{cell_m})$
for $i = 1 : N$ **do**
  Eval $f(I_{cell_e}(i), V_{cell_m}(i), \theta)$
  while $|f(I_{cell_e}(i), V_{cell_m}(i), \theta)| > tol$ **do**
    Eval $I_{cell_e}(i)$ using Eq. (3-6)
    Eval $f(I_{cell_e}(i), V_{cell_m}(i), \theta)$
  end while
end for
PRINT I_{cell_e}

curve. This curve can be obtained through different methods: experimental I-V curve [150], using MPPT information when the shading condition is present [151], considering variations of temperature in the behavior of the I-V curve [152], applying Lambert-W function to solve the model [153], using sweep voltage considering an electronic DC load [154] and by means of a mathematical reduction [155]. Here, the idea is to find the set of parameters that best reproduces the I-V curve of a cell from a circuital model. Therefore, it is proposed to minimize an objective function, such as an error metric between the measured data (I-V curve) I_{cell_m} and the estimated data I_{cell_e}, under a given test scenario (T and I_{rr}), as Eq. (3-8) shown. The selected error metric is the root mean square error (RMSE) as shown in Eq.(3-7).

$$\mathbf{O.F.}(\theta) = \mathbf{RMSE}\left(I_{cell_e}(\theta), I_{cell_m}\right) \tag{3-7}$$

$$min\left\{\mathbf{O.F.}(\theta)\right\} = min\left\{\sqrt{\frac{1}{N}\sum_{i=1}^{N}(I_{cell_e}(\theta) - I_{cell_m})^2}\right\} \tag{3-8}$$

It is also necessary to define a set of constraints to limit the optimization problem, for this case, it will be given by the search range of each parameter θ, through a minimum limit θ^{min} and a maximum limit θ^{max}. Eq. (3-9) presents a formulation to generate a set of parameters named θ_1 within the defined search space $\{\theta^{min}, \theta^{max}\}$. Here the function $rand[length(\theta)]$ will generate a vector with the same length as the set of θ parameters, with random values between 0 and 1.

$$\theta_1 = \theta^{min} + (\theta^{max} - \theta^{min}). * rand[length(\theta)] \tag{3-9}$$

4 Non-invasive procedure for extraction of the I-V cell curve in photovoltaic panels

As presented in Section 2.3, no non-invasive procedures still allow obtaining I-V curves of cells in commercial panels. This means procedures that do not require physical intervention in the panels that could affect their integrity and can be reversed without the need to carry out complex processes. Therefore, removing the bypass diode of a PV panel is not considered invasive to the PV module or PV cells. The contribution of this chapter is the proposal of a noninvasive procedure to obtain the I-V curve per cell in panels in such a way that the panels do not have to be physically intervened to measure the cell level in both the first and second quadrants, using a reduced number of measurement equipment, and thus being applied in other photovoltaic systems.

4.1. Series string analysis

The I-V curve of the shaded cell is taken from the following analysis. Consider a string of N cells where all cells share the same current since they are connected in series. Only one cell is partially shaded (cell N). Hence, its short circuit current will be lower than the others (see Figure **4-1**) because it receives a lower amount of irradiation than the others. In this way, at the operating point called I_1, the voltage contribution of each cell, shaded or not, is positive. However, at the I_2 operating point, shaded cell will have negative voltages for positive currents because it consumes some energy produced by nonshaded $N-1$ string cells.

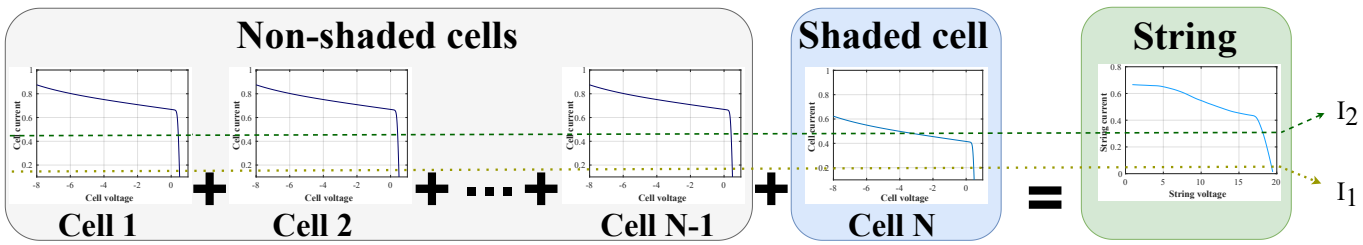

Figure 4-1: Cell contribution for an N-cell string.

In general, it is possible to calculate the string voltage for a given operating current point I_p through the sum of the voltage contributions of each non-shaded cell (V_{NS}) plus the voltage contribution of the shaded cell. From a general context, as shown in the Eq. (4-1), it would be possible to calculate the voltage on nonshaded cells in I_P, as the mean value of the contribution of $N-1$ voltage of nonshaded, multiplied by $N-1$. The string voltage (V_{string}) will be given by (V_{NS}) calculated through the mean value and the voltage of the shaded cell (V_{SHC}) (see Eq.(4-2)).

$$\begin{aligned} V_{NS}(I_p) =& Vcell_1(I_p) + Vcell_2(I_p) + Vcell_3(I_p) + \cdots + Vcell_{N-1}(I_p) \\ =& (N-1) * \left(\frac{1}{N-1}\right) \sum_{i=1}^{N-1} Vcell_i(I_p) \end{aligned} \tag{4-1}$$

$$\begin{aligned} V_{string}(I_p) =& V_{NS}(I_p) + V_{SHC}(I_p) \\ =& (N-1) * \left(\frac{1}{N-1}\right) \sum_{i=1}^{N-1} Vcell_i(I_p) + V_{SHC}(I_p) \end{aligned} \tag{4-2}$$

From the Eq. (4-2), it is possible to obtain the voltage in the shaded cell (V_{SHC}) as the difference between the string voltage (V_{string}) and the voltage contribution of the non-shaded cells (V_{NS}).
Performing a comparison with the data obtained from the experimental curves (see Figure **4-2** (b)) and simulated curves (see Figure **4-2** (a)), voltage contribution of the $N-1$ non-shaded cells (V_{NS}) can be extracted from a panel I-V curve without shading as follows:

- Given the series connection of the cells, the panel voltage will be equal to the addition of cell voltage contributions $V_{PV}(I_p) = \sum_{i=1}^{N} Vcell_i(I_p)$.
- The voltage contribution of $N-1$ nonshaded cell can be given as a scaled form of V_{PV} (See Eq. (4-3)).

$$V_{NS}(I_p) \approx (N-1) \left[\frac{1}{N} \sum_{i=1}^{N} Vcell_i(I_p)\right] \tag{4-3}$$

The string voltage when a cell is shaded ($V_{string}(I_p)$), can be obtained experimentally by measuring the voltage in a panel terminal when a portion of a cell is shaded.
From Eq. (4-2), V_{SHC} can be evaluated as follows:

$$V_{SHC}(I_p) = V_{string}(I_p) - V_{NS}(I_p) \tag{4-4}$$

To extend the shaded cell voltage calculation V_{SHC} to a set of current operating points, it is necessary to guarantee that the voltages V_{string} and V_{NS} are taken at the same current

values. If this condition is not reached, it is possible to interpolate them using the same current vector

Figure **4-2**(a) presents the simulation results of a 36-cell string, where only one cell is shaded, and its I-V curve is colored red. The green curve represents the contribution of cells without shading (NS), that is, a total of $N - 1 = 35$ cells. Finally, the I-V string curve, in black, is the summation of the voltage contribution from the red and green curves. The dashed green curve represents the mirror of the IV curve corresponding to the cells without shading. From the intersection of the second quadrant curve of the shaded cell and the dashed curve, it is possible to determine the greatest power dissipated by the shaded cell. For example, for Figure **4-2**(a), this value corresponds to -3.93 W. This information allows the detection of hot spots in photovoltaic panels [156]. Figure **4-2**(b) presents the experimental results in a PV panel without bypass diode, considering, this value correspond to -3.93 only one shaded cell, and obtaining two I-V curves with and without shading cell (green and black, respectively). Then, the red curve is obtained using the proposed procedure, which will be described in detail in the following subsections.

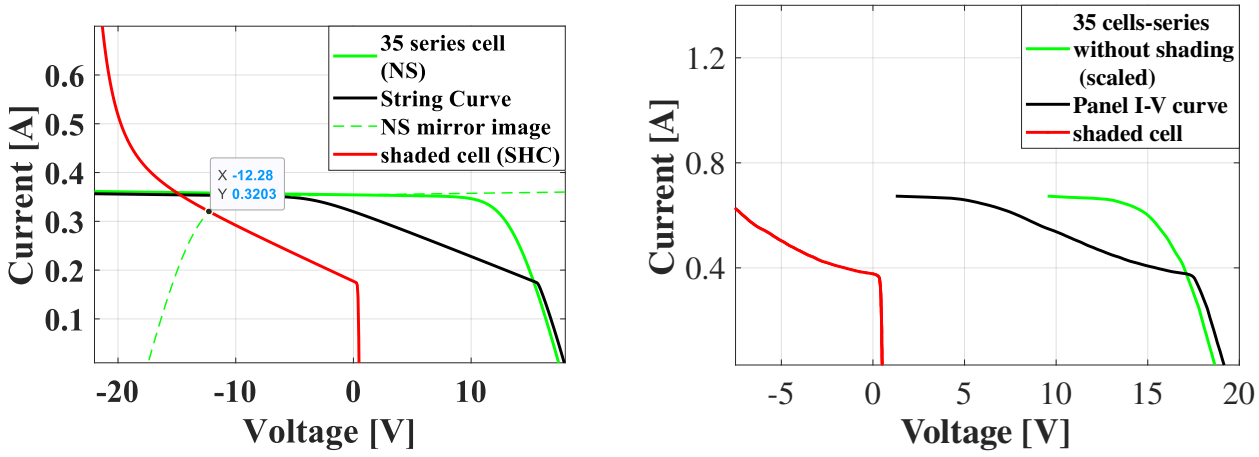

(a) (b)

Figure 4-2: Graphical analysis of shading phenomena: (a) from simulation and (b) from experimental analysis

4.2. Experimental platform

Two ERDM SOLAR panels with module type HYBRITEC-10/12 (one mc-SI and another pc-SI), were selected to obtain an I-V cell curves dataset. Table **4-1** reports the most important electrical parameters of the datasheet for the modules. In each case, a cell with a 50 % shaded area was selected to experimentally obtain its I-V curve in the first and second quadrants. An opaque object generates the shadow in the selected area of the cell to avoid

incident radiation. Therefore, the experimental I-V curves, of both mc-SI and pc-SI cells, were generated under real operating conditions, with an irradiance of 1008 W/m^2 and a temperature of 320.65 K. The experimental setup shown in Figure **4-3** was used to obtain cell I-V curves in a panel. Two panels with the same reference (a) and (b) were used, an oscilloscope R&S®RTE1204 records the current and voltage of the panel (c), a sweep voltage was achieved with the DC electronic load BK 8514 (d). Irradiance and temperature were measured with the MACSOLAR SLM018c-2 (e) and the FLUKE 63 infrared thermometer (f), respectively. Finally, the short-circuit current of panel (b) was measured with a multimeter. The DC electronic load BK 8514 was programmed using serial communication to perform a sweep voltage until 110 % $\times V_{oc}$ panel value, with intervals of 1 ms between each pair of points on the curve. A voltage sweep was selected to obtain greater detail in terms of current data near the short circuit region; that is, where the behavior in the second quadrant begins. If a current sweep had been chosen, it is possible that a lower resolution would be obtained in this region, which is quite important for the estimation of the parameters that affect the second quadrant. the aim was to ensure that the exposure time in each test was as small as possible to avoid changes in irradiation. Figure **4-8** shows the experimental I-V curves.

Using the previously described procedure, the shaded cell's behavior was calculated, and those results are presented in Figure **4-9**. There is a noticeable difference in the second-quadrant behavior for pc-SI and mc-SI cells, related to the reverse-mode operation. The following subsection describes, in detail, the proposed procedure.

Table 4-1: Datasheet parameters for ERDM-SOLAR 10/12 panel

Parameters	V_{mp}	I_{mp}	V_{oc}	I_{sc}	P_{max}	Cells	Bypass diodes
Value	17.4V	0.58A	21.8V	0.69A	10W	36	1

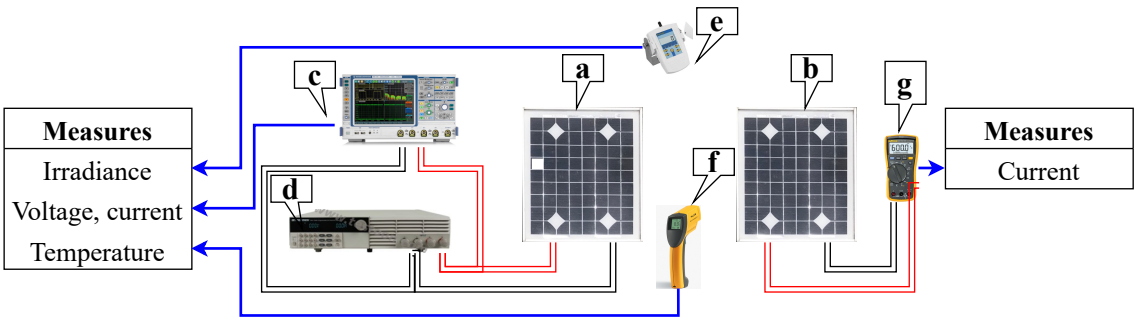

Figure 4-3: Experimental stage.

4.3. Procedure description

The procedure for obtaining the I-V curve at the cell level in photovoltaic panels is presented in Figure **4-4** and described as follows:

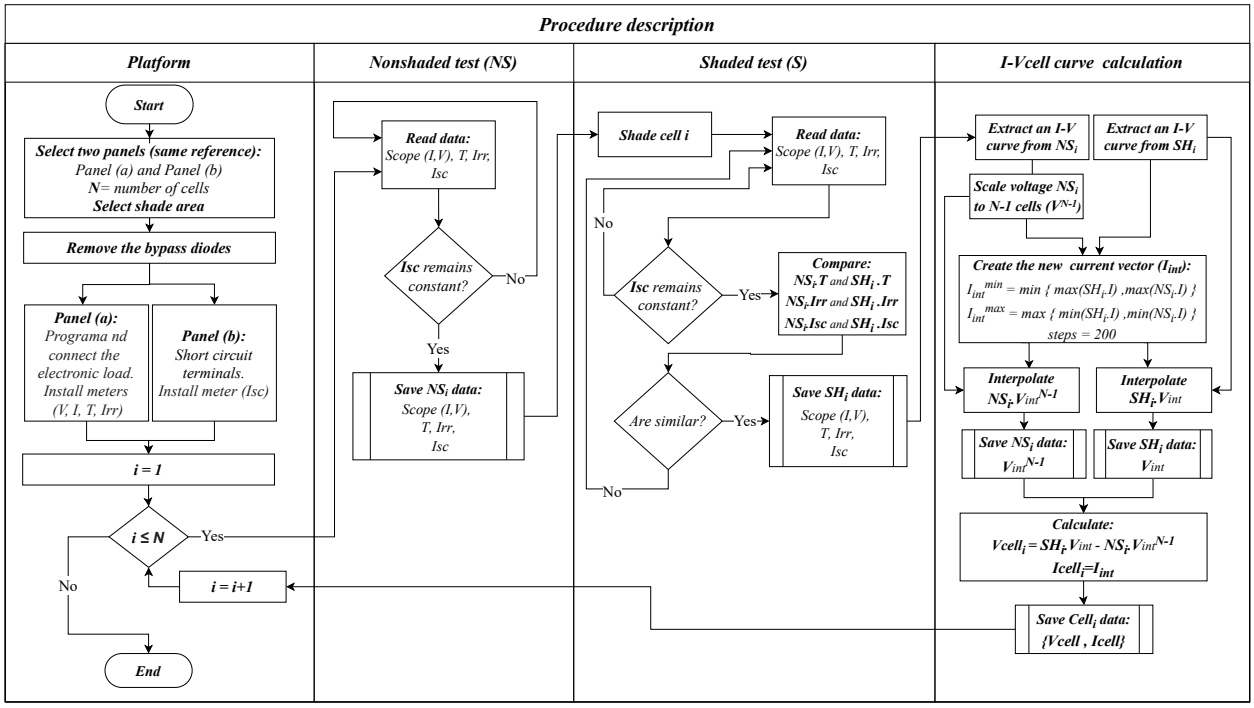

Figure 4-4: Proposed procedure for obtaining the I-V curve at the cell level in photovoltaic panels.

1. Select two panels of the same reference (panels (a) and (b)); the junction box with the bypass diodes must be accessible to disconnect the bypass diodes.

2. The bypass diode included in panel (a) must be removed.

3. To guarantee that curves are acquired under similar weather conditions, panel (b) must be short-circuited, and it is necessary to measure its current I_{sc} because it is directly related to irradiance. In this way, if the current did not change significantly, it can be assumed that the irradiation did not change considerably.

4. The curve of the panel (a) without shadowing (V_{panel} and I_{panel}) is acquired, as well as the irradiation and temperature. In addition, the short-circuit current I_{sc} data value from panel (b) is taken using a digital multimeter, to identify considerable changes in irradiation during the test.

5. To select a cell, refer to the numbering indicated in Figure **4-5**. The numbers represent the rows, while the letters represent the columns where the cell is located on the panel. For the mc-SI panel, the cell range is from A1 to D9, and for the pc-SI panel, it is from A1 to C12.

6. The shaded I-V curve of the panel (a) can be obtained by shading a certain percentage of its area. In this case, a solid shadow covering 50 % of the cell area was selected. The measurement of I_{sc} in panel (b) holds significance as it provides valuable information about changes in irradiation. The reference panel (b) to which the current is measured through the multimeter will deliver the short-circuit current at the time of the test. This current has a direct relationship with the irradiation perceived by the panel. For Panel 1, most tests returned a short circuit current value between 0.67 A, 0.68 A, or 0.69 A. The variation in irradiance concerning that difference in current measurements of 0.01A, or 1.6 % referring to relative error, corresponds to a change in irradiance between 10 W/m^2 and 20 W/m^2. Concerning Panel 2, current variations ranged from 0.57 A to 0.66 A in steps of 0.01 A. The measures were acquired using a multimeter with a resolution 0.1 mV, and precision is equal to 0.15 %. Hence, a notable change in irradiation corresponded to a variation in the short-circuit current measurement of 0.01 A.

7. Both curves, with and without shading, must be acquired under similar irradiation and temperature conditions. The acquisition time required for a complete curve is 200 ms. The time between curves is 20 ms. Figure **4-6** and Figure **4-7** show an example of the data recorded by the scope for mc-SI panel (a):

   - Figure **4-6** (a) presents the panel voltage and current without shading. Data was taken at $T = 47.8$ ℃, $I_{rr} = 1008$ W/m^2, and $I_{sc} = 0.68$ A in panel (b).
   - Figure **4-7** (b) presents the panel voltage and current when A_1 cell is shaded, at $T = 46.7$ ℃, $I_{rr} = 1007$ W/m^2, and $I_{sc} = 0.68$ A in panel (b).

   At least three curves were acquired for each test with or without shading, as shown in Figure **4-7** and Figure **4-6**, respectively. Then, the information is segregated by curves in terms of current (I_1, I_2, and I_3); if significant variations in their shape are found when superimposing them, the test must be repeated. Figures 4.6(b) and 4.7(b) present the comparison of 3 of the analyzed curves. For these examples, no differences are found in the curves, so the test information is suitable and does not need to be repeated.

8. Then, a current-voltage data set is extracted. the curve is labeled according to the cell under analysis, as shown in Figure **4-8**. Figure (a) shows the curves of the mc-SI panel without shading (NS-A1) and when cell A1 is shaded to 50 % its area (SH-A1). Figure (b) presents the experiment in the pc-SI panel when cell A2 is analyzed; that is, the

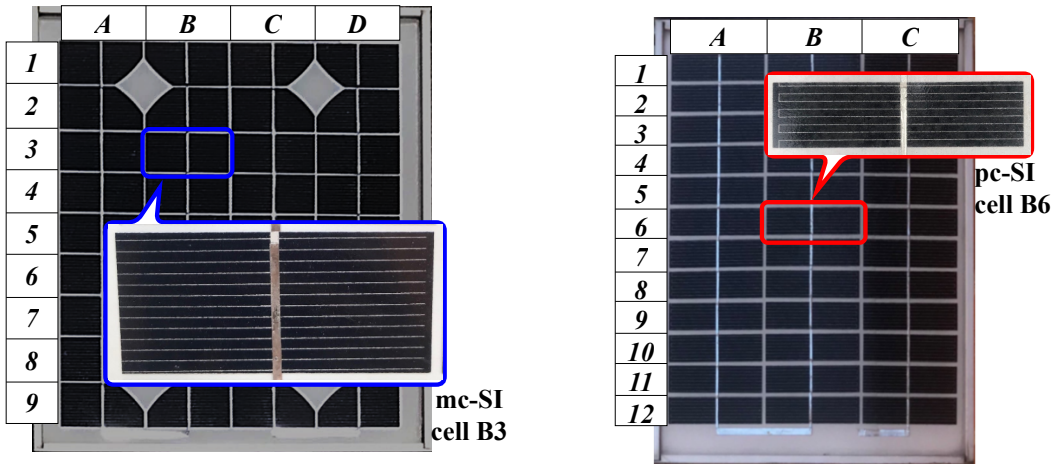

(a) (b)

Figure 4-5: Cell labeling in photovoltaic panels: (a) monocrystalline mc-SI (b) polycrystalline pc-SI

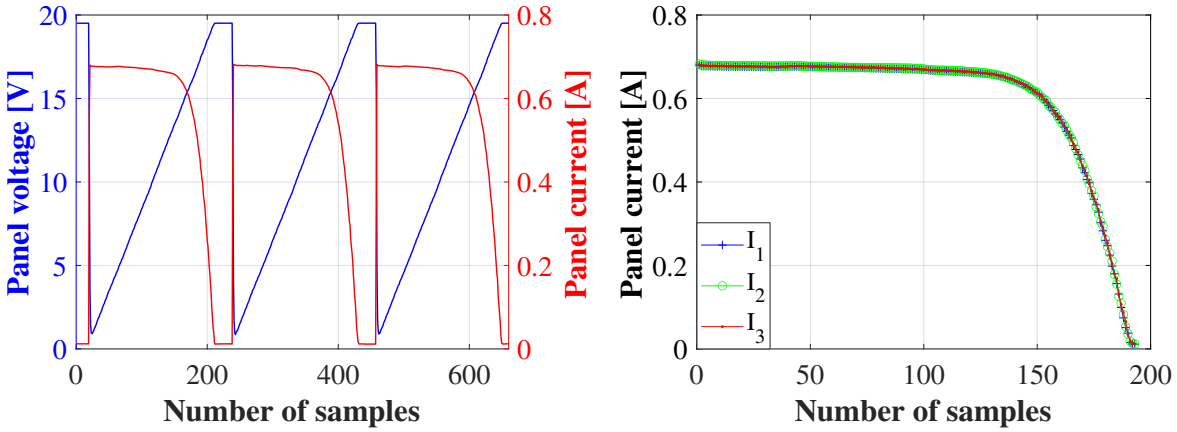

(a) (b)

Figure 4-6: Voltage and current data from the monocrystalline panel: (a) without shadowing and (b) with a 50 % shaded area of the A1 cell

panel curve without shading (NS-A2) and the panel I-V curve when cell A1 has been shaded (SH-A2). Table **4-2** presents the irradiation and temperature information for acquiring shaded and non-shaded data. As can be seen, the data sets were obtained under similar conditions. Cell labeling is carried out according to Figures **4-5** (a) and (b).

9. The I-V curve of the shaded cell is reconstructed by subtracting between the two I-V curves, with and without shading in terms of voltage (see Figure **4-8**). Following the

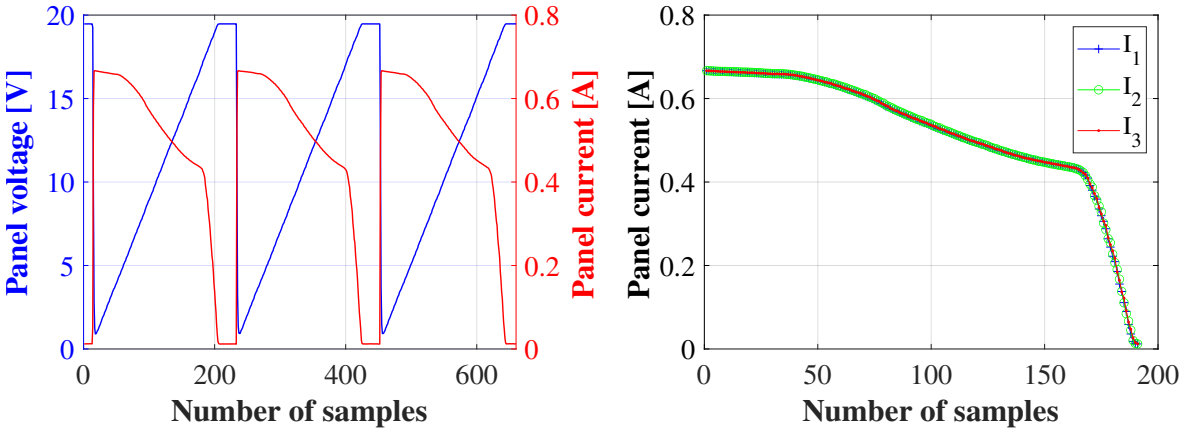

(a) (b)

Figure 4-7: Voltage and current data from the monocrystalline panel: (a) without shadowing and (b) with a 50 % shaded area of the A1 cell

Table 4-2: Meteorological data measured during experimental tests presented in Figure **4-8**

	mc-SI Panel (a)		**pc-SI Panel (a)**	
	NS-A1	**SH-A1**	**NS-A2**	**SH-A2**
Temperature (°C)	47.8	46.7	47.5	47.1
Irradiance (W/m^2)	1008	1007	945	942
I_{sc} for panel (b) (A)	0.68	0.68	0.60	0.60

description provided in Subsection 4-1, it is necessary:

- To calculate the contribution of the nonshaded cells V_{NS}; hence, it is necessary to scale the curve without shading to the contribution of $N-1$ cells. Thus, the output voltage vector of the panel corresponding to the $N-1$ cells will be $V_{NS}^{N-1} = V_{NS} * \frac{(N-1)}{N}$. Those results can be observed in Figure **4-2** (b) in green.
- Considering that all cells of the panel share a series connection, for the subtraction between the shaded I-V curve of the voltage vectors V_{SH} and the non-shaded scaled I-V curve V_{NS}^{N-1}, it must be guaranteed that both curves have been evaluated for the same current values of the panel. Therefore, a current vector must be created I_{sub}. The range of I_{sub} is defined in (4-5) and (4-6).

$$I_{sub}^{min} = max\left[min(I_{SH}), min(I_{NS_{scaled}})\right] \tag{4-5}$$

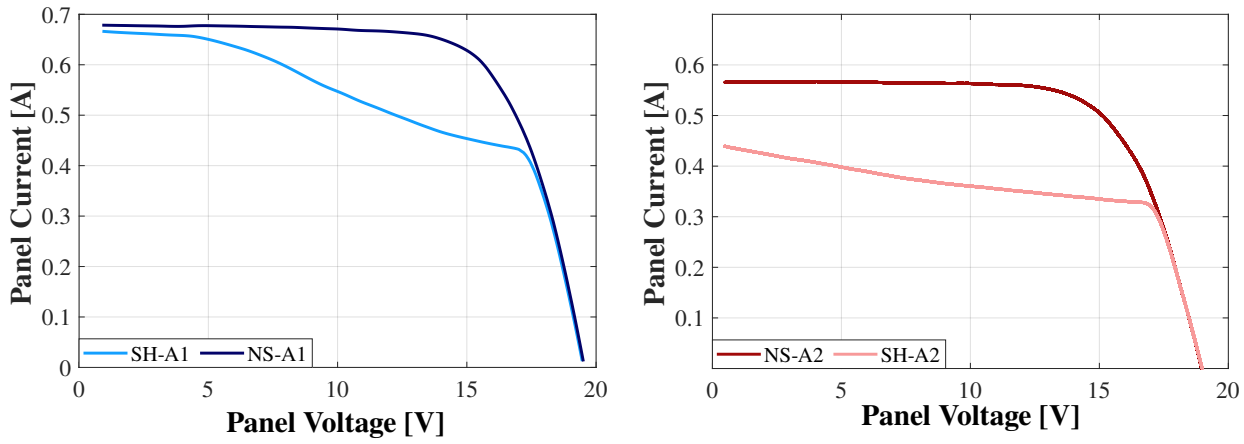

(a) (b)

Figure 4-8: Experimental I-V curves: Nonshadowed (NS) and shadowed (SH): (a) for mc-SI panel (a) cell A1 and (b) pc-SI panel (a) cell A2

$$I_{sub}^{max} = min\left[max(I_{SH}), max(I_{NS_{scaled}})\right] \tag{4-6}$$

The minimum limit is the highest value between the minimum currents of both curves (SH and scaled NS). The upper limit will be the lowest value within the maximum current value of both curves. The points in I_{sub} can be between 150 and 200.After reviewing the state of the art related to parameter estimation for photovoltaic cells/panels, it was found that many of the analyzed works used a data set of 25 or 101 samples for voltages and currents (see 2.4). It must be considered that these studies were developed only to analyze behavior in the first quadrant. Therefore, it was defined as a set of 150 to 200 data, enough to estimate the parameters in both the first and second quadrants. On average, for each cell of the trading panel, 116 samples were used for the first quadrant and 78 for the second quadrant.

- Next, both voltage vectors V_{SH} and V_{NS}^{N-1} are interpolated using the current vector I_{sub}. These vectors are named $V_{SH_{int}}$ and $V_{NS_{int}}^{N-1}$, respectively.
- Finally, the estimated I-V cell curve is obtained by subtracting $V_{SH_{int}}$ and $V_{NS_{int}}^{N-1}$. Figure **4-9** shows the results of the procedure for (a) the A2 cell in the mc-SI panel and (b) the A1 cell in the pc-SI panel. It can be seen that both curves present information from the first and second quadrants. In addition, it is also possible to observe important variations in the short-circuit current and the behavior in the reverse mode operation.

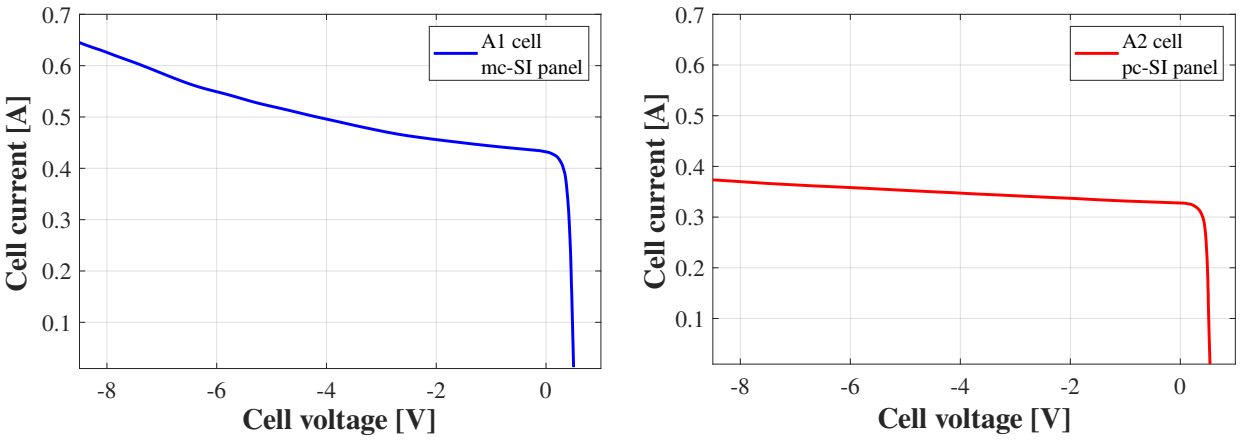

(a) (b)

Figure 4-9: I-V cell curve of: mc-SI 4.9(a) and 4.9(b) pc-SI technologies

10. Repeat steps five to nine for all the cells in the panel to obtain the IV cell curve in the first and second quadrants, for which it is required:
    - A voltage sweep is programmed into an electronic load to generate the I-V curve on the panel.
    - I-V curves were acquired at panel terminals without shading and when a cell is shaded.
    - Then both curves are subtracted interpolating the voltages of both curves in terms of the same current vector. The current vector used approximately 200 points equally spaced.

Figure **4-9** presents the IV curves at the cell level for each panel technology (mc-SI and pc-SI). It is possible to note some differences in the behavior in the first and second quadrants. For example, considering that the experimental stage was obtained with similar values of temperature and irradiation, and, that both panels have the same nominal information, the short circuit current I_{sc} presents a visible difference. Regarding the behavior in the second quadrant, it is possible to observe that the magnitude of the breakdown voltage V_{br} is lower for the pc-SI cell than for the mc-SI cell. The mc-SI cell shows the beginning of exponential growth in this region, while the pc-SI cell only exhibits the ohmic region in the second quadrant because, under the test, it was not possible to acquire information close to the breakdown voltage (V_{br}). Table **4-3** consolidates information about some points of interest on the curve. Some relevant differences are present in the short circuit current (I_{sc}) and the maximum power point (P_{mpp}).
The procedure outlined in this section enables the estimation of cell behavior within the first and second quadrants of a commercial panel. Each curve provides detailed information

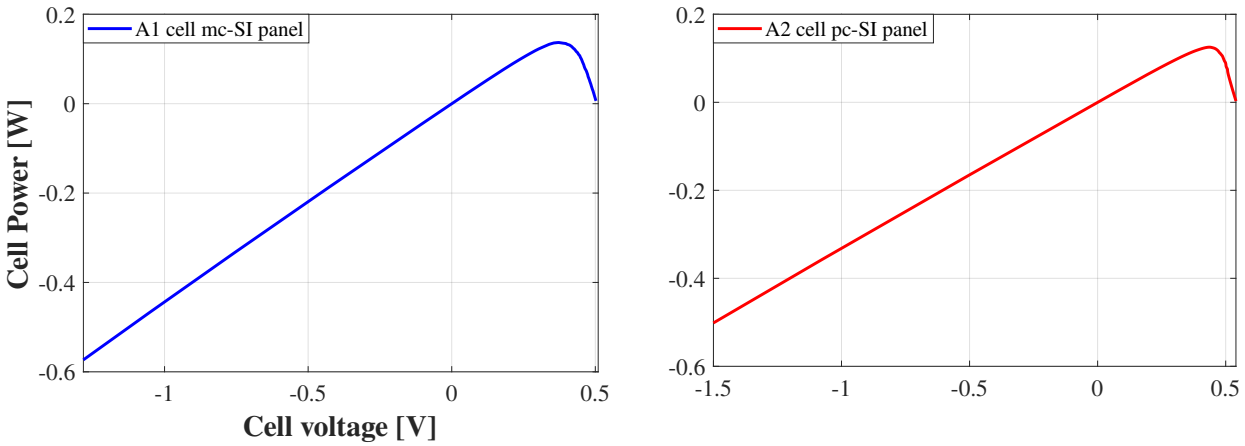

(a) (b)

Figure 4-10: P-V cell curve of: mc-SI 4.10(a) and 4.10(b) pc-SI technologies

Table 4-3: IV curve cell interest points for mc-SI panel (a) and pc-SI panel (a)

	V_{mpp}	I_{mpp}	V_{oc}	I_{sc}	P_{mpp}
mc-SI A1 cell	0.37V	0.36A	0.50V	0.43A	0.13W
pc-SI A2 cell	0.47V	0.23A	0.54V	0.32A	0.12W

on irradiance, temperature, voltage, and current data. This procedure was applied to two panels featuring different technologies, namely mc-Si and pc-SI. The cell-level information obtained will serve as input for the analyses presented in Chapters 5 and 6. The proposed method presents a non-invasive option for obtaining cell curves in photovoltaic panels' first and second quadrants. However, some improvements can be implemented. The first one is by implementing the tests in a controlled environment, ensuring constant irradiation and temperature, for which a specialized panel testing laboratory is required. The second one is developing a data acquisition system, which automatically takes voltage, current, irradiation, and temperature data to be stored in the cloud for further analysis. This development can reduce data processing times considerably.

5 Evaluation of cell models for both direct and reverse representation

This section shows a behavior comparison between the three models, the SDM, Bishop, and DRM, when reproducing the current vs. voltage curve for both Q_1 and Q_2. To achieve this, it was necessary:

- Identify the parameters required by each model.
- Define the data set that will be used for the estimation.
- Select the metrics for validation.

Initially, SDM, which in literature, has been widely used to represent behavior in the first quadrant. Here, it will represent both quadrants (Q_1 and Q_2). It will use experimental data from both quadrants. The focus will be on the representation of Q_2. Bishop, which is used to represent both quadrants, also will use experimental information in Q_1 and Q_2. The focus will be on the representation of Q_1. Finally, for DRM, the analysis will be divided into two sections, Q_1 and Q_2. The first will use the experimental data from the first quadrant (Q_1) to estimate the SDM parameters. For the model segment representing the second quadrant, the experimental data in Q_2 will be used and calculated as explained in [32]. This information is consolidated in Table **5-1**. Those results were validated by comparing two error measures (RMSE and MAPE) obtained from the reconstruction of an experimental I-V cell curve for each model, that is, in both Q_1 and Q_2. Furthermore, the results of the estimation of some points of interest, such as the short-circuit current (I_{sc}), the open-circuit voltage (V_{oc}), and the voltage and current at the maximum power point (V_{mpp}, I_{mpp}) were evaluated and analyzed for each model.

Table 5-1: Comparison scenario for the three models.

Model	**Model parameters**	**I-V experimental data**
SDM	$[I_{ph}, R_s, R_{sh}, I_0, n]$	Q_1 and Q_2
Bishop	$[I_{ph}, R_s, R_{sh}, I_0, n, V_{br}, m, a]$	Q_1 and Q_2
DRM	$[I_{ph}, R_s, R_{sh}, I_0, n]$ $[V_1, R_1, V_2, R_2, V_3, R_3]$	Q_1 Q_2

The proposed methodology for evaluating the electrical model at the cell level, in both the direct and reverse modes, is summarized in Figure **5-1**.

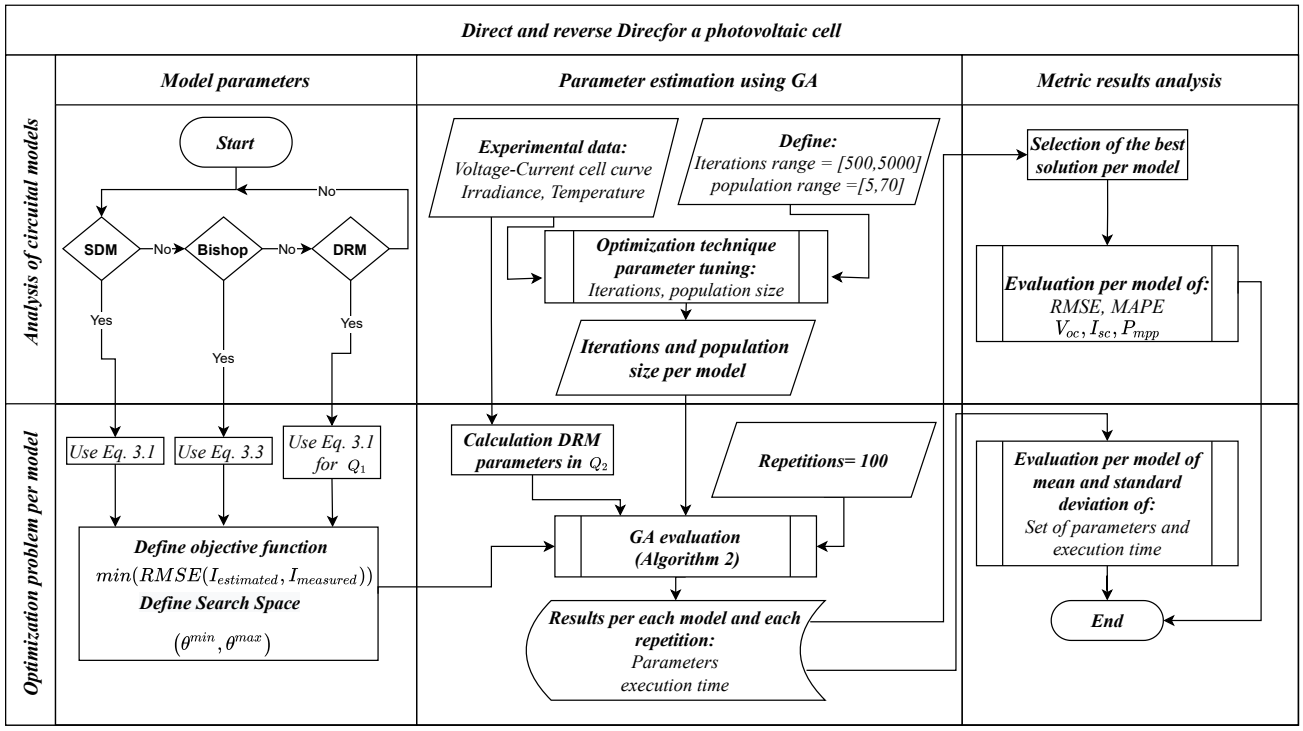

Figure 5-1: Evaluation of the electrical model at the cell level in the direct and reverse modes.

5.1. Proposed parameter estimation technique

The parameter estimation problem for each model presented in Section 3.5 was solved using Genetic Algorithms. Each step of the estimation process, explained in the following subsections, is related to the fitness function and the search space constraints, which must be accurately defined to avoid falling into a local minimum. A set of constraints must also be defined and determined by the search space of the parameters when modeling PV cells. The literature describes the search space for the SDM and DDM of PV cells [14, 157] to represent only Q_1. Those ranges can be applied to parameters common in the Bishop model and in the DRM; however, search ranges for the parameters that determine the behavior of PV cells in Q_2 are also required. In the DRM, these ranges can be obtained using information contained in the experimental data of the I–V curve.

5.1.1. Initial population

A set of p solution vectors is randomly generated within the search space (see Eq.(3-9)) to establish the current population Θ_{ini} as shown in the Eq. (5-1). Here, the size of the solution vectors depends on the number of parameters in each model (see Table **5-2**). All solution vectors in the initial population must be different to meet the diversity criterion. Then, the fitness function of each solution vector is evaluated and stored as shown in the Eq.(5-2), and the minimum value is selected as the *incumbent*.

$$\Theta_{ini} = \begin{bmatrix} \theta_1 \\ \theta_2 \\ \theta_3 \\ \vdots \\ \theta_p \end{bmatrix} \tag{5-1}$$

$$O.F.(\Theta_{ini}) = \begin{bmatrix} RMSE\left(I_{cell_e}(\theta_1), I_{cell_m}\right) \\ RMSE\left(I_{cell_e}(\theta_2), I_{cell_m}\right) \\ RMSE\left(I_{cell_e}(\theta_3), I_{cell_m}\right) \\ \vdots \\ RMSE\left(I_{cell_e}(\theta_p), I_{cell_m}\right) \end{bmatrix} \tag{5-2}$$

5.1.2. Selection

A section of the initial population, with a length given by a random integer (r), is chosen to generate a new population. Therefore, to complete this new population, $p - r$ solution vectors must be created (Θ_{adj}). Next, a pair of solution vectors, which are named parents, are selected for the crossover stage (see Figure **5-2**).

5.1.3. Crossover

In this stage, the two selected solution vectors are combined to produce new vectors called offspring, which the parents cross at a selected point. This will ensure that each offspring contains information from both parents. The crossover process is explained in Figure **5-3**.

5.1.4. Mutation

As can be seen in Figure **5-3**, two descendants were created, named $Offspring_1$ and $Offspring_2$. It is necessary to introduce some variation in both descendants (mutation), preserving the information inherited from their parents. Also, it is possible to decide whether or not the offspring will be mutated based on a randomized number that can take values of 0 or 1.

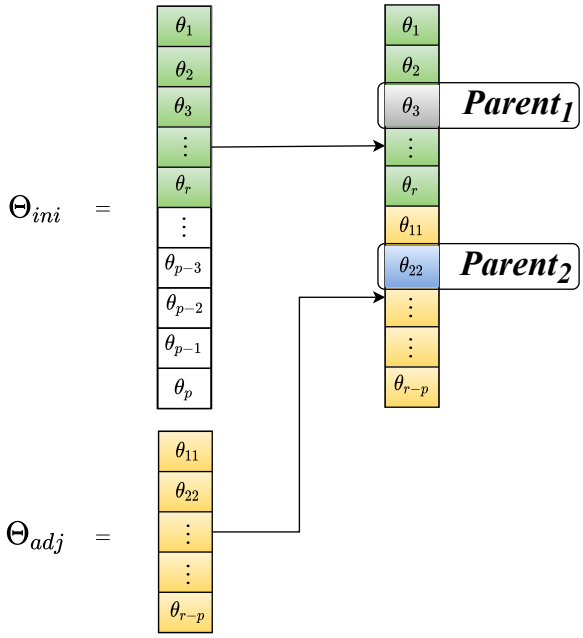

Figure 5-2: Selection process.

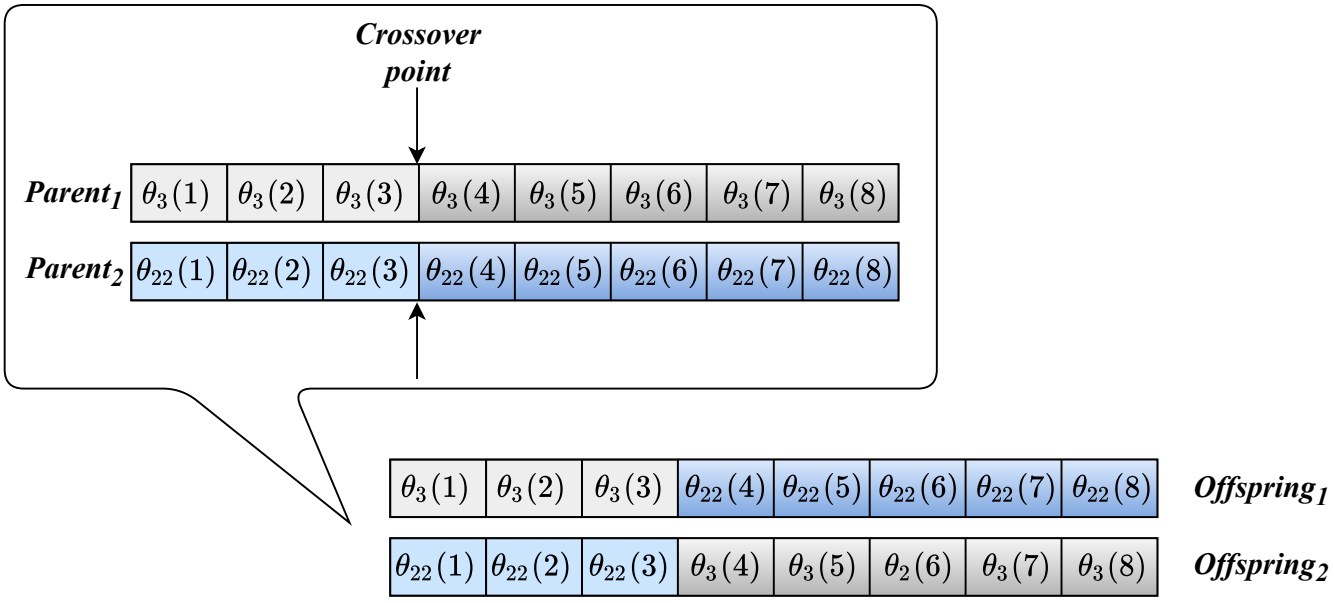

Figure 5-3: Crossover process.

If the value is 0, no mutation is performed; mutation occurs if it is 1. If the decision is to mutate the offspring, the parameter to be mutated is randomly selected and replaced by a random value within its search range. Figure **5-4** shows this process.

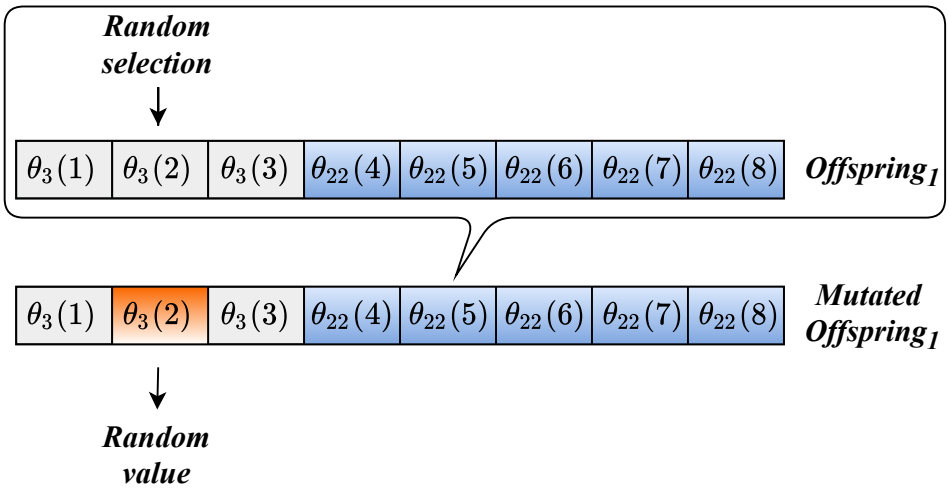

Figure 5-4: Mutation process.

5.1.5. Population update

The two mutated descendants must be evaluated in the model, to establish which is the best offspring, that is, the one with a lower value of $O.F.$

To update the population, the algorithm repeats the selection, crossover, and mutation processes until a set of p offspring is created.

The offsprings and the initial population are concatenated, creating a new group of size $2p$. Then, the new group is sorted according to the evaluation of their fitness function (smallest to largest). Only the first p solution vectors of the new group will be selected as the initial population of the next generation.

5.1.6. Stopping criterion

The stop criterion is the maximum number of iterations for the estimation process (itermax), called generations. Algorithm 2 presents the pseudocode of the GA described above.

5.1.7. Objective function (O.F.)

The objective function (**O.F.**) of the optimization problem addressed in this study is to minimize the root mean square error ($RMSE$) between the cell current measured in the experimental tests (I_{cell_m}) and the value estimated with the optimization technique, as shown in Eq. (3-7). $I_{cell_e}(\theta)$ is the cell output current and depends on the model used for its representation. For example, for SDM, it is presented in Eq. (3-1) and for the Bishop model in (3-3). In the case of DRM, only the parameters of the first quadrant will be estimated using Eq.(3-1). Table **5-2** provides the coding for the optimization problem discussed in this section; θ is the solution vector, which includes the model's unknown parameters to be

Algorithm 2: Pseudocode of GA applied to PV cell parameter estimation.

Data: Experimental $I-V$ data, p, $itermax$, θ^{min}, θ^{max}
Result: θ

```
iter=1;
Generate initial population Θ_ini;
Evaluate the O.F. and constraints;
Select the best solution;
while iter = 2 : itermax do
    for i = 1 : p do
        Select r vectors of initial population;
        Create p − r vectors randomly Θ_adj;
        Generate the new population by combining selected and created vectors;
        Select two parents randomly from the new population;
        Create offspring 1 and 2 by recombining parents;
        Mutate offspring;
        Evaluate offspring O.F.;
        Select the best offspring (min(O.F.));
        offspring population (i) =best offspring ;
    end
    New population= [initial population; offspring population];
    New Population sorted = Sort(New population (min to max O.F.)) ;
    Initial population= New Population sorted(1:p);
    Select the first position of New Population sorted as incumbent θ_inc;
end
```

identified. As mentioned earlier, the specific coding depends on the chosen PV model, as each model has different parameters.

Table 5-2: Optimization problem formulation for each model.

Model	$I_{cell_e}(\theta)$	**Parameters to estimate** (θ)	**Constraints**
SDM	(3-1)	$[I_{ph}, R_s, R_{sh}, I_0, n]$	**Eqs.** (5-7), (5-4), (5-5), (5-6), (5-3)
Bishop	(3-3)	$[I_{ph}, R_s, R_{sh}, I_0, n, V_{br}, m, a]$	**Eqs.** (5-7), (5-4), (5-5), (5-6), (5-3), (5-10), (5-9), (5-8)
DRM	(3-1) for Q_1	$[I_{ph}, R_s, R_{sh}, I_0, n]$	**Eqs.** (5-7), (5-4), (5-5), (5-6), (5-3)

5.1.8. Problem constraints

The restrictions of the optimization problem correspond to the search ranges of the parameters to be estimated, which are defined in equations (5-7), (5-4), (5-5), (5-6), (5-3), (5-10), (5-9), and (5-8). Those parameters correspond to the models reported in Section 3, where the search ranges should be respected to ensure a correct estimation of the parameters in each model as presented in Table **5-2**.

$$I_{ph_{min}} \leq I_{ph} \leq I_{ph_{max}} \tag{5-3}$$
$$R_{s_{min}} \leq R_s \leq R_{s_{max}} \tag{5-4}$$
$$R_{sh_{min}} \leq R_{sh} \leq R_{sh_{max}} \tag{5-5}$$
$$I_{0_{min}} \leq I_0 \leq I_{0_{max}} \tag{5-6}$$
$$n_{min} \leq n \leq n_{max} \tag{5-7}$$
$$V_{br_{min}} \leq V_{br} \leq V_{br_{max}} \tag{5-8}$$
$$m_{min} \leq m \leq m_{max} \tag{5-9}$$
$$a_{min} \leq a \leq a_{max} \tag{5-10}$$

5.2. Tuning of GA for each model

The I–V curve for the validation process was obtained using the procedure described in Chapter 4 applied to the A1 cell in the monocrystalline panel (mc-SI) (see Section 4.3). In this case, the I-V curve obtained has the electrical characteristics shown in Table **5-3**, and the panel was exposed to an irradiance of 1008 W/m^2 and a temperature of 47.8°C.

Table 5-3: Electrical characteristic from the I-V cell curve

Parameters	V_{mp}	I_{mp}	V_{oc}	I_{sc}
Value	0.37V	0.36A	0.50V	0.43A

Table **5-4** reports the constraints used to estimate the parameters of each model addressed in this study. Thus, the ranges in Table **5-4** were selected as search ranges; those values were taken from the literature [158, 159, 138, 139, 160, 140, 161, 162, 163]. The photovoltaic current (I_{ph}) was adjusted to a range of $\pm 10\,\%$ of the short-circuit current of the test (I_{sc}), this based on the fact that I_{sc} is caused by the generation and collection of light-generated carriers, therefore I_{sc} and I_{ph} are very close values.
The input parameters required for the GA, the number of individuals per population, and the maximum number of iterations were defined by evaluating the algorithm results in a range of $\{5, 70\}$ individuals per population and $\{500, 5000\}$ iterations. An example of this tuning is

Table 5-4: Parameter constraints.

Parameter	Minimum value	Maximum value
I_{ph} $[A]$	$90\,\% * I_{sc}$	$110\,\% * I_{sc}$
I_0 $[A]$	1×10^{-10}	1×10^{-7}
n	0.05	4
R_s $[\Omega]$	1×10^{-5}	2
R_{sh} $[\Omega]$	20	100
V_{br} $[V]$	-50	-10
m	2	8
a	1×10^{-3}	30×10^{-3}

shown in Figure **5-5**, where the SDM parameters were estimated. As observed in Figure **5-5**, there is an increase in the number of individuals per population and a decrease in the average value of the objective function with a decreasing number of iterations. Figure **5-6** shows the contour of the surface, which reports that the objective function reaches its minimum value with 65 individuals after 1500 iterations. The models were simulated in MATLAB® R2021a on a computer with an Intel Core i5–5200U 2.2GHz processor, 8GB of RAM, and Windows 10 pro. The results obtained with each model, which are presented in the next subsection, were contrasted with the I–V curve obtained experimentally.

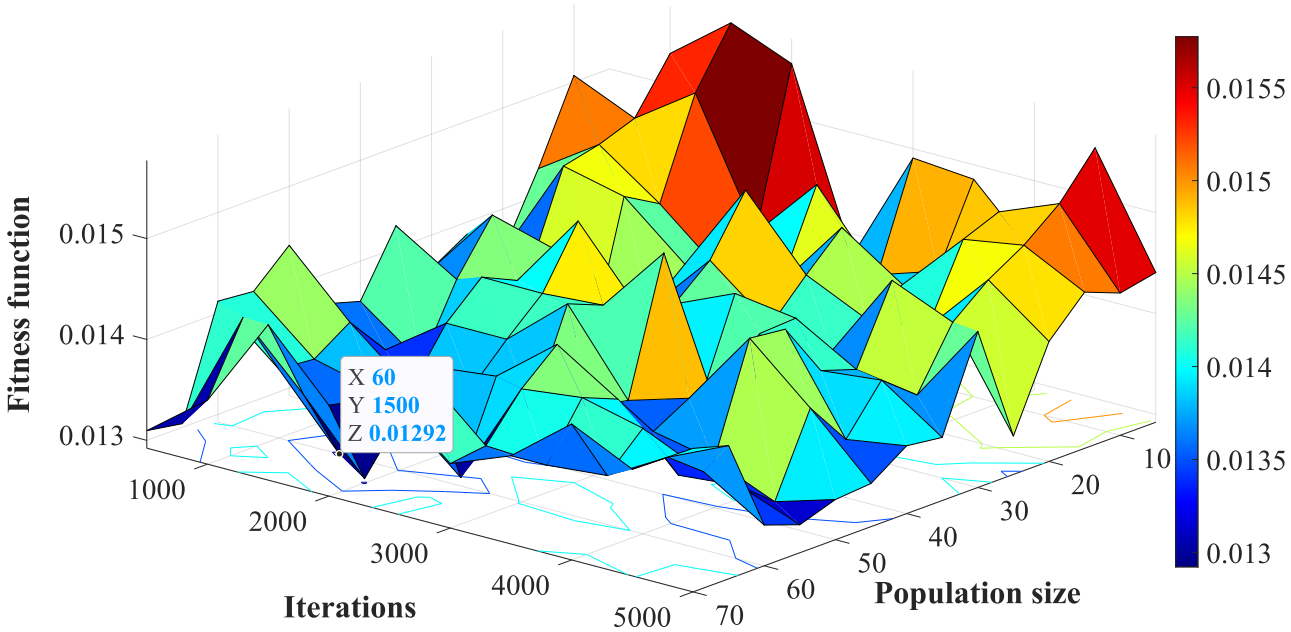

Figure 5-5: Selection of GA parameters for SDM: Mesh

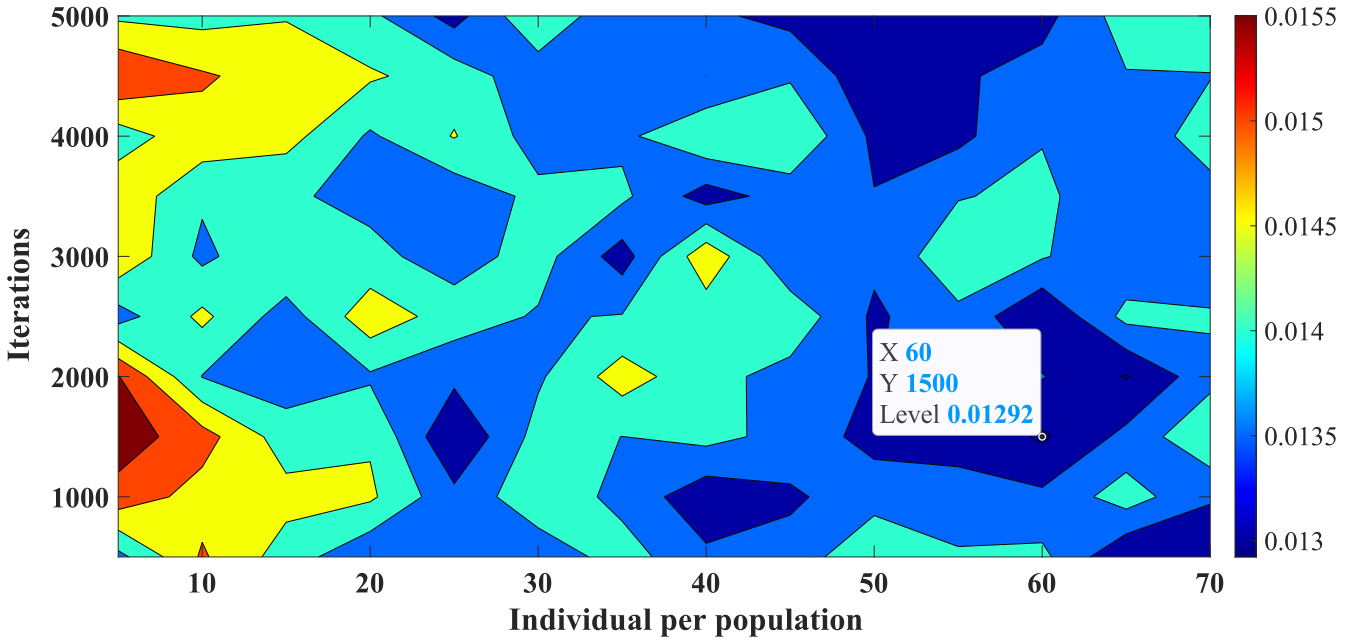

Figure 5-6: Selection of GA parameters for SDM: Contour

Parameter tuning was performed to determine the best number of individuals and iterations to estimate the parameters of each model; that is, they allow finding the smallest **O.F.** value. Table **5-5** shows the results of the tuning process for each model. Regarding the population size, Bishop's model requires only 5 individuals, a low value considering the values obtained for SDM and DRM. While the maximum number of iterations for the Bishop model and DRM is 500, the SDM requires triple that value. As Bishop's model will be evaluated considering the smallest population size and maximum iterations, the computation time is expected to be shorter than for the parameter estimation of the other models.

Table 5-5: Selection of GA variables for each model.

Model	Individual per population	Number of iterations
SDM	60	1500
Bishop	5	500
DRM	60	500

5.3. Estimation result

With the GA variables provided in Table **5-5**, and for each model, 100 repetitions of the parameter estimation algorithm (Algorithm 2) were performed for each model. To evaluate the repeatability of the solutions, the mean value and standard deviation of each estimated parameter of the SDM, Bishop model, and DRM were calculated. These metrics were also calculated for **O.F.**, the mean absolute percentage error (MAPE), and the computational time of each model, as reported in Table **5-6**. The calculation of MAPE is shown in (5-11). This metric is useful because provides a measure of relative error in percentage terms. Additionally, it penalizes both positive and negative errors evenly. However, it should be taken into account that the calculation of this metric can be amplified by small values in the denominator (zero or close to zero).

$$\textbf{MAPE} = \frac{1}{N}\sum_{i=1}^{N}\left|\frac{I_{cell_e}(i) - I_{cell_m}(i)}{I_{cell_m}(i)}\right| \tag{5-11}$$

Table 5-6: Parameters estimated for each model (mean ± standard deviation %).

Parameter	SDM	Bishop	DRM
I_{ph} [A]	$0.43 \pm 4.57\,\%$	$0.43 \pm 5.62\,\%$	$0.43 \pm 5.80\,\%$
I_0 [10^{-8} A]	$5.66 \pm 44.8\,\%$	$5.72 \pm 44.35\,\%$	$5.11 \pm 59.06\,\%$
n	$1.17 \pm 5.61\,\%$	$1.36 \pm 16.11\,\%$	$1.17 \pm 6.90\,\%$
R_s [Ω]	$0.21 \pm 40.97\,\%$	$0.61 \pm 63.05\,\%$	$0.26 \pm 46.45\,\%$
R_{sh} [Ω]	$47.40 \pm 18.48\,\%$	$58.01 \pm 28.60\,\%$	$51.87 \pm 51.21\,\%$
V_{br} [V]	$--$	$-24.58 \pm 37.22\,\%$	$--$
m	$--$	$-5.68 \pm 31.22\,\%$	$--$
a	$--$	$0.016 \pm 54.69\,\%$	$--$
RMSE	$0.026 \pm 35.81\,\%$	$0.047 \pm 37.36\,\%$	$0.032 \pm 40.73\,\%$
MAPE	$0.15 \pm 60.50\,\%$	$0.39 \pm 46.46\,\%$	$0.62 \pm 45.16\,\%$
Time [s]	$49.80 \pm 1.74\,\%$	$1.27 \pm 47.17\,\%$	$3.12 \pm 6.60\,\%$

According to Table **5-6**, the parameters I_0, R_s and R_{sh} have the highest standard deviation, although the mean values of RMSE and MAPE are considerably low for the three models. This showed the impact of the R_{sh} parameter on the zone near I_{sc}, which is the beginning of the Q_2 zone. The low computation time of Bishop's model implies that the tuning parameters of GA are suitable for the number of parameters to estimate. In the case of SDM, the computation time is higher since it has three times more iterations. A proper estimation of its parameters is a crucial task to ensure accurate parameter estimation in Q_2.

The DRM parameters in reverse mode, presented in Figure **3-8**, were estimated following the instructions provided in [83]. First, it was necessary to identify the zones that could be

linearized; in this case, the blue, red, and gray regions highlighted in Figure **5-7** are the zones to be linearized. Breakdown voltages V_{br1}, V_{br2}, and V_{br3} correspond to the points on the curve where a linear zone begins, that is, $0V$, $2.318V$ and $5.979V$, respectively. The values of the resistors ($R_1 = 90\Omega$, $R_2 = 40\Omega$ and $R_3 = 26.31\Omega$), which correspond to the slopes of the linear zones, were calculated through Ohm's law using the extreme points of the corresponding linear zone.

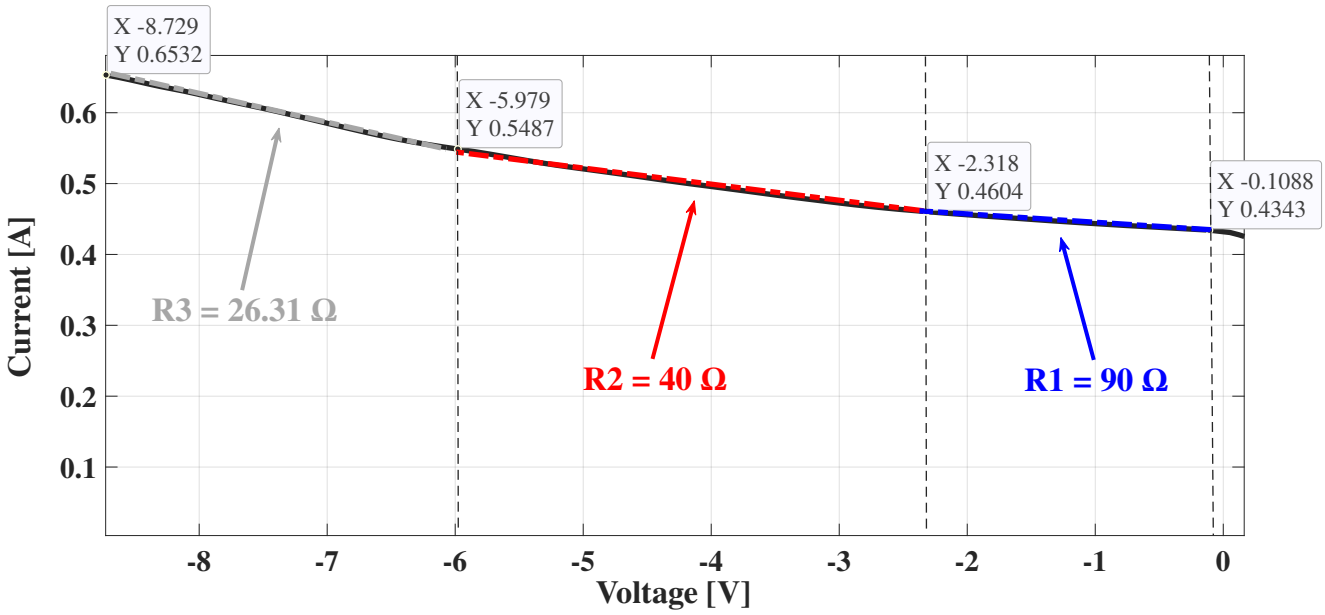

Figure 5-7: Estimation of DRM parameters for Q_2.

The circuit in Figure **3-8** was simulated in Simulink to obtain the I–V curve for the DRM. Then, an interpolation with the voltage vector of the experimental data was performed to compare the results of the cell current estimated by the DRM with those predicted by the SDM and Bishop model.

Figure **5-8** illustrates the I–V curves obtained with each model using the best population function results taken from Table **5-8**. In Q_1, the three models show high precision between the simulation and the experimental data. In Q_2, the Bishop model provides the best result, while the SDM and the DRM exhibit a decrease in accuracy.

The DRM accuracy depends on the linear zones chosen for the curve characterization, as well as on the precise calculation of the number of branches. Moreover, the estimation of the parameters that define the DRM model in the first quadrant is similar to the SDM, and those were estimated using only the information of the experimental I-V curve in the

first quadrant. Finally, these parameters also affect the behavior of the models in the second quadrant (Q_2).

In addition, it is observed that the estimation provided by the SDM did not have a good approximation in Q_2. This model presents a linear behavior for Q_2. Therefore, the breakdown voltage is not observed. Here, for the parameterization of this model, the whole information of the experimental I-V curve was used (Q_1 and Q_2). Table **5-7** presents the evaluation results of the error metrics for the estimation in Q_1, Q_2, and Q_1-Q_2. For the experimental I-V curve, there are 197 data, 129 corresponding to Q_1 and the remaining 68 to Q_2.

Table 5-7: Error metrics for the I-V curve reconstruction using the best solution.

Quadrant	Model	RMSE	MAPE
Q_1	**SDM**	0.0067	0.0695
	Bishop	0.0075	0.0292
	DRM	0.1618	0.5551
Q_2	**SDM**	0.0142	0.0223
	Bishop	0.0123	0.0209
	DRM	0.0332	0.0529
Q_1-Q_2	**SDM**	0.0099	0.0532
	Bishop	0.0094	0.0263
	DRM	0.1208	0.3228

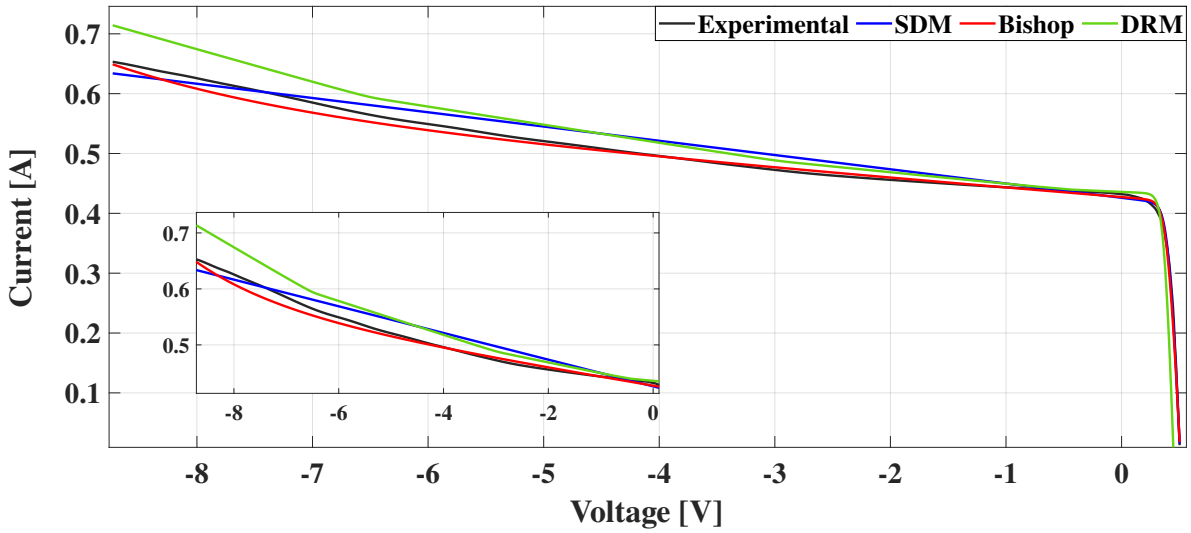

Figure 5-8: Comparison between the experimental and estimated curves in Q_1 and Q_2 (zoom-in for Q_2).

Table 5-8: Parameters used for the best solution.

Parameter	SDM	Bishop	DRM
I_{ph} [A]	0.41	0.43	0.42
$10^{-8} * I_0$ [A]	8.35	6.77	3.63
n	1.19	1.16	1.13
R_s [Ω]	0.14	0.15	0.15
R_{sh} [Ω]	41.82	49.92	26.13
V_{br} [V]	−−	−18.90	−−
m	−−	−3.53	−−
a	−−	0.02	−−
V_{br_1} [V]	−−	−−	0
R_1 [Ω]	−−	−−	90
V_{br_2} [V]	−−	−−	−2.31
R_2 [Ω]	−−	−−	40
V_{br_3} [V]	−−	−−	−5.97
R_3 [Ω]	−−	−−	26.31

Table **5-9** presents the relative percent error of the main points of interest, that is, I_{sc}, V_{oc}, and P_{mpp}. The three models show low error values in the estimation of P_{mpp}, making them suitable for applications where the delivered power needs to be estimated [164].
As observed in Figure **5-9**, the SDM and the Bishop model exhibit high accuracy for the representation of Q_1, especially at the Maximum Power Point (MPP), which is the most relevant point for power analysis (see Figure **5-10**). For the DRM, there is a significant difference in the estimation of V_{oc}, while the estimation of I_{sc} exhibits a lower difference. However, both differences affect the estimated location of the MPP compared to the one obtained in the experimental stage.

Table 5-9: Relative percent error of some points of interest in the I–V and P–V curves.

Parameter	SDM	Bishop	DRM
I_{sc} [A]	4.15	0.69	2.45
V_{oc} [V]	7.94	0.07	15.26
I_{mpp} [A]	13.45	5.61	14.22
V_{mpp} [V]	0	2.07	11.34
P_{mpp} [W]	2.66	0.43	4.01

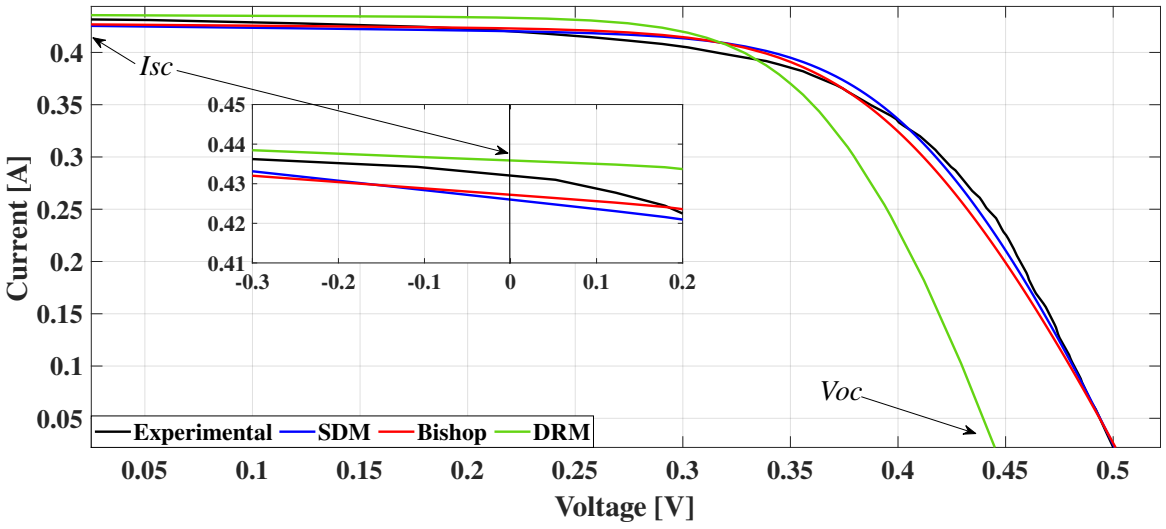

Figure 5-9: Comparison between the experimental and estimated curves (zoom-in for I_{sc}).

Figure **5-10** shows the power vs. voltage (P–V) curves obtained with each model near the MPP. The relative estimation errors for some important points in Q_1 are consolidated in Table **5-9**. In this case, the Bishop model and SDM provide the best results for MPP estimation based on the experimental data. The Bishop model exhibits the smallest estimation error of 0.43 %, while the error provided by SDM is 2.66 %. On the other hand, the DRM presents an error of 4.01 %, which is the highest deviation obtained.

Finally, Figure **5-11** shows the errors obtained for the best estimation of SDM, Bishop's model, and DRM. For Q_1, in terms of RMSE, the SDM provides the best result for I–V characterization, while for Q_2, the Bishop model exhibits the lowest error, comparing the results of RMSE and MAPE. Considering the estimation analysis of both quadrants, the best representation is given by the Bishop model, both from the RMSE and MAPE perspectives. It is important to clarify that 129 points were considered for Q_1 and 68 for Q_2, as a result of applying the procedure described in Section 4.3. In the case of DRM, the I–V characterization depends on the accurate estimation of the parameters in Q_1, which highlights the impact of R_{sh} as previously discussed. However, this model is analyzed because the parameters that represent the first quadrant are similar to those of the SDM model, so they can be taken from the literature, and the estimation of the parameters for the second quadrant is based on the calculation of the slope in each linearized section of the curve.

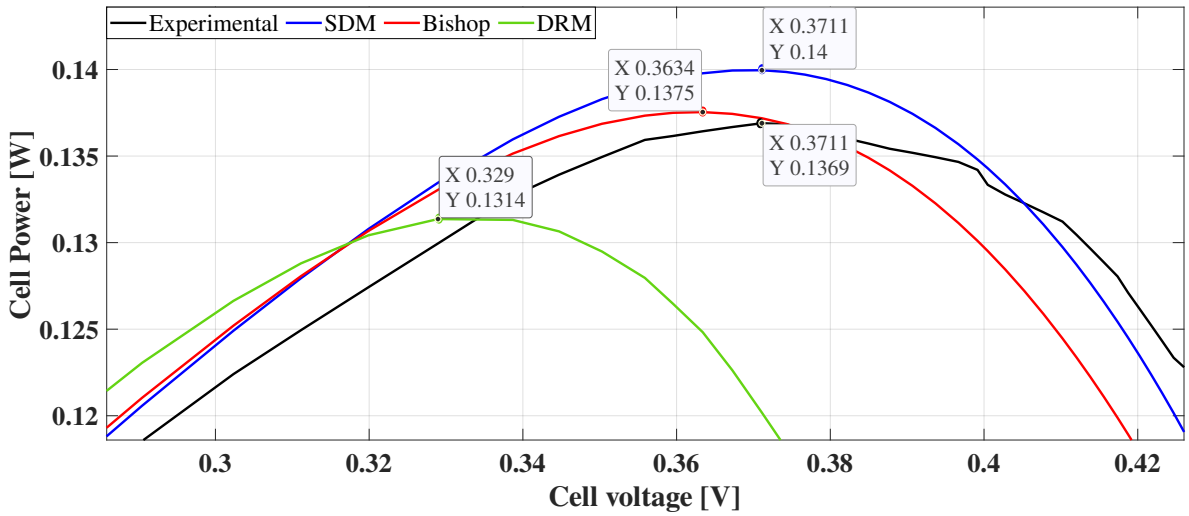

Figure 5-10: Maximum power point for each model.

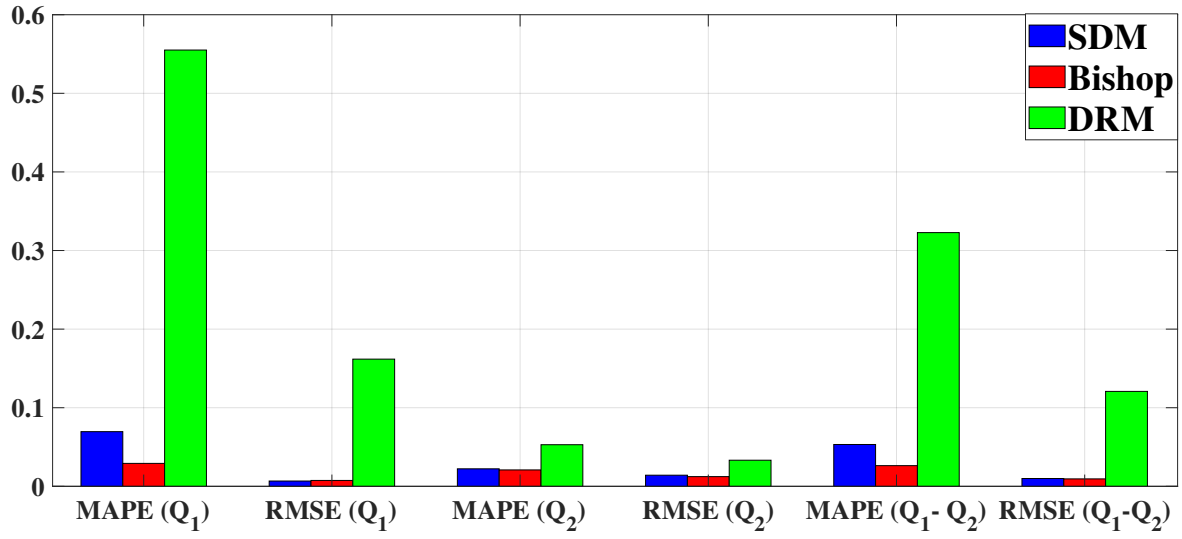

Figure 5-11: Discriminated errors by quadrant for each model.

5.4. Discussion

This section presented a simple strategy for I-V curve characterization of a PV cell considering three models. This proposed strategy uses GA and Simulink to extract the parameters from the experimental I-V curve. The analysis of the results demonstrated that the SDM model does not correctly reproduce the cell behavior when the current increases exponentially while the voltage at the cell terminals increases negatively (Q_2).

The parameter estimation of the DRM model was carried out in two stages. The first stage considers the parameters of the SDM model that has been widely studied in the literature. With respect to the second quadrant, the parameters can be easily calculated by linearizing the function in stages. However, the estimation of the parameters per quadrant has a negative influence on the accuracy of the model. When estimating the parameters of the first quadrant, exclusively using the experimental information related to that quadrant, the critical parameter R_{sh} is not correctly identified, which is one of the parameters that impose the behavior in the second quadrant. Moreover, the results reveal the need for a mathematical formulation that allows the whole set of parameters to be estimated for this particular model. Here, this procedure was developed with the evaluation of the circuital model in Simulink, which required the estimation of the five parameters for Q_1 described in Table **5-2**, and the calculation of the parameters for Q_2 (see Figure **5-7**), independently.

It is also important to highlight that the proposed procedure can be used, along with PV array modeling methodologies, to analyze the behavior of cells operating in both Q_1 and Q_2, which is needed for power analysis and loss estimation during partial shading conditions. Future works could consider estimating the energy per day, month, or year using the electrical representation described for the PV cell modeling. Also, another future work could consider applying other optimization techniques to solve the parameter estimation problem, which may reduce both estimation errors and computation time.

Finally, this contribution was published in the following journal paper: Restrepo-Cuestas, B.J.; Durango-Flórez, M.; Trejos-Grisales, L.A.; Ramos-Paja, C.A. "Analysis of Electrical Models for Photovoltaic Cells under Uniform and Partial Shading Conditions." Computation 2022, 10, 111. This article can be found on the publisher's website at `https://www.mdpi.com/2079-3197/10/7/111`. The journal's homepage is located at `https://www.mdpi.com/journal/computation`, and the publisher's copyright information can be found at `https://www.mdpi.com/journal/computation/about`.

6 Proposed methodology for estimation of Bishop model parameters

Optimization techniques have been widely used for estimating the parameters of cells or photovoltaic modules primarily for the SDM or the DDM. However, those models do not represent the behavior of the cell in the second quadrant in a proper way. Although, the Bishop model improves the representation of the behavior of the cell in the second quadrant, procedures for estimating its parameters are not reported in the literature. Most of the works concerning PV cell or arrays analysis based on the Bishop model, adopt the parameters from other studies previously reported. Therefore, in this chapter, a methodology to estimate the parameters of the Bishop mathematical model to represent a PV cell, in both the first and second quadrants, is proposed. Because of the high number of parameters to be identified and the implicit, and non-linear, relationship between the output current and voltage of the Bishop model, an optimization approach based on a Chu-Beasley genetic algorithm is used. Genetic algorithms are the most widely used optimization technique in the parameter estimation of photovoltaic systems [55, 56, 54]. This technique presents an advantage in execution time due to its advanced criterion. In this chapter, a variation of the Chu-Beasly algorithm is proposed, which selects the descendant randomly in each iteration, avoiding the evaluation of **O.F.** for each generated offspring.The reduction in computing time is an important advantage since this model could also be adjusted and used in the diagnosis of panel failures, degradation analysis, and estimation of power losses due to partial shading.

The parameter estimation methodology of the Bishop model was established using a comparison between two estimation scenarios. The first scenario is based on the information found in the literature review; that is, the parameters for Q_2 are not estimated, but rather the values of the parameters most commonly found in the literature are used. Regarding the parameters associated with the SDM (n, R_s, R_{sh}, I_0, I_{ph}), it is possible to find defined ranges for different cell technologies in the literature. However, the parameters' ranges that affect the second quadrant behavior (a, m, and V_{br}) have not been extensively studied; therefore, those ranges will be described in Section 6.3.1. While for Q_1, the estimation of the set of parameters of θ_{SDM} is made using only the experimental values of voltage and current of the cell in the first quadrant (see Table **6-1**).

The second scenario evaluates the behavior of the Bishop model when the complete set of its parameters is estimated (θ_{BM}). In this case, the experimental values of cell voltage and current in both Q_1 and Q_2, are used (see Table **6-1**).

Both estimation stages use Eq. 3-8 as the fitness function, and are validated using the I-V curves of two PV cells (mc-SI and pc-SI). For each case, the repeatability of the estimation response was evaluated using the parameters mean value and standard deviation after running the estimation process 100 times. Also, the **O.F.**, the computation time, and some evaluation of accuracy metrics, such as RMSE, MAPE, and MBE (mean bias error), were used to compare the behavior of both estimation scenarios. A summary diagram of the methodology proposed in this chapter is presented in Figure **6-1**.

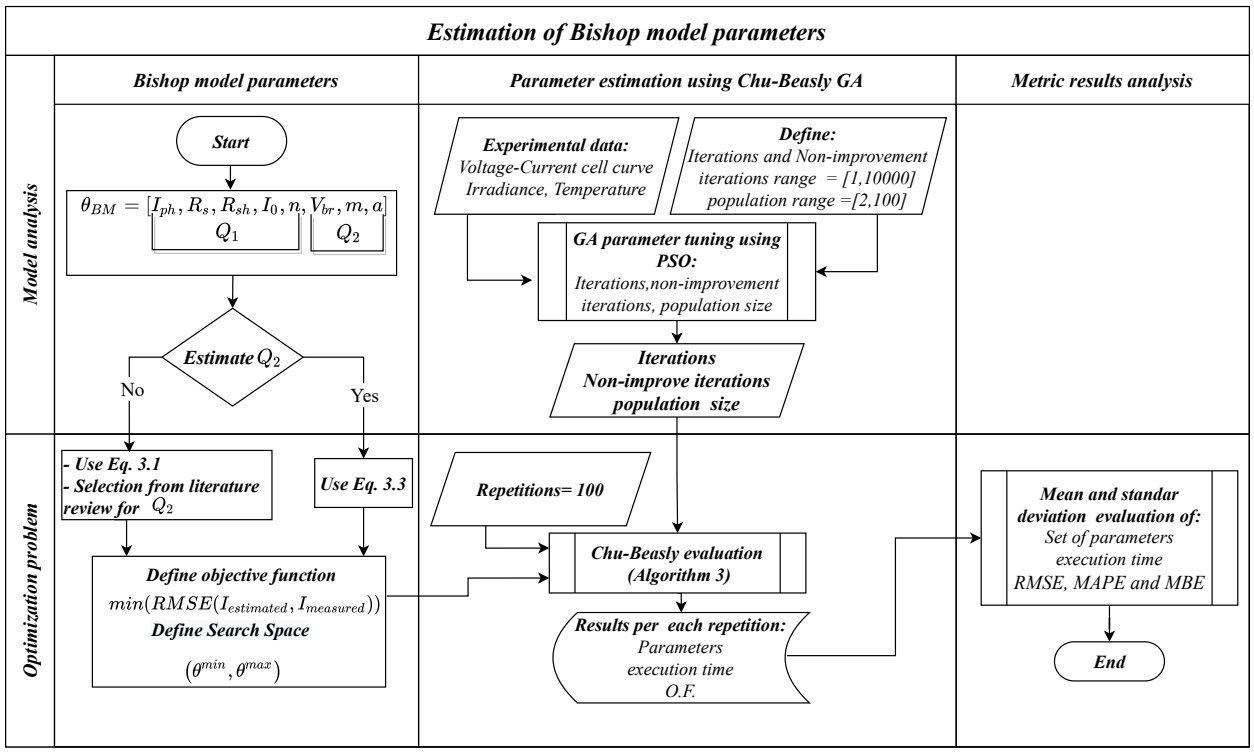

Figure 6-1: Evaluation of the electrical model at the cell level in the direct and reverse modes.

Table 6-1: Detailed information for each estimation stage.

	Stage 1	**Stage 2**
$I_{cell_e}(\theta)$	Eq. (3-1)	Eq. (3-3)
Parameters to estimate (θ)	$\theta_{SDM} = [I_{ph}, R_s, R_{sh}, I_0, n]$	$\theta_{BM} = [I_{ph}, R_s, R_{sh}, I_0, n, a, V_{br}, m]$
Parameters from literature	$\{a, V_{br}, m\}$	–
I-V curve information	Q_1	$Q_1 - Q_2$
Set of constraints	Eqs. (5-7), (5-4), (5-5) (5-6), (5-3)	Eqs. (5-7), (5-4), (5-5), (5-6) (5-3),(5-10), (5-9), (5-8)

6.1. Chu–Beasley Genetic Algorithm applied to the problem of parameter estimation

The Chu-Beasley algorithm is a modified version of the basic genetic algorithm. Its main characteristic is to replace a single individual in the population in each generation. This individual must meet both the diversity and feasibility criteria; that is, it must be different from the others that form the population and respect the variable search ranges that define the problem [165]. From the optimization problem defined in Section 3.5, through the equations (3-7), and (3-8), the procedure for parameter estimation using the Chu-Beasly algorithm will be explained. This chapter proposes two stages to solve that problem: (1) estimation of the SDM parameters and (2) estimation of Bishop parameters that can be used to represent the cell-level PV profiles in the first and second quadrants, where the GA is used to find the optimal parameter estimation. This technique employs the same stages presented in Subsection 5.1:

- Generation of the initial population Θ_{ini}, conformed by p solution vectors. Each solution, called individual, has a length equal to the number of parameters to be estimated. Each individual is generated randomly, respecting the search range of each parameter as shown in Eq. 3-9. All individuals must be evaluated to obtain their **O.F.** and select as incumbent the lower valuable. Here, the population constitutes a different set each time the algorithm is run. In this way, it is desired to reach the neighborhood of the global minimum, taking different paths in each solution, understanding that a good solution will be achieved that may not always be the same.

- Iterative generation of descendants:
  - Selection of two different parents randomly from Θ_{ini} (see Figure **6-2**). To achieve this, the function $randperm(p, 2)$ from Matlab was used. This function selects 2 unique integers that represent the position of parents, selected randomly from 1 to p.
  - Obtain the offspring with a crossover of the parents information, selecting a crossover point. The function *randi* from Matlab allows generating a value, with random integers uniformly distributed in a predefined interval, which is used to obtain the crossover point.This stage produces two descendants. An example of the crossover stage can be seen in Figure **5-3**.
  - To define if the mutation is performed, a randomized number that can take values of 0 (for not mutate) or 1 (to mutate) is used. If the mutation is decided, the parameter to be mutated is randomly selected and replaced by a random value within its search range (see Figure **5-4**). This process applies to the two descendants created in the crossover stage.

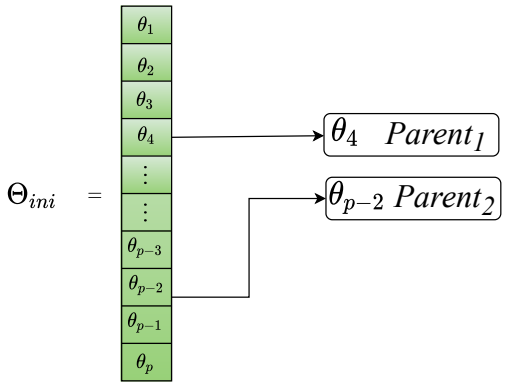

Figure 6-2: Selection stage in GA estimation

- The descendant that will continue the process is also randomly selected. Once it is selected, its objective function is evaluated.
- The selected descendant must achieve the diversity criterion. If this condition is fulfilled, in the parent update stage, this descendant will replace the worst parent in the initial population (i.e., the one with the highest **O.F.**). Then, the new population is sorted according to the O.F. value (lowest to highest). If this new individual has the best **O.F.** in the entire population, it will replace the incumbent. At this point, a generation has ended.

- The iterative process continues (generations) until one of the two stopping criteria is met: (1) a maximum number of iterations to be evaluated in the estimation process ($iter_{max}$) and (2) a maximum number of consecutive iterations in which the incumbent is not improved ($iter_{nmax}$).

Finally, Algorithm 3 shows the pseudocode implementation of the GA used for the parameter estimation of the Bishop model.

6.2. Summary of the proposed procedure

The proposed methodology for estimating the parameters of a photovoltaic cell, considering the behavior in both the first and second quadrants, is summarized in the following stages (see Figure **6-3**):

6.2.1. Experimental analysis

For the analysis contemplated in this chapter cell current and voltage information is required. Therefore, the procedure described in Section 4.3 was applied. In the direction of analyzing the behavior of the curves for both panel technologies, were selected cell A1 of the mc-SI

Algorithm 3: Pseudocode proposed for Chu-Beasly GA.

Data: Experimental $I-V$ data, p, $iter_{max}$, $iter_{nmax}$, θ^{min}, θ^{max}
Result: θ

```
iter=1;
Generate initial population Θ_ini randomly (according to θ^min, θ^max);
Evaluate O.F. for Θ_ini;
Sort Θ_ini according to O.F. (lower to higher);
Select the best solution (min O.F.);
while iter = 2 : itert_max do
    Select two parents randomly from the initial population;
    Select one crossover point randomly;
    Create two descendants by recombining parents at crossover point;
    Define randomly Mutate between 0 and 1;
    if Mutate==1 then
        Select parameter to mutate in both descendants;
        Select a random value of the parameter in its range;
    else
        Do not mutate offspring
    end
    Randomly select the descendant of the generation;
    Evaluate the selected descendant O.F.;
    Replace the parent with the highest O.F. value with the selected descendant in
     Θ_ini;
    Sort Θ_ini according to O.F. (lower to higher);
    if The best solution was updated==1 then
        iter_nmax = 0
    else
        iter_nmax = iter_nmax + 1
    end
    if Was any stopping criteria met? then
        Finish the estimation process;
        Print results;
        Break;
    else
        Continue;
    end
end
```

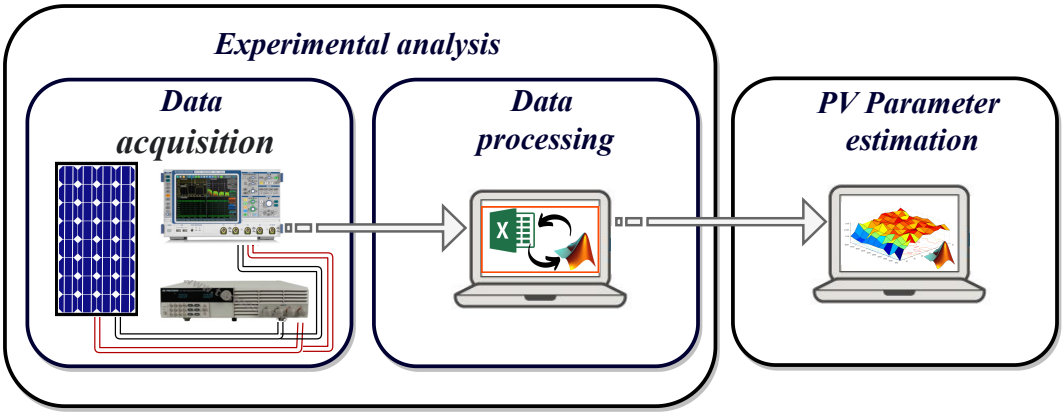

Figure 6-3: Evaluation of the electrical model at the cell level in the direct and reverse modes.

panel and cell A2 of the pc-SI panel (see Figure **4-9**). The irradiation and temperature conditions at which the data were acquired are stated in Table **4-8**, and some points of interest for both curves are listed in Table **4-3**.

6.2.2. PV parameter estimation

The estimation of Bishop's model parameters requires, in addition to the curves of the experimental stage, the definition of the search ranges for each parameter depending on the cell technology under analysis. In this work, a range is proposed for the technologies used in the tests (mc-SI and pc-SI); however, it is required to establish new search ranges for cells with different technologies.

Then, it is possible to use an optimization technique to solve the PV parameter estimation problem. This work adopts the Chu-Beasly GA (see Section 6.1), which requires some adjustment parameters such as the number of maximum iterations $iter_{max}$, the number of maximum non-improvement iterations $iter_{nmax}$, and the population size p. Therefore, the PSO algorithm was used to find the value for each of these parameters, which allows the best behavior of the genetic algorithm.

It is necessary to clarify that the entire estimation process was coded in Matlab, without using any Genetic or optimization toolboxes, which provides complete control of its operations and access to the internal variables to improve its performance. Since the function that relates the cell voltage and current in the Bishop model is implicit, its evaluation is carried out through the Newton-Raphson technique (see Algorithm 1).

The behavior of the estimation process is validated through its evaluation for a considerable number of repetitions of the process, in this case, 100 repetitions were performed. With this information, it is obtained some of the accuracy metrics associated with the estimation of each parameter: the evaluation of the objective function, the computational time, and some

other error measures.

6.3. Estimation stages

6.3.1. Estimation of the Q_1 parameters (stage 1)

In the first stage of the parameter estimation, the five parameters that define the behavior of the curve in the first quadrant (R_s, R_{sh}, I_{ph}, I_0 and η) were calculated. The ranges in Table **6-2** were taken from the literature [158, 159, 138, 139, 160, 140, 161]. The photovoltaic current (I_{ph}) was adjusted to a range of $\pm 5\,\%$ of the short-circuit current of the test (I_{sc}). This value depends directly on the short circuit current, which in turn is linked to the irradiation of the test, so it will always be necessary to adjust said range, according to the cell technology used.

Table 6-2: Ranges for the estimation of parameters in the first quadrant.

Limits	n	R_s [Ω]	R_{sh} [Ω]	I_0 [A]	I_{ph} [A]
Min	0.05	1×10^{-5}	5	1×10^{-10}	$95\,\% \times I_{sc}$
Max	4	2	500	1×10^{-7}	$105\,\% \times I_{sc}$

The Chu-Beasly GA is adjusted to obtain the best solution in terms of the objective function. In other words, it is necessary to implement another optimization algorithm to obtain the parameters that best fit the minimization of the problem. This was achieved by implementing the PSO algorithm due to its simplicity and fast convergence [166, 167]. The following parameters are used as tuning values: population size (individuals or particles) with a search range of $\{2, 100\}$, number of iterations (maximum iterations allowed in the GA) with a search range of $\{1, 10000\}$, and number of non-improvement iterations (this determines the point at which the algorithm stops performing convergence or minimizing the objective function) with a search range of $\{1, 10000\}$. The results obtained from this tuning process were $p = 11$, $iter_{max} = 8761$, and $iter_{nmax} = 4061$.

As part of the estimation process, the technique was evaluated 100 times per cell to analyze metrics such as the mean value and standard deviation for each estimated SDM parameter and also for **O.F.** (see Table **6-3**). Table **6-4** presents the results of some metric errors such as RMSE, MAPE, and the mean bias error (MBE). MBE provides a direct measure of the estimation bias (see (6-1)). The results show a slight deviation for the RMSE metric, used as an objective function, but this deviation is relatively high for MBE, especially for Cell 2. This may be a result of this metric not considering magnitude. That is, it is possible to obtain both positive and negative error values, which causes the standard deviation of the data to increase. In general, the three metrics present small mean values, which ensured a high accuracy on the I–V curves reproduction.

As indicated in Table **4-1**, the shortcircuit current of the panels that were used for the tests in this chapter is 0.69A. In this case, the cell that is the object of study was shaded 50 % of its area with a solid shadow, so the short circuit current of the shaded cell will decrease considerably. This current is expected to be less than the short circuit current of the module so that second quadrant shaded cell operation can be experienced.

$$\mathbf{MBE} = \frac{1}{N}\sum_{i=1}^{N}\left(I_{cell_e}(i) - I_{cell_m}(i)\right) \tag{6-1}$$

Table 6-3: Ranges of parameters estimated for the SDM model (mean ± standard deviation).

Parameter	**Cell 1 (mc-SI)**	**Cell 2 (pc-SI)**
I_{ph} [A]	$0.43 \pm 0.17\,\%$	$0.32 \pm 0.24\,\%$
I_0 [A]	$9.29 \times 10^{-8} \pm 23.01\,\%$	$9.12 \times 10^{-8} \pm 23.69\,\%$
n	$1.18 \pm 3.23\,\%$	$1.29 \pm 2.77\,\%$
R_s [Ω]	$0.12 \pm 3.41\,\%$	$0.08 \pm 4.57\,\%$
R_{sh} [Ω]	$15.05 \pm 2.07\,\%$	$485.06 \pm 14.36\,\%$
O.F.	$3.40 \times 10^{-3} \pm 7\,\%$	$8.10 \times 10^{-3} \pm 1.69\,\%$
Time [s]	$2.49 \times 10^{3} \pm 112\,\%$	$1.34 \times 10^{3} \pm 78.3\,\%$

Table 6-4: Accuracy measures for estimation with the SDM model (mean ± standard deviation).

Accuracy measures	**Cell 1 (mc-SI)**	**Cell 2 (pc-SI)**
RMSE	$0.003 \pm 7\,\%$	$0.008 \pm 1.6\,\%$
MAPE	$0.014 \pm 10.6\,\%$	$0.28 \pm 1.93\,\%$
MBE	$-1.6 \times 10^{-5} \pm 100\,\%$	$-2.8 \times 10^{-6} \pm 1559\,\%$

Analyzing Cell 1 (mc-SI), the highest relative deviations were found in I_{sat} with 23.3 %. Concerning Cell 2 (pc-SI), the highest relative deviations were found in parameters I_{sat} and R_{sh}, with 23.3 % and 14 %, respectively. Instead, the other parameters, for both cells, exhibited variations under 5 %. The mean RMSE of Cell 1, evaluated as the objective function, was lower than the value obtained for Cell 2; however, the relative deviations for Cell 2 were lower than in the case of Cell 1.

Figures 6.4(b) and 6.5(b) present the convergence of a sample of repetitions of the estimation algorithm. Both figures show that, starting from different initial values and arriving at similar values of **O.F.**

The best and worst solutions provided by the 100 estimations were also analyzed and compared based on the value of the objective function provided by the GA. Table **6-5** presents the sets of parameters that provide each cell's best and worst performance for the SDM. Furthermore, Figures 6.4(a) and 6.5(a) show the comparison between the I-V curves estimated with the best parameters and the experimental data for Cells 1 and 2, respectively. Those figures show a satisfactory reproduction of the I-V curve first quadrant using the SDM parameters obtained with the proposed GA. The most significant differences are presented in I_{ph} and R_{sh}, comparing the parameters of both cells.

Table 6-5: Sets of parameters of the best and worst solutions for the SDM of each PV cell.

Parameter	**Cell 1 (mc-SI)**		**Cell 2 (pc-SI)**	
	Best	**Worst**	**Best**	**Worst**
I_{ph} [A]	0.43	0.42	0.32	0.33
I_0 [A]	1×10^{-7}	4×10^{-9}	3.96×10^{-9}	9.99×10^{-8}
n	1.20	0.99	1.07	1.3
R_s [Ω]	0.12	0.15	0.1	0.08
R_{sh} [Ω]	15	15	92.14	67.07
O.F.	0.003	0.004	0.007	0.008
Time [s]	6.2×10^3	6.1×10^3	170.6	39.97

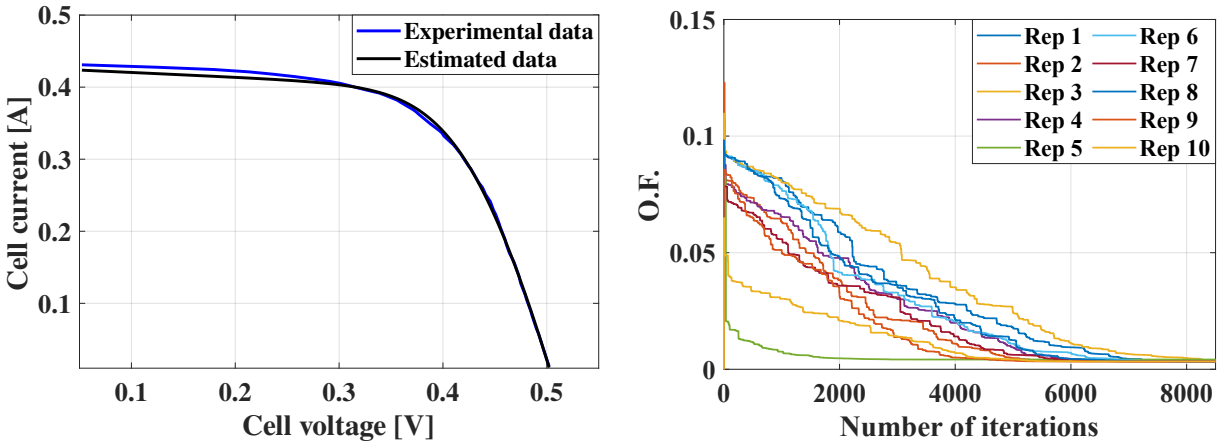

(a) (b)

Figure 6-4: Parameter estimation results for Cell 1 (mc-SI) using the SDM model: 6.4(a) Comparison of I-V curves using the best solution, 6.4(b) convergence results for a sample of 10 repetitions

To reproduce the second quadrant of the I-V curve, an exhaustive search was carried out in the literature to find the parameters of the Bishop model used for PV cells, modules, or

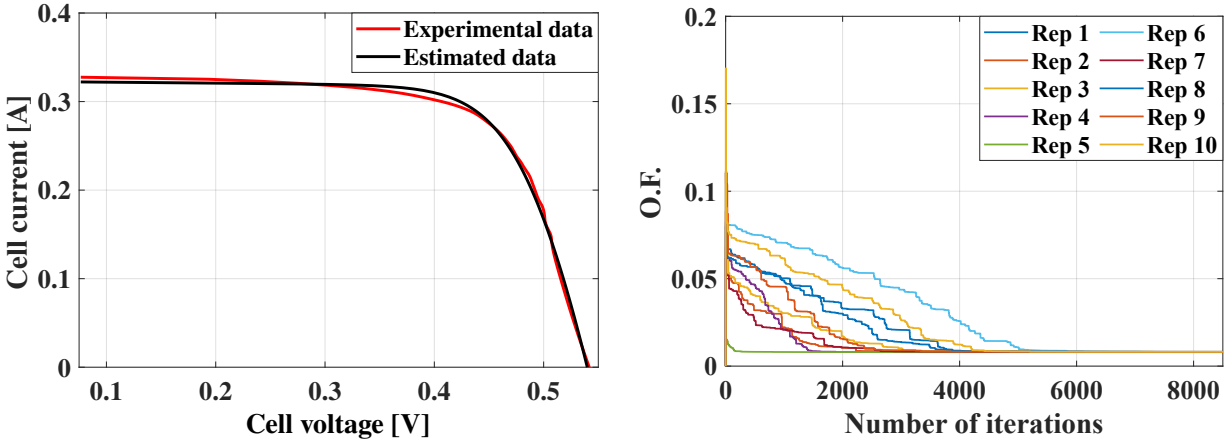

(a) (b)

Figure 6-5: Parameter estimation results for Cell 2 (pc-SI) using the SDM mode: 6.5(a) Comparison of I-V curves using de best solution, 6.5(b) convergence results for a sample of 10 repetitions

panels. This literature review confirmed that second-quadrant studies are commonly performed using parameters similar to those proposed in [23], with minor variations. It was found that the works define the parameters such as the breakdown voltage of the semiconductor junction (V_{br}), the fraction of ohmic current involved in avalanche breakdown (a), and the avalanche breakdown exponent (m) [23, 22, 105, 112, 106]. In some other cases, (a) and (m) are defined as constants [107, 168, 25, 21] or adjustment coefficients [31, 169]. Furthermore, only a few studies have reported the procedure to obtain these parameters. Table **6-6** lists some of the second quadrant studies found in the literature, the values adopted for the second quadrant parameters, the technology of the cell under study, and the source from which the parameters were adopted; in Table N.I. means the information is not indicated in the reference.

The most commonly adopted values in the literature for the parameters of the second quadrant, observed in Table **6-6**, are $a = 2 \times 10^{-3}$, $m = 3$, and $V_{br} = -28V$ for Cell 1 and $V_{br} = -26V$ for Cell 2. Using those values to estimate the behavior of both experimental cells (Cell 1 and Cell 2) through the Bishop model, leads to the results reported in **6-7**. Table **6-7** includes these values and also contains the MAPE and MBE metrics. The table shows how all metrics grow consistently with respect to metrics of the parameter estimation of the SDM model. Here the RMSE values increase considerably compared to the values obtained in Table **6-5**. Observing the set of parameters that provide the best solutions in both cases, the most considerable changes can be observed in I_{sat} and R_{sh}.

Figures 6.6(a) and 6.6(b) show the I-V reproduction for Cell 1 and Cell 2, respectively, when the best set of parameters are used in the Bishop model (see Table **6-8**). Both Figures show

Table 6-6: Values of the Bishop model parameters for the second quadrant.

Reference	a	V_{br} [V]	m	**Cell technology**	**Parameters source**
[23]	2×10^{-3}	-15	3.7	mc-SI	ESTI data base
[168]	2×10^{-3}	-20	3	N. I.	N. I.
[107]	2×10^{-3}	-15	6	N. I.	N. I.
[103]	0.1	-14	2	N. I.	N. I.
[25]	2×10^{-3}	-21.29	3	N. I.	N. I.
[114]	2×10^{-3}	-21.29	3	N. I.	[25, 168]
[22]	0.35	-15	3.8	mc-SI	N. I.
[105]	0.1	-20	3	N. I.	N. I.
[112]	2×10^{-3}	-15	3	N. I.	N. I.
[21]	2×10^{-3}	-15	3	N. I.	[107]
[106]	1×10^{-2}	-14.4	3	N. I.	N. I.
[31]	0.1	-10 V to -30	3.4 to 4	mc-SI and pc-SI	N. I.
[169]	0.1	-10	1.1	mc-SI	N. I.

Table 6-7: Accuracy measures for estimation for the Bishop model using the SDM parameters (mean $\pm$ standard deviation).

Accuracy measures	**Cell 1 (mc-SI)**	**Cell 2 (pc-SI)**
RMSE	$0.15 \pm 2.84\,\%$	$0.024 \pm 9.76\,\%$
MAPE	$0.15 \pm 2.30\,\%$	$0.23 \pm 2.31\,\%$
MBE	$-8.3 \times 10^{-2} \pm 2.83\,\%$	$9.4 \times 10^{-3} \pm 37.68\,\%$

a wrong reproduction of the second-quadrant behavior of real PV cells under real operation conditions. The RMSE values of cells 1 and 2 were 0.1512 A and 0.0149 A, respectively, much higher than the RMSE obtained in the first quadrant.

In Figures 6.6(a) and 6.6(b), it is possible to observe that although Bishop's model is used to represent the behavior of PV cells, its fitting is not correct in the second quadrant. Indeed, the estimated I-V curves do not present a shape similar to that of the experimental curves. Furthermore, as the negative voltage increases, the difference between the estimated and experimental curves becomes noticeable. The main reason is that the estimation includes only information from the first quadrant to find the SDM parameters.

Therefore, this test is evidence of the need to also estimate the parameters of the second quadrant instead of adopting the values reported in [23] for any condition. The following subsection addresses such a second estimation stage.

Table 6-8: Sets of parameters of the best and worst solutions for the Bishop model using SDM results of each PV cell.

Parameter	Cell 1 (mc-SI)		Cell 2 (pc-SI)	
	Best	**Worst**	**Best**	**Worst**
I_{ph} [A]	0.42	0.43	0.32	0.33
I_0 [A]	9.99×10^{-8}	9.99×10^{-8}	9.99×10^{-8}	9.99×10^{-8}
n	1.20	1.20	1.30	1.30
R_s [Ω]	0.13	0.13	0.08	0.08
R_{sh} [Ω]	17.52	15	243.151	67.07
a	2×10^{-3}	2×10^{-3}	2×10^{-3}	2×10^{-3}
m	-3	-3	-3	-3
V_{br} [V]	-28	-28	-26	-26
O.F.	0.11	0.15	0.01	0.04
Time [s]	38.22	46.28	38.72	39.97

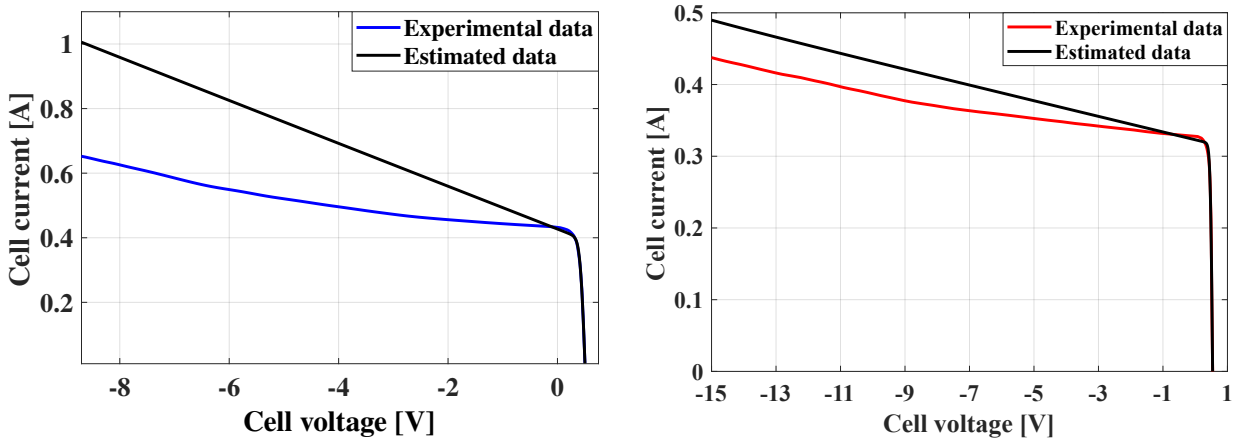

(a) (b)

Figure 6-6: Comparison of I-V curves using the Bishop model with the parameters of the SDM estimation and: 6.6(a) Cell 1 (mc-SI) $a = 2 \times 10^{-3}$, $m = 3$, $V_{br} = -28$ V, 6.6(b) Cell 2 (pc-SI) $a = 2 \times 10^{-3}$, $m = 3$, $V_{br} = -26$ V

6.3.2. Estimation of the Bishop model parameters (stage 2)

The second estimation stage was carried out for the two cells with different technologies previously described (Cell 1 and Cell 2) to observe variations in the parameters of the second quadrant. In this case, in addition to the search ranges defined in Table **6-2**, the ranges of parameters a, V_{br}, and m were also defined. Generally, the literature takes the information presented in Bishop regarding these three parameters. The only range that

Bishop establishes is for the avalanche exponent m, which can vary between 3 and 4. However, once the estimation stage began, it was noticed that some of the parameters collided at the limits of the search range. So, it was necessary to expand these ranges. The information in Table **6-6** was considered to define the search ranges of the variables a, m, and V_{br}. These additional ranges were obtained by analyzing the impact of each parameter on the I-V curve in the second quadrant. This procedure was carried out using simulations of the Bishop model, verifying which values allowed a reconstruction of the I-V curve close to the experimental ranges obtained from the real cells. Subsequently, the validation of the established parameter ranges was carried out by analyzing the results in the estimation stage. These new parameter ranges are detailed in Table **6-9**.

Table 6-9: Ranges for parameter estimation in the second quadrant.

Limits	a	V_{br} [V]	m
Min	2×10^{-3}	-50	2
Max	15×10^{-3}	-20	6

In this case, the results of PSO sintonization gave as results $p = 14$, $iter_{max} = 9709$, and $iter_{nm} = 1261$ for the GA parameters. With the parameters defined for the GA, the estimation of the Bishop model was repeated 100 times. Table **6-10** reports the variations in the model parameter estimation. Furthermore, Table **6-11** presents the parameters that provide the best and worst estimations obtained in 100 repetitions. The results show a lower execution time for the worst solution for Cell 1 and Cell 2. Since a maximum number of non-improvement iterations has been defined, it is possible that, in these cases, the algorithm has fallen into a local minimum. The electrical variables were acquired with the R&S®RTE1204 Oscilloscope. According to the datasheet. This equipment has an accuracy for DC measurements of $\pm 1.5\,\%$. Four variations in cell voltage and current values were proposed to analyze the impact of said precision on parameter estimation: 1. $\{1.015 * V_{cell}$, $1.015 * I_{cell}\}$, 2. $\{1.015 * V_{cell}$, $0.985 * I_{cell}\}$, 3. $\{0.985 * V_{cell}$, $1.015 * I_{cell}\}$, and 4. $\{0.985 * V_{cell}$, $0.985 * I_{cell}\}$. Comparing the results obtained with the variations in $\{V_{cell}$, $I_{cell}\}$ and the consolidated information in Table **6-11**, the deviations of the parameters are within the deviations of the estimate for the original data without variations, when the estimation stage was repeated 100 times. Therefore, no significant changes are observed in estimating parameters associated with the precision of the measuring equipment.

In this estimation process, the highest relative deviations were found in the same parameters: I_{sat}, V_{br}, m, and a. For Cell 1, those maximum variations were 13.3 %, 23.2 %, 33.3 %, and 22.22 %, respectively; while for Cell 2, were 24.4 %, 17.5 %, 24.5 %, and 32.5 %, respectively; finally, the other parameters reported variations under 5 %. The mean RMSE for Cell 1 (mc-SI), evaluated as the objective function, was lower than the value for Cell 2; however, the deviations were higher for Cell 2 (pc-SI).

Table 6-10: Parameters estimated for the Bishop model (mean ± standard deviation).

Parameter	Cell 1 (mc-SI)	Cell 2 (pc-SI)
I_{ph} [A]	$0.41 \pm 0.33\,\%$	$0.32 \pm 0.25\,\%$
I_0 [A]	$9.61 \times 10^{-8} \pm 12.65\,\%$	$9 \times 10^{-8} \pm 24.4\,\%$
n	$1.19 \pm 1.05\,\%$	$1.2 \pm 2.5\,\%$
R_s [Ω]	$0.13 \pm 2.37\,\%$	$0.08 \pm 5.6\,\%$
R_{sh} [Ω]	$51.69 \pm 3.98\,\%$	$182.9 \pm 3.1\,\%$
V_{br} [V]	$-18.45 \pm 23.25\,\%$	$-37 \pm 17.5\,\%$
m	$4.59 \pm 34.22\,\%$	$5.3 \pm 24.5\,\%$
a	$0.02 \pm 22.88\,\%$	$0.02 \pm 32.5\,\%$
O.F.	$4.7 \times 10^{-3} \pm 0.03\,\%$	$0.007 \pm 2.8\,\%$
Time [s]	$408.90 \pm 81.99\,\%$	$528.1 \pm 109.1\,\%$

Table 6-11: Best and worst parameter solutions for the Bishop model of each PV cell.

Parameter	Cell 1 (mc-SI)		Cell 2 (pc-SI)	
	Best	**Worst**	**Best**	**Worst**
I_{ph} [A]	0.41	0.42	0.32	0.32
I_0 [A]	9×10^{-8}	9×10^{-8}	2×10^{-9}	9×10^{-8}
n	1.1	1.2	1	1.3
R_s [Ω]	0.13	0.14	0.1	0.09
R_{sh} [Ω]	52.5	53.6	155.4	179.9
V_{br} [V]	−28.1	−18.3	−25.9	−40.9
m	7.5	4.5	4.4	6.1
a	0.029	0.028	0.005	0.024
O.F.	0.004	0.005	0.006	0.008
Time [s]	632.6	162.6	580.8	56.8

Table **6-12** presents the accuracy metrics evaluated for estimating Bishop's model. When comparing the results presented in Table **6-7** and Table **6-12**, it is observed that the average values of each metric considered for the assessment of Bishop's model parameters are considerably lower than those presented in estimation stage 1. RMSE, MAPE, and MBE errors are based on comparisons between the experimental and estimated current values. Then, a value of 0.15 A in the RMSE and MAPE values for Cell 1 is considerably high compared with its $I_{sc} = 0.43$ A.

Comparing the results obtained in Table **6-7** and Table **6-12**, for Cell 1, the average values for Stage 2 of the RMSE, MAPE, and MBE errors are significantly lower than for Stage 1. However, Stage 2 presents considerable variability concerning MAPE and MBE. For Cell 2,

the RMSE of Stage 2 is significantly lower than for Stage 1, indicating higher estimation precision. The standard deviation in MBE for stage 2 in both cells is very high, suggesting large variability in bias between different observations.

Finally, Figures 6.7(a) and 6.8(a) compare the estimated I-V curves of Cell 1 and Cell 2 with the experimental data, respectively, using the parameters obtained in the best solution. Both figures include a zoom-in Q_1 that presents the estimation results in the regions near I_{sc} and V_{oc}. Those comparisons evidence the satisfactory performance of the Bishop model in the second quadrant, using the parameters estimated with the proposed GA. Therefore, this approach provides a much more accurate solution compared with using the Bishop parameters reported in [23] for these real PV cells.

Figures 6.7(b) and 6.8(b) present a representative sample of the convergence of the estimation algorithm for Cell 1 and Cell 2, respectively. In both figures, it is possible to observe the decrement of **O.F.** as the number of iterations increases, and also that after 7000 iterations all solution paths reach a similar **O.F.** value, thus providing a similar accuracy in the second quadrant.

In addition, it is observed that the estimation provided by the SDM did not have a good approximation in Q_2. This model presents a linear behavior for Q_2. Therefore, the breakdown voltage is not observed. Here, for the parameterization of this model, the whole information of the experimental I-V curve was used (Q_1 and Q_2).

Table **6-13** presents the evaluation results of the error metrics for the estimation in Q_1, Q_2, and Q_1-Q_2 in both cells. For the experimental Cell 1 I-V curve, there are 197 data, 129 corresponding to Q_1 and the remaining 68 to Q_2. For the experimental Cell 2 I-V curve, there are 201 data, 152 corresponding to Q_1 and the remaining 49 to Q_2.

The table shows how, for Cell 2, the error values are consistent for Q_1, Q_2, and the complete set of experimental data (Q_1-Q_2). In the three evaluations, the errors for the estimation proposed in stage 2; that is, when the complete set of Bishop model parameters is estimated, it presents the lowest error values. However, for Cell 1, only for the evaluation in Q_1, stage 1 presents the lowest error values but only when RMSE and MBE are calculated.

Table 6-12: Accuracy measures for estimation with the Bishop parameters (mean ± standard deviation).

Accuracy measures	**Cell 1 (mc-SI)**	**Cell 2 (pc-SI)**
RMSE	$0.004 \pm 3.9\,\%$	$0.007 \pm 2.9\,\%$
MAPE	$0.018 \pm 25.9\,\%$	$0.20 \pm 12.34\,\%$
MBE	$-7.3 \times 10^{-5} \pm 185.4\,\%$	$-6.4 \times 10^{-5} \pm 196.18\,\%$

Table **6-14** presents the relative percent error of the main points of interest, that is, I_{sc}, V_{oc}, and P_{mpp}. The two stages show low error values in the estimation of P_{mpp}, below 2 %, making them suitable for applications where the delivered power needs to be estimated [164].

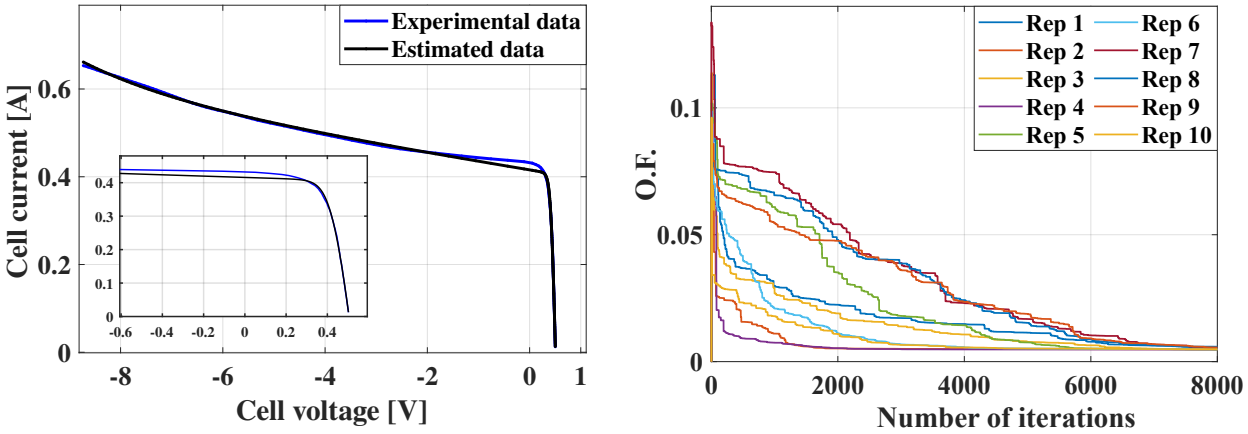

(a) (b)

Figure 6-7: Parameter estimation results for Cell 1 (mc-SI) using the Bishop model: 6.7(a) Comparison of I-V curves using the best solution (zoom-in Q_1), 6.7(b) convergence results for a sample of 10 repetitions

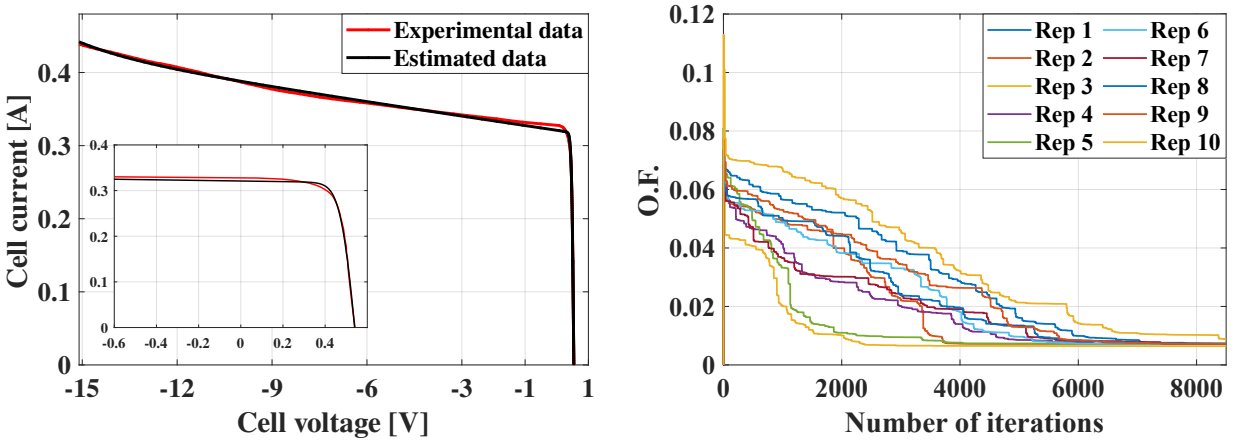

(a) (b)

Figure 6-8: Parameter estimation results from Cell 2 (pc-SI) using the Bishop model: 6.8(a) Comparison of I-V curves using the best solution (zoom-in Q_1), 6.8(b) convergence results for a sample of 10 repetitions

For Cell 1, the most significant error is found in I_{sc} when calculated through stage 2. For Cell 2, the most significant errors are found in I_{mpp}, for stage 1 equal to 4.43 % and stage 2 3.42 %. Concerning V_{mpp}, stage 1 presents an error of 2.85 %. The other calculated errors are below 2 %.

Table 6-13: Error metrics discriminated by quadrant for the best solution

		Cell 1			Cell 2		
		RMSE	**MAPE**	**MBE**	**RMSE**	**MAPE**	**MBE**
Q_1	Stage 1	0.0037	0.0182	4.03×10^{-5}	0.0082	0.0024	-2.25×10^{-4}
	Stage 2	0.0045	0.0174	-2.26×10^{-4}	0.0072	4.72×10^{-4}	-3.04×10^{-5}
Q_2	Stage 1	0.1995	0,3366	-0.1885	0.0272	0.0541	0.0219
	Stage 2	0.0042	0.0061	2.81×10^{-4}	0.0025	0.0058	8.36×10^{-5}
Q_1-Q_2	Stage 1	0.1172	0.1281	-0.065	0.0152	0.015	0.0052
	Stage 2	0.0044	0.0135	-5.11×10^{-5}	0.0064	0.011	-2.86×10^{-6}

Table 6-14: Relative percent error of some points of interest in the I–V and P–V curves

	Cell 1			Cell 2		
Variable	**Experimental**	**Stage 1**	**Stage 2**	**Experimental**	**Stage 1**	**Stage 2**
V_{oc} **[V]**	0.5023	0	0	0.5414	0.36	0.36
I_{sc} **[A]**	0.4343	0.02	3.79	0.3298	0.81	1.66
I_{mpp} **[A]**	0.3689	0.24	0.54	0.2864	4.43	3.42
V_{mpp} **[V]**	0.3711	0	1.5	0.4375	2.85	1.76
P_{mpp} **[W]**	0.1369	1.24	1.97	0.1253	0.79	1.59

6.4. Discussion

Comparing the results of the two stages for the parameter estimation, it was established that the estimation of the complete set of parameters of the Bishop model achieves better performance compared to estimating only the five parameters of the SDM and using the parameters of the second quadrant reported in Table **6-6**.

A comparison of the parameter estimation results (stages 1 and 2) shows that the parameters for the first quadrant are similar for both Cell 1 and Cell 2. The most significant difference in the estimation stages is R_{sh}, which affects the behavior in the second quadrant of the Bishop model. For this parameter, Cell 1 exhibited differences of 36.19Ω between the SDM and Bishop model from its mean values (see Table **6-3** and Table **6-10**), and 37.5Ω from the best results (see Table **6-5** and Table **6-11**). For Cell 2, the difference becomes considerably larger, with 302.1Ω when comparing the parameter mean value and 63.26Ω for the difference of best values. This analysis shows that I-V experimental curves, which include the first and second quadrants, are necessary for estimating the parameters of the Bishop model.

This study found differences in the behavior of the mc-SI and pc-SI I-V curves at important points, such as the short circuit current I_{sc} and the maximum power point (V_{mpp}, I_{mpp}). Those variations are reflected in the estimation of the parameters of the Bishop model, as shown in Table **6-10**. Such differences are noticeable not only in the first quadrant but also in the second quadrant since the three parameters defining that behavior (a, m, and V_{br})

show considerable variations depending on the type of cell technology. Therefore, parameters and search ranges should be defined according to the technology of the cells under analysis. It is important to emphasize that the parameters of the first quadrant also affect both the result of estimating the parameters of the second quadrant and the reproduction of the I-V curve in that quadrant; therefore, using values reported in the literature introduces significant errors in the estimation of the I-V curve. The solution presented in this Chapter is a tool for improving the analysis of the cell when it is exposed to partial shading, and its representation is performed with using the Bishop model. In this way, tools oriented to quantify shading losses and study degradation caused by hot spots, and aging, among other issues, can be developed by using the proposed methodology; thus, it provides a suitable compromise between accuracy and complexity.

Finally, future studies should focus on evaluating the performance of other optimization techniques to estimate the parameters of photovoltaic cells for the first and second quadrants using the Bishop model. Moreover, performing experiments on a large number of commercial photovoltaic cells, with different technologies (thin-film, bifacial, PERC, among others) could be useful for the scientific community, since accurate parameters for both the first and second quadrants are needed to analyze cells of those technologies. However, it is important to evaluate the performance of the proposed approach by considering different operating conditions with respect to temperature and irradiance.

This contribution was published in the journal paper:Restrepo-Cuestas, B.J.; Montano, J.; Ramos-Paja, C.A.; Trejos-Grisales, L.A.; Orozco-Gutierrez, M.L. “Parameter Estimation of the Bishop Photovoltaic Model Using a Genetic Algorithm.”Appl. Sci. 2022, 12, 2927. This article can be found on the publisher’s website at `https://www.mdpi.com/2076-3417/12/6/2927`. The journal’s homepage is located at `https://www.mdpi.com/journal/applsci`, and the publisher’s copyright information can be found at `https://www.mdpi.com/journal/applsci/about`.

7 Conclusions

This doctoral thesis has presented a methodology for modeling commercial panels at the cell level, under partial shading, using experimental I-V curves. This methodology allows analyzing the cell behavior in the first quadrant, which is in direct operation mode when the cell produces power, and in the second quadrant when the cell consumes power due to mismatching conditions.

From the literature review, it was possible to find that SDM has been widely used, from its application to different panel technologies to the estimation of parameters using analytical or optimization techniques for its solution. However, its application is limited to the module or panel level since it is not possible to capture the behavior at the cell level for the second quadrant.

It was also found that the Bishop model is used to represent photovoltaic systems; this allows their representation from a cell, module, or panel in the first and second quadrants. However, the model has not been widely studied, and no proposal for the estimation of its parameters was found.

On the other hand, the DRM presented in some articles allows associating the first quadrant with the SDM and adjusting the second quadrant through simple linearizations of the curve. Of the three models analyzed, this is the least common. It was possible to observe that it requires the development of a mathematical formulation that allows evaluating the current and the voltage in terminals through a set of equations, otherwise, it will only be possible to evaluate it through circuit simulators.

Once the models have been analyzed, it is necessary to obtain cell-level curves that provide information in both the first and second quadrants. Therefore, Chapter 4 presents a non-invasive procedure for panels that allows, through voltage and current data taken at its terminals, to estimate the behavior of one of its cells that has been affected by partial shading. This procedure seeks to avoid damage to the physical structure of the panel since, in order to obtain a direct measurement of the voltage at the terminals of the affected cell, it would be necessary to affect the encapsulating material.

The chapter details the experimental platform used and the procedure to obtain the I-V curves, which includes the process required to obtain the curves at the cell level. This procedure was applied in two panels with the same characteristics but different technologies (monocrystalline and polycrystalline). Each panel has 36 cells connected in series. As a result of this chapter, a database of I-V curves per panel was obtained, formed by of a curve for each cell where the behavior is observed in the first and second quadrants when the cell is

shaded at 50 % of the area, also including temperature information and test irradiation. In addition, I-V curves from a single cell with different sizes of the shaded area were acquired.
Based on the curves obtained in Chapter 4, Chapter 5 presents a strategy for the I-V characterization of a PV cell considering three PV models: the SDM, the Bishop model, and the DRM. The proposed strategy uses GA and Simulink to extract the parameters from an experimental I-V curve. The analysis results demonstrate that the SDM model does not correctly reproduce the cell behavior when the current grows exponentially while the voltage at the cell terminals grows negatively (Q_2).
The parameter estimation of the DRM model, which was carried out in two stages, demonstrated that estimating the parameters per quadrant has a negative influence on the model's accuracy. When estimating the parameters of the first quadrant, exclusively using the experimental information related to that quadrant, the critical parameter R_{sh} is not correctly identified, which is one of the parameters that impose the behavior in the second quadrant. Moreover, the results reveal the need for a mathematical formulation that allows estimating the whole set of parameters of this particular model. Here, this procedure was developed with the circuital model evaluation in Simulink, which required the estimation of the five parameters for Q_1 and the calculation of the parameters for Q_2, in an independent way.
It is also important to highlight that the proposed procedure can be used, along with PV array modeling methodologies, to analyze the behavior of cells operating in both Q_1 and Q_2, which is needed for power analysis and loss estimation during partial shading conditions or other mismatching phenomena.
The results demonstrated that the Bishop model presents the best behavior of the three models analyzed. In this way, Chapter 6 focused on the parameter estimation of the Bishop model. This analysis considers the information found in the literature review.
Most of the studies estimate the parameters of the Bishop model that are common with the SDM; however, some of the parameters that dictate the behavior of the second quadrant are not estimated but are defined as fit parameters. Therefore, it was proposed to analyze the results from two perspectives: First, estimate the parameters of the SDM model and select values for the other parameters; and Second, estimate the complete set of parameters of the Bishop model.
Comparing the results of the two stages of the parameter estimation, it was established that the estimation of the complete set of parameters that form the Bishop model achieves a better performance in comparison to estimating only the five SDM parameters and using second-quadrant parameters found reported in [23].
A comparison of the parameter estimation results (Stages 1 and 2) shows that the parameters for the first quadrant are similar for both Cell 1 and Cell 2. The most significant difference in the estimation stages is R_{sh}, which affects the second quadrant behavior in the Bishop model. This analysis shows that I-V experimental curves, which include the first and second quadrants, are necessary for estimating the parameters of the Bishop model.
As it was discussed in Chapter 4, the results presented differences in the behavior of the I-V

curve of mc-SI and pc-SI cells at important points, such as the short-circuit current I_{sc} and the maximum power point (V_{mpp}, I_{mpp}). Those variations are reflected in the estimation of the parameters of the Bishop model which are noticeable not only in the first quadrant, but also in the second quadrant, since the three parameters defining that behavior (a, m, and V_{br}) show considerable variations depending on the type of cell technology. Therefore, not only parameters but also search ranges should be defined according to the technology of the cells under analysis.

It is important to emphasize that the parameters of the first quadrant also affect both the result of estimating the parameters of the second quadrant and the reproduction of I-V curve at that quadrant; therefore, using values taken from the literature introduces significant errors in the estimation of the I-V curve. The solution presented in this thesis is a tool to improve the analysis of the cell when it is exposed to partial shading and its representation through the Bishop model is also supported. In this way, tools oriented to quantifying shading losses and the study of degradation caused by hot spots and aging, among other issues, can be developed by using the presented methodology, thus providing a suitable compromise between accuracy and complexity.

Finally, the procedure to calculate the voltage-current curve in commercial panels at the cell level, including information in both the first and second quadrants was developed. In addition, the subsequent stage of estimating parameters of the Bishop model for its representation considers real conditions of operation such as partial shading, achieving estimation with RMSE of the order of 4×10^{-3}, which are comparable with the best estimations of procedures reported in the literature but those works are focused on the first quadrant only. Furthermore, the trade-off between precision and complexity means that the methodology can be used in applications that evaluate energy losses due to partial shading, search for the maximum power point, and detect faults in photovoltaic panels.

Manufacturers of commercial panels can use the procedure to provide information in the data sheet about the behavior of the cells in the second quadrant, such as breakdown voltage. Furthermore, the experimental procedure presented in Section 4.3 can be replicated by researchers to provide models with parameters tuned to cell-level behavior in commercial panels. be to evaluate other optimization techniques, such as PSO, both in parameter performance and in computational load and execution times.

Future studies should be focused on evaluating the performance of different optimization techniques, such as PSO, for estimating the parameters of photovoltaic cells for both the first and second quadrants using the Bishop model. Moreover, performing experiments on a large number of commercial PV cells with different technologies (thin-film, bi-facial, PERC, among others) could be useful for the scientific community since accurate parameters for both the first and second quadrants could be provided. On the other hand, it is important to evaluate the performance of the proposed approach by considering different operating conditions regarding temperature and irradiance, to evaluate the variation in the estimated parameters.

References

[1] IRENA and CPI. *Global Landscape of Renewable Energy Finance 2023*. International Renewable Energy Agency, 2 edition, 2023.

[2] Meteorología y Estudios Ambientales Instituto de Hidrología and Unidad de Planeación Minero Energética. Atlas Interactivo - Radiación IDEAM, 2015.

[3] Freddy Ricardo Torres Fernández. Análisis del marco normativo del sector eléctrico colombiano, impactos en la regulación eléctrica de la ley 1715 de 2014. *Ingeniería Eléctrica*, 2016.

[4] UPME. Estadísticas incentivos tributarios fuentes no convencionales de energía. Technical report, Ministerio de Minas y Energía, 2023.

[5] Ali Q Al-Shetwi, Muhamad Zahim Sujod, and Frede Blaabjerg. Low voltage ride-through capability control for single-stage inverter-based grid-connected photovoltaic power plant. *Solar energy*, 159:665–681, 2018.

[6] Albert Polman, Mark Knight, Erik C Garnett, Bruno Ehrler, and Wim C Sinke. Photovoltaic materials: Present efficiencies and future challenges. *Science*, 352(6283):aad4424, 2016.

[7] Nikola L Georgijevic, Marko V Jankovic, Srdjan Srdic, and Zoran Radakovic. The detection of series arc fault in photovoltaic systems based on the arc current entropy. *IEEE Transactions on Power Electronics*, 31(8):5917–5930, 2016.

[8] B Chitti Babu and Suresh Gurjar. A novel simplified two-diode model of photovoltaic (pv) module. *IEEE journal of photovoltaics*, 4(4):1156–1161, 2014.

[9] Vivek Tamrakar, SC Gupta, and Yashwant Sawle. Single-diode and two-diode pv cell modeling using matlab for studying characteristics of solar cell under varying conditions. *Electrical & Computer Engineering: An International Journal (ECIJ)*, 4(2):67–77, 2015.

[10] Kashif Ishaque, Zainal Salam, et al. A comprehensive matlab simulink pv system simulator with partial shading capability based on two-diode model. *Solar energy*, 85(9):2217–2227, 2011.

[11] JC Sánchez Barroso, JPM Correia, N Barth, S Ahzi, and MA Khaleel. A pso algorithm for the calculation of the series and shunt resistances of the pv panel one-diode model. In *2014 International Renewable and Sustainable Energy Conference (IRSEC)*, pages 1–6. IEEE, 2014.

[12] MA Abo-Sennah, MA El-Dabah, and Ahmed El-Biomey Mansour. Maximum power point tracking techniques for photovoltaic systems: a comparative study. *International Journal of Electrical & Computer Engineering (2088-8708)*, 11(1), 2021.

[13] Zhaodong Wen, Jun Chen, Xian Cheng, Haiyan Niu, and Xuetao Luo. A new and simple split series strings approach for adding bypass diodes in shingled cells modules to reduce shading loss. *Solar Energy*, 184:497–507, 2019.

[14] Juan David Bastidas-Rodriguez, Giovanni Petrone, Carlos Andrés Ramos-Paja, and Giovanni Spagnuolo. A genetic algorithm for identifying the single diode model parameters of a photovoltaic panel. *Mathematics and Computers in Simulation*, 131:38–54, 2017.

[15] Jieming Ma, TO Ting, Ka Lok Man, Nan Zhang, Sheng-Uei Guan, and Prudence WH Wong. Parameter estimation of photovoltaic models via cuckoo search. *Journal of applied mathematics*, 2013, 2013.

[16] Jianbo Bai, Yang Cao, Yuzhe Hao, Zhen Zhang, Sheng Liu, and Fei Cao. Characteristic output of pv systems under partial shading or mismatch conditions. *Solar Energy*, 112:41–54, 2015.

[17] SeyedKazem Hosseini, Shamsodin Taheri, Masoud Farzaneh, and Hamed Taheri. An approach to precise modeling of photovoltaic modules under changing environmental conditions. In *2016 IEEE Electrical Power and Energy Conference (EPEC)*, pages 1–6. IEEE, 2016.

[18] A Rezaee Jordehi. Parameter estimation of solar photovoltaic (pv) cells: A review. *Renewable and Sustainable Energy Reviews*, 61:354–371, 2016.

[19] Fabricio Bradaschia, Marcelo C Cavalcanti, Aguinaldo José do Nascimento, Emerson Alves da Silva, and Gustavo Medeiros de Souza Azevedo. Parameter identification for pv modules based on an environment-dependent double-diode model. *IEEE Journal of Photovoltaics*, 9(5):1388–1397, 2019.

[20] Salam J. Yaqoob, Ameer L. Saleh, Saad Motahhir, Ephraim B. Agyekum, Anand Nayyar, and Basit Qureshi. Author correction: Comparative study with practical validation of photovoltaic monocrystalline module for single and double diode models. *Scientific Reports*, 11(1):21822, 2021.

[21] F Belhachat and C Larbes. Modeling, analysis and comparison of solar photovoltaic array configurations under partial shading conditions. *Solar Energy*, 120:399–418, 2015.

[22] Eloy Díaz-Dorado, Jose Cidras, and Camilo Carrillo. Discrete i–v model for partially shaded pv-arrays. *solar energy*, 103:96–107, 2014.

[23] JW Bishop. Computer simulation of the effects of electrical mismatches in photovoltaic cell interconnection circuits. *Solar cells*, 25(1):73–89, 1988.

[24] European Commission. European solar test installation.

[25] Hajime Kawamura, Kazuhito Naka, Norihiro Yonekura, Sanshiro Yamanaka, Hideaki Kawamura, Hideyuki Ohno, and Katsuhiko Naito. Simulation of i–v characteristics of a pv module with shaded pv cells. *Solar Energy Materials and Solar Cells*, 75(3-4):613–621, 2003.

[26] DL King, JK Dudley, and WE Boyson. Pvsim {copyright}: A simulation program for photovoltaic cells, modules, and arrays. Technical report, Sandia National Lab.(SNL-NM), Albuquerque, NM (United States), 1996.

[27] Guangyu Liu, Sing Kiong Nguang, and Ashton Partridge. A general modeling method for i–v characteristics of geometrically and electrically configured photovoltaic arrays. *Energy Conversion and Management*, 52(12):3439–3445, 2011.

[28] Abdallah Zegaoui, Pierre Petit, Michel Aillerie, Jean-Paul Sawicki, and Jean-Pierre Charles. Experimental validation of photovoltaic direct and reverse mode model. influence of partial shading. *Energy Procedia*, 18:1247–1253, 2012.

[29] Zewei Yang, Kailin Liao, Jun Chen, Lei Xia, and Xuetao Luo. Output performance analysis and power optimization of different configurations half-cell modules under partial shading. *Optik*, 232:166499, 2021.

[30] Manit Seapan, Yoshihiro Hishikawa, Masahiro Yoshita, and Keiichi Okajima. Detection of shading effect by using the current and voltage at maximum power point of crystalline silicon pv modules. *Solar Energy*, 211:1365–1372, 2020.

[31] Idriss Hadj Mahammed, Amar Hadj Arab, Yahia Bakelli, Messaouda Khennene, Samir Hamid Oudjana, Amor Fezzani, Layachi Zaghba, et al. Outdoor study of partial shading effects on different pv modules technologies. *Energy Procedia*, 141:81–85, 2017.

[32] Abdallah Zegaoui, Mohamed Boutoubat, Jean-Paul Sawicki, Fatma Zohra Kessaissia, Abdelkader Djahbar, and Michel Aillerie. Enhanced model of photovoltaic cell/panel/array considering the direct and reverse modes. In *AIP Conference Proceedings*. AIP Publishing LLC, 2018.

[33] J Montano, AF Tobón, JP Villegas, and M Durango. Grasshopper optimization algorithm for parameter estimation of photovoltaic modules based on the single diode model. *International Journal of Energy and Environmental Engineering*, pages 1–9, 2020.

[34] Giuseppina Ciulla, Valerio Lo Brano, Vincenzo Di Dio, and Giovanni Cipriani. A comparison of different one-diode models for the representation of i–v characteristic of a pv cell. *Renewable and Sustainable Energy Reviews*, 32:684–696, 2014.

[35] Shangce Gao, Kaiyu Wang, Sichen Tao, Ting Jin, Hongwei Dai, and Jiujun Cheng. A state-of-the-art differential evolution algorithm for parameter estimation of solar photovoltaic models. *Energy Conversion and Management*, 230:113784, 2021.

[36] Giovanni Petrone, Carlos Andrés Ramos-Paja, and Giovanni Spagnuolo. *Photovoltaic sources modeling*. John Wiley & Sons, 2017.

[37] Ahmed A El Tayyan. An approach to extract the parameters of solar cells from their illuminated iv curves using the lambert w function. *Turkish Journal of Physics*, 39(1):1–15, 2015.

[38] Vun Jack Chin, Zainal Salam, and Kashif Ishaque. Cell modelling and model parameters estimation techniques for photovoltaic simulator application: A review. *Applied Energy*, 154:500–519, 2015.

[39] Shubham Raj, Ankit Kumar Sinha, and Ashish K Panchal. Solar cell parameters estimation from illuminated i-v characteristic using linear slope equations and newton-raphson technique. *Journal of Renewable and Sustainable Energy*, 5(3):033105, 2013.

[40] Abir Chatterjee, Ali Keyhani, and Dhruv Kapoor. Identification of photovoltaic source models. *IEEE Transactions on Energy conversion*, 26(3):883–889, 2011.

[41] Dhruv Kler, Yagyadatta Goswami, KPS Rana, and Vineet Kumar. A novel approach to parameter estimation of photovoltaic systems using hybridized optimizer. *Energy Conversion and Management*, 187:486–511, 2019.

[42] O Hachana, KE Hemsas, GM Tina, and C Ventura. Comparison of different metaheuristic algorithms for parameter identification of photovoltaic cell/module. *Journal of renewable and sustainable energy*, 5(5):053122, 2013.

[43] Andrés Tobón, Julián Peláez-Restrepo, Jhon Montano, Mariana Durango, Jorge Herrera, and Asier Ibeas. Mppt of a photovoltaic panels array with partial shading using the ipsm with implementation both in simulation as in hardware. *Energies*, 13(4):815, 2020.

[44] Andres Felipe Tobon Mejia. Estimación de los parámetros del modelo de un solo diodo del módulo fotovoltaico aplicando el método de optimización basado en búsqueda de patrones mejorado. *Revista Ingenierías Universidad de Medellín*, 20(38), 2021.

[45] Attia A El-Fergany. Parameters identification of pv model using improved slime mould optimizer and lambert w-function. *Energy Reports*, 7:875–887, 2021.

[46] Yann-Chang Huang, Chao-Ming Huang, Shin-Ju Chen, and Sung-Pei Yang. Optimization of module parameters for pv power estimation using a hybrid algorithm. *IEEE Transactions on Sustainable Energy*, 11(4):2210–2219, 2019.

[47] Hatem R Alamri, Hegazy Rezk, Heba Abd-Elbary, Hamdy A Ziedan, and Ahmed Elnozahy. Experimental investigation to improve the energy efficiency of solar pv panels using hydrophobic sio2 nanomaterial. *Coatings*, 10(5):503, 2020.

[48] Zuowen Liao, Zhikun Chen, and Shuijia Li. Parameters extraction of photovoltaic models using triple-phase teaching-learning-based optimization. *IEEE Access*, 8:69937–69952, 2020.

[49] Xu Chen, Hong Yue, and Kunjie Yu. Perturbed stochastic fractal search for solar pv parameter estimation. *Energy*, 189:116247, 2019.

[50] Hongliang Zhang, Ali Asghar Heidari, Mingjing Wang, Lejun Zhang, Huiling Chen, and Chengye Li. Orthogonal nelder-mead moth flame method for parameters identification of photovoltaic modules. *Energy Conversion and Management*, 211:112764, 2020.

[51] N Shankar, N Saravanakumar, et al. Solar photovoltaic module parameter estimation with an enhanced differential evolutionary algorithm using the manufacturer's datasheet information. *Optik*, 224:165700, 2020.

[52] Oscar Danilo Montoya, Carlos Alberto Ramírez-Vanegas, and Luis Fernando Grisales-Norena. Parametric estimation in photovoltaic modules using the crow search algorithm. *International Journal of Electrical and Computer Engineering*, 12(1):82, 2022.

[53] Derick Mathew, Chinnappa Rani, Muthu Rajesh Kumar, Yue Wang, Richard Binns, and Krishna Busawon. Wind-driven optimization technique for estimation of solar photovoltaic parameters. *IEEE Journal of Photovoltaics*, 8(1):248–256, 2017.

[54] Naima Hamid, Rachida Abounacer, Mohammed Idali Oumhand, M'barek Feddaoui, and Driss Agliz. Parameters identification of photovoltaic solar cells and module using the genetic algorithm with convex combination crossover. *International Journal of Ambient Energy*, 40(5):517–524, 2019.

[55] Madhav Kumar et al. Modelling and parameter estimation of solar cell using genetic algorithm. In *2019 International Conference on Intelligent Computing and Control Systems (ICCS)*, pages 383–387. IEEE, 2019.

[56] Cecilia Tang and Hang Zhou. Inverse modelling of pv power prediction based on ga method. In *IOP Conference Series: Earth and Environmental Science*, volume 675, page 012080. IOP Publishing, 2021.

[57] Angel Marinov, Svetlozar Zahariev, Ivelin Ivanov, and Toncho Papanchev. Genetic algorithm for generation of pv panel curves from datasheets. In *2021 17th Conference on Electrical Machines, Drives and Power Systems (ELMA)*, pages 1–4. IEEE, 2021.

[58] Jhon Jairo Montano, Luis F Grisales Noreña, Andres Felipe Tobon, and Daniel Gonzalez Montoya. Estimation of the parameters of the mathematical model of an equivalent diode of a photovoltaic panel using a continuous genetic algorithm. *IEEE Latin America Transactions*, 20(4):616–623, 2022.

[59] Mahmoud S Ismail, Mahmoud Moghavvemi, and TMI Mahlia. Characterization of pv panel and global optimization of its model parameters using genetic algorithm. *Energy Conversion and Management*, 73:10–25, 2013.

[60] Hussein M Waly, Haitham Z Azazi, Dina SM Osheba, and Awad E El-Sabbe. Parameters extraction of photovoltaic sources based on experimental data. *IET Renewable Power Generation*, 13(9):1466–1473, 2019.

[61] Safi Allah Hamadi, Aissa Chouder, Mohamed Mounir Rezaoui, Saad Motahhir, and Ameur Miloud Kaddouri. Improved hybrid parameters extraction of a pv module using a moth flame algorithm. *Scientific Reports*, 10(22), 2021.

[62] Ahmed Bouraiou, Messaoud Hamouda, Abdelkader Chaker, Mohammed Sadok, Mohammed Mostefaoui, and Salah Lachtar. Modeling and simulation of photovoltaic module and array based on one and two diode model using matlab/simulink. *Energy Procedia*, 74:864–877, 2015.

[63] Sangram Bana and RP Saini. A mathematical modeling framework to evaluate the performance of single diode and double diode based spv systems. *Energy Reports*, 2:171–187, 2016.

[64] Achim Woyte, Johan Nijs, and Ronnie Belmans. Partial shadowing of photovoltaic arrays with different system configurations: literature review and field test results. *Solar energy*, 74(3):217–233, 2003.

[65] Kashif Ishaque, Zainal Salam, Hamed Taheri, et al. Modeling and simulation of photovoltaic (pv) system during partial shading based on a two-diode model. *Simulation Modelling Practice and Theory*, 19(7):1613–1626, 2011.

[66] Suneel Raju Pendem and Suresh Mikkili. Modeling, simulation and performance analysis of solar pv array configurations (series, series–parallel and honey-comb) to extract maximum power under partial shading conditions. *Energy Reports*, 4:274–287, 2018.

[67] Cai Yunmei, Li Xiangwei, et al. Study of bypass diodes configuration on pv modules with partial shaded. In *2019 Chinese Control And Decision Conference (CCDC)*, pages 511–515. IEEE, 2019.

[68] S Malathy and R Ramaprabha. Comprehensive analysis on the role of array size and configuration on energy yield of photovoltaic systems under shaded conditions. *Renewable and Sustainable Energy Reviews*, 49:672–679, 2015.

[69] Samkeliso Shongwe and Moin Hanif. Comparative analysis of different single-diode pv modeling methods. *IEEE Journal of photovoltaics*, 5(3):938–946, 2015.

[70] Adel A Elbaset, Hamdi Ali, and Montaser Abd El Sattar. New seven parameters model for amorphous silicon and thin film pv modules based on solar irradiance. *Solar energy*, 138:26–35, 2016.

[71] R Rajesh and M Carolin Mabel. A comprehensive review of photovoltaic systems. *Renewable and sustainable energy reviews*, 51:231–248, 2015.

[72] H Rahimi Mirazizi and MA Shafiyi. A comprehensive analysis of partial shading effect on output parameters of a grid-connected pv system. *International Journal of Electrical and Computer Engineering*, 8(2):749, 2018.

[73] Ch Saha, N Agbu, R Jinks, and M Nazmul Huda. Review article of the solar pv parameters estimation using evolutionary algorithms. *MOJ Solar and Photoenergy Systems*, 2(2):66–78, 2018.

[74] A Elkholy and AA Abou El-Ela. Optimal parameters estimation and modelling of photovoltaic modules using analytical method. *Heliyon*, 5(7):e02137, 2019.

[75] Salwan Tajjour, Shyam Singh Chandel, Hasmat Malik, Majed A Alotaibi, and Taha Selim Ustun. A novel metaheuristic approach for solar photovoltaic parameter extraction using manufacturer data. In *Photonics*, volume 9, page 858. MDPI, 2022.

[76] Vandana Khanna, BK Das, Dinesh Bisht, PK Singh, et al. A three diode model for industrial solar cells and estimation of solar cell parameters using pso algorithm. *Renewable Energy*, 78:105–113, 2015.

[77] Qinzhi Hao, Zhongliang Zhou, Zhenglei Wei, and Guanghui Chen. Parameters identification of photovoltaic models using a multi-strategy success-history-based adaptive differential evolution. *IEEE Access*, 8:35979–35994, 2020.

[78] MF AlHajri, KM El-Naggar, MR AlRashidi, and AK Al-Othman. Optimal extraction of solar cell parameters using pattern search. *Renewable energy*, 44:238–245, 2012.

[79] Ayman Youssef, Mohammed El-Telbany, and Abdelhalim Zekry. The role of artificial intelligence in photo-voltaic systems design and control: A review. *Renewable and Sustainable Energy Reviews*, 78:72–79, 2017.

[80] Rituraj Tamrakar and Archana Gupta. A review: extraction of solar cell modelling parameters. *International journal of innovative research in electrical, electronics, instrumentation and control engineering*, 3(1):55–60, 2015.

[81] Lei Luo, Fei Yan, Ying-quan Zou, and Huang-jie Gong. A fast photovoltaic array simulation method for arbitrary configuration. In *2016 35th Chinese Control Conference (CCC)*, pages 8584–8587. IEEE, 2016.

[82] Shahida Khatoon, Mohd Faisal Jalil, et al. Feasibility analysis of solar photovoltaic array configurations under partial shading conditions. In *2015 Annual IEEE India Conference (INDICON)*, pages 1–6. IEEE, 2015.

[83] Abdallah Zegaoui, P Petit, M Aillerie, JP Sawicki, AW Belarbi, MD Krachai, and JP Charles. Photovoltaic cell/panel/array characterizations and modeling considering both reverse and direct modes. *Energy Procedia*, 6:695–703, 2011.

[84] Shiva Moballegh and Jin Jiang. Modeling, prediction, and experimental validations of power peaks of pv arrays under partial shading conditions. *IEEE Transactions on Sustainable Energy*, 5(1):293–300, 2013.

[85] Ali M Humada, Salih Y Darweesh, Khalid G Mohammed, Mohammed Kamil, Samen F Mohammed, Naseer K Kasim, Tahseen Ahmad Tahseen, Omar I Awad, and Saad Mekhilef. Modeling of pv system and parameter extraction based on experimental data: Review and investigation. *Solar Energy*, 199:742–760, 2020.

[86] Fabio Ricco Galluzzo, Pier Enrico Zani, Marina Foti, Andrea Canino, Cosimo Gerardi, and Salvatore Lombardo. Numerical modeling of bifacial pv string performance: Perimeter effect and influence of uniaxial solar trackers. *Energies*, 13(4):869, 2020.

[87] Sundeep Gali. Energy yield model for bifacial pv systems: A study and analysis of temperature & rear irradiance models, 2017.

[88] Matthieu Chiodetti. Bifacial pv plants: performance model development and optimization of their configuration, 2015.

[89] Daniel Riley, Clifford Hansen, Joshua Stein, Matthew Lave, Johnson Kallickal, Bill Marion, and Fatima Toor. A performance model for bifacial pv modules. In *2017 IEEE 44th Photovoltaic Specialist Conference (PVSC)*, pages 3348–3353. IEEE, 2017.

[90] ML Orozco-Gutierrez, JM Ramirez-Scarpetta, G Spagnuolo, and C Ax Ramos-Paja. A technique for mismatched pv array simulation. *Renewable Energy*, 55:417–427, 2013.

[91] Mohammadmehdi Seyedmahmoudian, Saad Mekhilef, Rasoul Rahmani, Rubiyah Yusof, and Ehsan Taslimi Renani. Analytical modeling of partially shaded photovoltaic systems. *Energies*, 6(1):128–144, 2013.

[92] Juan David Bastidas-Rodríguez, Luz Adriana Trejos-Grisales, Daniel Gonzalez-Montoya, Carlos Andrés Ramos-Paja, Giovanni Petrone, and Giovanni Spagnuolo. General modeling procedure for photovoltaic arrays. *Electric Power Systems Research*, 155:67–79, 2018.

[93] S Sheik Mohammed, D Devaraj, and TP Imthias Ahamed. Modeling, simulation and analysis of photovoltaic modules under partially shaded conditions. *Indian Journal of Science and Technology*, 9(16):1–8, 2016.

[94] Hiren Patel and Vivek Agarwal. Matlab-based modeling to study the effects of partial shading on pv array characteristics. *IEEE transactions on energy conversion*, 23(1):302–310, 2008.

[95] S Moballegh and J Jiang. Partial shading modeling of photovoltaic system with experimental validations. In *2011 IEEE Power and Energy Society General Meeting*, pages 1–9. IEEE, 2011.

[96] Sara Gallardo-Saavedra and Björn Karlsson. Simulation, validation and analysis of shading effects on a pv system. *Solar Energy*, 170:828–839, 2018.

[97] PK Sadhu et al. Matlab-based simulation to analyze the aftermath of partial shading on solar cell. In *2018 International Conference on Power Energy, Environment and Intelligent Control (PEEIC)*, pages 437–441. IEEE, 2018.

[98] Suneel Raju Pendem and Suresh Mikkili. Modeling, simulation, and performance analysis of pv array configurations (series, series-parallel, bridge-linked, and honeycomb) to harvest maximum power under various partial shading conditions. *International journal of green energy*, 15(13):795–812, 2018.

[99] Ayşe Beşkirli and İdiris Dağ. Parameter extraction for photovoltaic models with tree seed algorithm. *Energy Reports*, 9:174–185, 2023.

[100] Duong Nguyen Dang, Thinh Le Viet, Hirotaka Takano, and Tuyen Nguyen Duc. Estimating parameters of photovoltaic modules based on current–voltage characteristics at operating conditions. *Energy Reports*, 9:18–26, 2023.

[101] Alain K Tossa, YM Soro, Y Azoumah, and D Yamegueu. A new approach to estimate the performance and energy productivity of photovoltaic modules in real operating conditions. *Solar energy*, 110:543–560, 2014.

[102] Assane Seck, Mouhamadou Thiam, Maguette Sarr, Mamadou Wade, and Ibrahima Ka. Comparative study of photovoltaic models using simulation and experimental studies. *International Journal of Renewable Energy Research (IJRER)*, 12(4):1704–1711, 2022.

[103] Liu Guangyu, Sing Kiong Nguang, Ashton Partridge, et al. A general modeling method for iv characteristics of geometrically and electrically configured photovoltaic arrays. *Energy conversion and management*, 52, 2011.

[104] Dominique Bonkoungou, Toussaint Guingane, Eric Korsaga, Sosthène Tassembedo, Zacharie Koalaga, Arouna Darga, and François Zougmore. A novel topology to improve pv module efficiency under partial shading conditions. *International Journal of Photoenergy*, 2022, 2022.

[105] A Fezzani, I Hadj Mahammed, and S Said. Matlab-based modeling of shading effects in photovoltaic arrays. In *2014 15th International Conference on Sciences and Techniques of Automatic Control and Computer Engineering (STA)*, pages 781–787. IEEE, 2014.

[106] Chokri Ahmed Belhadj, IH Banat, and Mohamed Deriche. A detailed analysis of photovoltaic panel hot spot phenomena based on the bishop model. In *2017 14th International Multi-Conference on Systems, Signals & Devices (SSD)*, pages 222–227. IEEE, 2017.

[107] Santiago Silvestre, Alfredo Boronat, and A Chouder. Study of bypass diodes configuration on pv modules. *applied energy*, 86(9):1632–1640, 2009.

[108] Ousmane W Compaore, Ghaleb Hoblos, and Zacharie Koalaga. Analysis of the impact of faults in a photovoltaic generator. In *2021 International Conference on Innovation and Intelligence for Informatics, Computing, and Technologies (3ICT)*, pages 68–73. IEEE, 2021.

[109] Abdesslam Belaout, Fateh Krim, and Adel Mellit. Neuro-fuzzy classifier for fault detection and classification in photovoltaic module. In *2016 8th International Conference on Modelling, Identification and Control (ICMIC)*, pages 144–149. IEEE, 2016.

[110] Todizara Andrianajaina, Eric Jean Roy Sambatra, Charles Bernard Andrianirina, Tsivalalaina David Razafimahefa, and Nicolas Heraud. Pv fault detection using the least squares method. In *2016 International Conference and Exposition on Electrical and Power Engineering (EPE)*, pages 846–851. IEEE, 2016.

[111] Volker Quaschning and Rolf Hanitsch. Numerical simulation of current-voltage characteristics of photovoltaic systems with shaded solar cells. *Solar energy*, 56(6):513–520, 1996.

[112] ML Orozco-Gutierrez, JM Ramirez-Scarpetta, G Spagnuolo, and CA Ramos-Paja. A method for simulating large pv arrays that include reverse biased cells. *Applied energy*, 123:157–167, 2014.

[113] Donatien Goron, Deliand Njomo. Mathematical modelling and simulation of a partially shaded photovoltaic module. *International Journal of Scientific & Engineering Research*, 7(2), feb 2016.

[114] Efstratios I Batzelis, Iason A Routsolias, and Stavros A Papathanassiou. An explicit pv string model based on the lambert w function and simplified mpp expressions for operation under partial shading. *IEEE Transactions on Sustainable Energy*, 5(1):301–312, 2013.

[115] Chris Deline, Aron Dobos, Steven Janzou, Jenya Meydbray, and Matt Donovan. A simplified model of uniform shading in large photovoltaic arrays. *Solar Energy*, 96:274–282, 2013.

[116] W Herrmann, W Wiesner, and W Vaassen. Hot spot investigations on pv modules-new concepts for a test standard and consequences for module design with respect to bypass diodes. In *Conference Record of the Twenty Sixth IEEE Photovoltaic Specialists Conference-1997*, pages 1129–1132. IEEE, 1997.

[117] M Danner and K Bucher. Reverse characteristics of commercial silicon solar cells-impact on hot spot temperatures and module integrity. In *Conference Record of the Twenty Sixth IEEE Photovoltaic Specialists Conference-1997*, pages 1137–1140. IEEE, 1997.

[118] MC Alonso, JM Ruiz, and F Chenlo. Experimental study of mismatch and shading effects in the iv characteristic of a photovoltaic module. *Solar Energy Materials & Solar Cells*, 90(3):329–340, 2006.

[119] Resu Iturri Buzunáriz. Revisión bibliográfica y caracterización de células solares en polarización inversa, 2011.

[120] Qi Zhang and Qun Li. Temperature and reverse voltage across a partially shaded si pv cell under hot spot test condition. In *2012 38th IEEE photovoltaic specialists conference*, pages 001344–001347. IEEE, 2012.

[121] Radhakrishnan Venkateswari and Natarajan Rajasekar. Review on parameter estimation techniques of solar photovoltaic systems. *International Transactions on Electrical Energy Systems*, 31(11):e13113, 2021.

[122] Thuan Thanh Nguyen, Thang Trung Nguyen, and Thanh Ngoc Tran. Parameter estimation of photovoltaic cell and module models relied on metaheuristic algorithms including artificial ecosystem optimization. *Neural Computing and Applications*, 34(15):12819–12844, 2022.

[123] S Mohammadreza Ebrahimi, Esmaeil Salahshour, Milad Malekzadeh, and Francisco Gordillo. Parameters identification of pv solar cells and modules using flexible particle swarm optimization algorithm. *Energy*, 179:358–372, 2019.

[124] Nikita Rawat and Padmanabh Thakur. Comparative analysis of hybrid and metaheuristic parameter estimation methods of solar pv. *Materials Today: Proceedings*, 65:3748–3756, 2022.

[125] Belkacem Aoufi, Oussama Hachana, Mohamed Amine Sid, and Giuseppe Marco Tina. Precise and fast parameter identification of mono-crystalline, poly-crystalline, and mono-facial photovoltaic modules using a new bat artificial bee colony optimizer. *Journal of Computational Electronics*, 21(2):491–512, 2022.

[126] Kunjie Yu, Boyang Qu, Caitong Yue, Shilei Ge, Xu Chen, and Jing Liang. A performance-guided jaya algorithm for parameters identification of photovoltaic cell and module. *Applied Energy*, 237:241–257, 2019.

[127] Maryam Naeijian, Abolfazl Rahimnejad, S Mohammadreza Ebrahimi, Nafiseh Pourmousa, and S Andrew Gadsden. Parameter estimation of pv solar cells and modules using whippy harris hawks optimization algorithm. *Energy Reports*, 7:4047–4063, 2021.

[128] Ahmed A Zaki Diab, Ameena Al Sumaiti, AA Ezzat, Amr E Rafaat, Kotin A Denis, and Ayat Gamal Abo El-Magd. New objective function of parameters extraction of photovoltaic modules for plummeting execution time complexity. *IET Renewable Power Generation*, 2022.

[129] M Premkumar, Pradeep Jangir, R Sowmya, Rajvikram Madurai Elavarasan, and B Santhosh Kumar. Enhanced chaotic jaya algorithm for parameter estimation of photovoltaic cell/modules. *ISA transactions*, 116:139–166, 2021.

[130] Mohammed Qaraad, Souad Amjad, Nazar K Hussein, Mahmoud Badawy, Seyedali Mirjalili, and Mostafa A Elhosseini. Photovoltaic parameter estimation using improved moth flame algorithms with local escape operators. *Computers and Electrical Engineering*, 106:108603, 2023.

[131] Arooj Tariq Kiani, Muhammad Faisal Nadeem, Ali Ahmed, Intisar Ali Sajjad, Aamir Raza, and Irfan A Khan. Chaotic inertia weight particle swarm optimization (ciwpso):

An efficient technique for solar cell parameter estimation. In *2020 3rd International Conference on Computing, Mathematics and Engineering Technologies (iCoMET)*, pages 1–6. IEEE, 2020.

[132] Manish Kumar Singla, Jyoti Gupta, Parag Nijhawan, Parminder Singh, Nimay Chandra Giri, Essam Hendawi, and Mohamed I Abu El-Sebah. Parameter estimation techniques for photovoltaic system modeling. *Energies*, 16(17):6280, 2023.

[133] Aala Kalananda Vamsi Krishna Reddy and Komanapalli Venkata Lakshmi Narayana. Extraction of optimal solar pv parameters using hybrid optimization techniques. In *2021 Innovations in Power and Advanced Computing Technologies (i-PACT)*, pages 1–7. IEEE, 2021.

[134] Mahmoud A El-Dabah, Ragab A El-Sehiemy, and Ahmed Abdelbaset. An improved rcga for parameter extraction of three-diode pv model. In *2022 23rd International Middle East Power Systems Conference (MEPCON)*, pages 1–6. IEEE, 2022.

[135] Shuijia Li, Qiong Gu, Wenyin Gong, and Bin Ning. An enhanced adaptive differential evolution algorithm for parameter extraction of photovoltaic models. *Energy Conversion and Management*, 205:112443, 2020.

[136] Ibrahim Anwar Ibrahim, MJ Hossain, Benjamin C Duck, and Mithulananthan Nadarajah. An improved wind driven optimization algorithm for parameters identification of a triple-diode photovoltaic cell model. *Energy Conversion and Management*, 213:112872, 2020.

[137] P Ashwini Kumari and P Geethanjali. Adaptive genetic algorithm based multi-objective optimization for photovoltaic cell design parameter extraction. *Energy Procedia*, 117:432–441, 2017.

[138] Rituraj Tamrakar and Archana Gupta. Extraction of solar cell modelling parameters using differential evolution algorithm. *Int. J. Innov. Res. Elec., Electron., Instrument. Contr. Engineering*, 3(11), 2015.

[139] Yourim Yoon and Zong Woo Geem. Parameter optimization of single-diode model of photovoltaic cell using memetic algorithm. *International Journal of Photoenergy*, 2015, 2015.

[140] Zhicong Chen, Lijun Wu, Peijie Lin, Yue Wu, and Shuying Cheng. Parameters identification of photovoltaic models using hybrid adaptive nelder-mead simplex algorithm based on eagle strategy. *Applied Energy*, 182:47–57, 2016.

[141] Hans S Rauschenbach. Electrical output of shadowed solar arrays. *IEEE Transactions on Electron Devices*, 18(8):483–490, 1971.

[142] MC Alonso-García and JM Ruíz. Analysis and modelling the reverse characteristic of photovoltaic cells. *Solar Energy Materials and Solar Cells*, 90(7-8):1105–1120, 2006.

[143] P Spirito and V Albergamo. Reverse bias power dissipation of shadowed or faulty cells in different array configurations. In *Fourth EC Photovoltaic Solar Energy Conference*, pages 296–300. Springer, 1982.

[144] CF Lopez Pineda. Experimental evaluation of reverse bias stress induced on photovoltaic modules for different configurations. *Solar & wind technology*, 3(2):85–88, 1986.

[145] R Ahmad, Ali F Murtaza, Hadeed Ahmed Sher, Umar Tabrez Shami, and Saheed Olalekan. An analytical approach to study partial shading effects on pv array supported by literature. *Renewable and Sustainable Energy Reviews*, 74:721–732, 2017.

[146] Hans S. Rauschenbach. Electrical output of shadowed solar arrays. *IEEE Transactions on Electron Devices*, 18(8):483–490, 1971.

[147] HA Koffi, A Kuditcher, VCK Kakane, EA Armah, AA Yankson, and JKA Amuzu. The shockley five-parameter model of a solar cell: A short note. *African Journal of Science, Technology, Innovation and Development*, 7(6):491–494, 2015.

[148] Robert L Boylestad and Louis Nashelsky. *Electronic devices and circuit theory*. Pearson Educación, 2002.

[149] Pierre Petit, Abdallah Zégaoui, Michel Aillerie, Jean-Paul Sawicki, and Jean-Pierre Charles. The transistor based direct and reverse mode model for photovoltaic strings and panels. *Energy Procedia*, 18:1240–1246, 2012.

[150] JA Ramos-Hernanz, JJ Campayo, J Larranaga, E Zulueta, O Barambones, J Motrico, U Fernandez Gamiz, and I Zamora. Two photovoltaic cell simulation models in matlab/simulink. *International Journal on Technical and Physical Problems of Engineering,(IJTPE)*, 4(1):45–51, 2012.

[151] Antony Xenophontos and Ali M Bazzi. Model-based maximum power curves of solar photovoltaic panels under partial shading conditions. *IEEE Journal of Photovoltaics*, 8(1):233–238, 2017.

[152] S Rustemli and F Dincer. Modeling of photovoltaic panel and examining effects of temperature in matlab/simulink. *Elektronika ir Elektrotechnika*, 109(3):35–40, 2011.

[153] Juan David Bastidas-Rodríguez, Edinson Franco, Giovanni Petrone, Carlos Andrés Ramos-Paja, and Giovanni Spagnuolo. Model-based degradation analysis of photovoltaic modules through series resistance estimation. *IEEE Transactions on Industrial Electronics*, 62(11):7256–7265, 2015.

[154] Antonino Laudani, Francesco Riganti Fulginei, and Alessandro Salvini. High performing extraction procedure for the one-diode model of a photovoltaic panel from experimental i–v curves by using reduced forms. *Solar Energy*, 103:316–326, 2014.

[155] Sofiane Kichou, Santiago Silvestre, Gustavo Nofuentes, Miguel Torres-Ramírez, Aissa Chouder, and Daniel Guasch. Characterization of degradation and evaluation of model parameters of amorphous silicon photovoltaic modules under outdoor long term exposure. *Energy*, 96:231–241, 2016.

[156] S Pace, J Bishop, and M Magni. Hot spots in solar cells. test procedures and study of related phenomena. In *Seventh EC Photovoltaic Solar Energy Conference: Proceedings of the International Conference, held at Sevilla, Spain, 27–31 October 1986*, pages 304–308. Springer, 1987.

[157] Vun Jack Chin, Zainal Salam, and Kashif Ishaque. An accurate and fast computational algorithm for the two-diode model of pv module based on a hybrid method. *IEEE transactions on Industrial Electronics*, 64(8):6212–6222, 2017.

[158] Yiqun Zhang, Peijie Lin, Zhicong Chen, and Shuying Cheng. A population classification evolution algorithm for the parameter extraction of solar cell models. *International Journal of Photoenergy*, 2016, 2016.

[159] Wenyin Gong and Zhihua Cai. Parameter extraction of solar cell models using repaired adaptive differential evolution. *Solar Energy*, 94:209–220, 2013.

[160] Jeisson Vélez-Sánchez, Juan David Bastidas-Rodríguez, Carlos Andrés Ramos-Paja, Daniel González Montoya, and Luz Adriana Trejos-Grisales. A non-invasive procedure for estimating the exponential model parameters of bypass diodes in photovoltaic modules. *Energies*, 12(2):303, 2019.

[161] Kashif Ishaque, Zainal Salam, Saad Mekhilef, and Amir Shamsudin. Parameter extraction of solar photovoltaic modules using penalty-based differential evolution. *Applied Energy*, 99:297–308, 2012.

[162] Jieming Ma. *Optimization approaches for parameter estimation and maximum power point tracking (MPPT) of photovoltaic systems*. PhD thesis, University of Liverpool, 2014.

[163] Dhiaa Halboot Muhsen, Abu Bakar Ghazali, Tamer Khatib, and Issa Ahmed Abed. A comparative study of evolutionary algorithms and adapting control parameters for estimating the parameters of a single-diode photovoltaic module's model. *Renewable energy*, 96:377–389, 2016.

[164] Jerry Kumar, Nanik Ram Parhyar, Manoj Kumar Panjwani, and Danish Khan. Design and performance analysis of pv grid-tied system with energy storage system. *International Journal of Electrical and Computer Engineering*, 11(2):1077, 2021.

[165] Hugo Andrés Ruiz, Eliana Mirledy Toro Ocampo, and Harold Salazar Isaza. Algoritmo genético modificado chu-beasley aplicado a la identificación de errores en la estimación de estado en sistemas eléctricos. *Scientia et technica*, 3(35):25–30, 2007.

[166] Luis Fernando Grisales-Noreña, Daniel Gonzalez Montoya, and Carlos Andres Ramos-Paja. Optimal sizing and location of distributed generators based on pbil and pso techniques. *Energies*, 11(4):1018, 2018.

[167] Jhon Montano, Andres Felipe Tobon Mejia, Andrés Alfonso Rosales Muñoz, Fabio Andrade, Oscar D. Garzon Rivera, and José Mena Palomeque. Salp swarm optimization algorithm for estimating the parameters of photovoltaic panels based on the three-diode model. *Electronics*, 10(24), 2021.

[168] Santiago Silvestre and A Chouder. Effects of shadowing on photovoltaic module performance. *Progress in Photovoltaics: Research and applications*, 16(2):141–149, 2008.

[169] Pierluigi Guerriero, Lorenzo Codecasa, Vincenzo d'Alessandro, and Santolo Daliento. Dynamic electro-thermal modeling of solar cells and modules. *Solar Energy*, 179:326–334, 2019.